In Vivo Study of Nuclear-Localized Protein-Protein Interactions in Plant Cells

Thesis

UNRESTRICTED

In Vivo Study of Nuclear-Localized Protein-Protein Interactions in Plant Cells

Fabio Formiggini
Laurea in Scienze Biologiche
Università degli Studi di Napoli "Federico II"
Italia

Doctor of Philosophy

Sponsoring Establishment
Stazione Zoologica Anton Dohrn
Napoli, Italia

September 2003

Submission date: 24 September 2003
Acceptance date: 30 December 2003

ProQuest LLC.
789 East Eisenhower Parkway
P.O. Box 1346
Ann Arbor, MI 48106 – 1346

Director of studies:	**Dr. Chris Bowler** **Laboratory of Molecular Plant Biology** **Stazione Zoologica "Anton Dohrn"** **Naples - Italy**
Internal Supervisor:	**Dr. Roberto Di Lauro** **Stazione Zoologica "Anton Dohrn"** **Naples - Italy**
External Supervisor:	**Dr. Gunther Neuhaus** **Institute of Biology II** **Department of Cell Biology** **University of Freiburg - Germany**

Al mio papà il cui caro ricordo mi ha sempre sostenuto, ed alla mia cara mamma che ha sempre creduto in me ed ha saputo darmi una grande lezione di umanità.

Acknowledgments

I wish to thank Prof. Dorus Gadella (University of Amsterdam, The Netherlands) for his invaluable advice about FRET, and my external advisor Dr. Gunther Neuhaus (University of Freiburg, Germany) and internal advisor Prof. Roberto Di Lauro for their precious suggestions.

A special thanks to my director of studies Dr. Chris Bowler who guided me through scientific research always stimulating my curiosity and teaching me scientific rigour and to the people of my laboratory who helped me in several occasions and provided, when necessary, important moral support. Many thanks also to all the numerous people of the Institute who helped me in many ways.

Finally, thanks Anna for your patience and your encouragement and Giorgio for your vitality and love.

ABSTRACT

Recent results suggest that key events controlling light regulated gene expression in plants are import of the phytochrome photoreceptors into the nucleus followed by their binding to transcription factors such as PIF3. Coupled with this, the degradation of positively acting intermediates such as the transcription factor HY5 by COP1 and the COP9 signalosome appears to be an important process whereby photomorphogenesis is repressed in darkness. Genetic analyses in Arabidopsis and tomato have revealed that the nuclear protein DET1 also plays a key role in the repression of photomorphogenesis. However, up until now the mechanisms underlying its function have remained obscure.

In this thesis through a series of in vitro experiments, persuasive evidence is provided that DET1 binds to non-acetylated amino-terminal tails of the core histone H2B in the context of the nucleosome. Furthermore, FRET imaging with GFP variants has been used to prove this interaction within the nucleus of living plant cells. DET1 is therefore a novel chromatin interacting protein which binds to nucleosomes via interaction with unmodified H2B tails. Given the dramatic photomorphogenic phenotypes of *det1* mutants, this result infers that chromatin remodelling plays a heretofore unsuspected role in regulating gene expression during photomorphogenesis.

An important part of this thesis was devoted to the establishment of a reliable FRET-based wide-field microscopy system for the detection of the interactions between GFP- (Green Fluorescent Protein) tagged proteins in living cells. Limits of some of the available techniques are shown together with many data proving that the established system is indeed able to reliably detect protein-protein interactions.

Moreover, given the emerging importance of chromatin remodelling in plants, the FRET-based microscopy system has been used with a histone-based construct in an attempt to reveal chromatin dynamics in living cells. Data are presented about changes

of chromatin structures, as detected by FRET measurements, occurring during the cell cycle of living BY-2 cells.

ABBREVIATIONS:

BY-2	Tobacco cell line induced from a pith of *Nicotiana tabacum* L. cv. Bright Yellow No. 2.
CCD	Charged-Coupled Device
dpFRET	donor photobleaching FRET.
E	Efficiency of FRET.
ECFP	Enhanced Cyan Fluorescent Protein.
EYFP	Enhanced Yellow Fluorescent Protein.
f%	Per cent frequency. Per cent fraction of pixels having a certain value of N_{FRET} or $netF'_A$.
f% CUM	Cumulative per cent frequency. Per cent fraction of pixels having N_{FRET} or $netF'_A$ values ranging from zero to a certain value. 100 - f% CUM provides the per cent fraction of pixels having values higher than the fixed one.
FRET	Fluorescence Resonance Energy Transfer.
GFP	Green Fluorescent Protein.
NDF	Neutral Density Filter.
P-value	"Output" of a statistical t-test. It is the probability that a difference found between the mean values of a certain quantity measured in two populations (for example, of cells differently treated) is due to chance, i.e. it is the probability that the two populations behave analogously (have the same "real" mean value) although they present different mean values. A P-value lower than 5% is considered significant to infer that the two populations are indeed different.
R	Distance between donor and acceptor of a FRET pair.
Ro	Förster distance: distance between donor and acceptor of a FRET pair for which FRET efficiency is 50%.
ROI	Region Of Interest.
$X_{(x, y)}$	Each values of the X quantity which is surveyed in a pixel of x, y coordinates.
τ^{bl}	Photobleaching time constant.

CONTENTS

INTRODUCTION

1.1 PLANT LIGHT SIGNAL TRANSDUCTION

Plants have evolved as sessile organisms whose success is evident from their wide ecological distribution. An important feature that contributed to this success is their ability to react to the multitude of information that constantly bombards them, for adapting to their changeable life environment, based on a sophisticated system of receptors and signal transduction pathways that generates appropriate responses. The number of signals that challenge plants during their life cycle is enormous: photosynthetic and photomorphogenic light, photoperiod, temperature, wind, CO_2, humidity and herbivores, to mention just a few of them, mediate specific responses that most often culminate in altered gene expression.

Among these signals, light plays a major role. This is not surprising considering that plants have to optimize their photosynthetic productivity by adapting to the available source of light. This depends on their capacity to sense, evaluate and respond to light quality, quantity and direction. Moreover, the proper timing of developmental phenomena, such as flowering, requires systems of measuring and responding to variation in daylength. This sophisticated detection of light is achieved through the use of several photoreceptors, comprising phytochromes (red/ far red receptors), cryptochromes and phototropins (UV-A/blue light receptors).

1.1.1 Phytochromes

Phytochromes have been intensively studied since their biochemical purification over 40 years ago (Butler et al., 1959). These photoreceptors are strongly involved in light-dependent plant development. They control plant growth and adjust plant developmental strategies to changes in the light environment (Kendrick and

Kronemberg, 1994). For example, phytochromes have been demonstrated to be profoundly involved (Smith, 1995) in processes such as germination, de-etiolation (development of etiolated plants upon light exposure. Etiolation is the plant development in darkness typical of seedlings in the initial stages of growth when they are still buried in the soil), proximity perception, shade avoidance, photosynthetic acclimation to vegetation shade and to high irradiance, floral induction, etc.

In higher plants phytochromes are encoded by small gene families. For example, in Arabidopsis, five genes *PHYA*, *PHYB*, *PHYC*, *PHYD* and *PHYE* have been identified (Sharrock and Quail, 1989; Clack et al., 1994; Nagy and Schäfer, 2002; Schäfer and Bowler, 2002). Each forms a homodimer of around 240 KDa which covalently binds a tetrapyrrole chromophore to the N-terminal half of each monomer (Montgomery and Lagarias, 2002), which confers light sensitivity. Each phytochrome can exist in two photointerconvertible conformations termed Pr and Pfr. Pfr is the biologically active form. In the dark, de novo synthesized phytochrome is in the Pr form which absorbs maximally wavelengths in the red regions (600-700 nm). Upon absorption of red light, phytochrome is photoconverted into the Pfr form which absorbs maximally in the far-red region (700-800 nm), thereby being converted back to Pr (Nagy and Schäfer, 2002).

Many efforts have been made to elucidate the molecular mechanisms of phytochrome activity. To date it has emerged that phytochromes have both a cytoplasmic- and a nuclear-localized activity. In the cytoplasm, they appear to function at least partially as light-regulated kinases (Yeh and Lagarias, 1998), whereas in the nucleus they directly interact with transcription factors, acting as modulators of transcription (Martinez-Garcia et al., 2000).

1.1.1.2 Cytoplasm-based phy signalling

Albeit indirect, important evidence for the cytoplasmic activity of phytochrome has derived from biochemical and pharmacological studies in which purified phytochromes and putative signalling intermediates were microinjected into tomato cells deficient in phytochrome chromophore biosynthesis. These experiments demonstrated that signalling controlled by phyA and phyB are mediated by heterotrimeric GTP-binding proteins, cGMP, calcium and calmodulin (Shacklock et al., 1992; Bowler et al., 1994). The involvement of G-proteins was subsequently confirmed by reverse genetics approaches (Okamoto et al., 2001) while the role of calcium was reinforced by the discovery of SUB1, a cytoplasmically-localized calcium binding protein that appears to negatively regulate cryptochrome and phyA responses (Guo et al., 2001).

Moreover, other evidence for the cytoplasmic activity of phytochromes derives from the identification, through yeast two hybrid screens and pull-down experiments, of a phytochrome interacting protein, denoted PKS1, which is constitutively localized in the cytoplasm (Fankhauser et al., 1999). This protein can be phosphorylated by oat phyA on Ser/Thr residues, but the significance of this reaction is still unknown (Fankhauser et al., 1999). Evidence for the role of PKS1 in cytoplasmically-localized phytochrome activity derives from the phenotype of a loss-of-function *pks1* mutant which shows enhanced responsiveness to red light. This implies that PKS1 might be a negative regulator of phyB signalling, maybe forming a cytoplasmic retention complex with phytochrome (Nagy and Schäfer, 2000).

1.1.1.3 Nuclear-localized phy activity

The idea of a nuclear-localized activity of phytochromes was initially ignored because, from the earlier biochemical and immunocytochemical studies on phytochrome localization, which were performed on phyA, it appeared that the majority of Pr and Pfr

forms were localized in the cytoplasm both in dark- and light-grown plants (McCurdy and Pratt, 1986; Speth et al., 1986; Speth et al., 1987). The cytoplasm was therefore considered to be the main compartment from which phytochromes directly operate, and this view was reinforced by the microinjection studies conducted during the early 1990s (see above). The pioneering study of Sakamoto and Nagatani (Sakamoto and Nagatani, 1996) on the subcellular localization of *Arabidopsis* phyB (light stable) and phyB-GUS fusion proteins showed that nuclei isolated from light-treated plants contained higher amounts of phyB than those from dark-grown plants, suggesting for the first time the importance of the import of phyB into the nucleus as part of the light signalling mechanism mediated by phytochromes.

Subsequent studies, in which phy-GFP fusions were used to investigate phytochrome localization (Kircher et al., 1999; Yamaguchi et al., 1999; Kim et al., 2000; Kircher et al., 2002; Nagy and Schäfer, 2002; Huq et al., 2003), ascertained that:

1) All five phytochrome species are imported into the nuclei upon light exposure (in the Pfr form).

2) Nuclear translocation of individual phytochromes is regulated differentially by light and correlates with the physiological responses associated to each molecular species, indicating that the import of the photoreceptor into the nucleus is a major regulatory step in phytochrome signalling.

3) Upon translocation to the nucleus each phytochrome forms discrete speckles which are believed to be linked to the physiological activity of the photoreceptor in the nucleus. It has been postulated (Nagy and Schäfer, 2002) that speckles represent either active transcriptional- or degradation-complexes containing a high number of physically and functionally interacting molecules, on the basis of the following observations: a) the size and light-dependent dynamics of speckle formation argue against them being an artifact of the GFP fusions; b) inactive phytochrome mutants do not form speckles

(Kircher et al., 2002); c) speckles formed upon light exposure have been shown to contain intimately interacting phyB and cry2 photoreceptors (Mas et al., 2000). These findings are highly significant considering that many phytochrome responses are dependent upon changes in gene expression (Tepperman et al., 2001; Wang et al., 2001; Schroeder et al., 2002).

Beside the localization studies, a battery of nuclear localized proteins interacting with phytochrome A and B have been identified by yeast two-hybrid screens and in vitro pull-down experiments, reinforcing the significance of phytochrome localized in the nucleus (Ahmad et al., 1998a; Ni et al., 1999; Choi et al., 1999; Colon-Carmona et al., 2000; Mas et al., 2000; Sweere et al., 2001; Quail, 2000). Among them, PIF3 (Phytochrome Interacting Factor 3) has been shown to be a constitutively nuclear localized basic helix-loop-helix (bHLH) transcription factor which binds G-box elements present within the promoters of many light regulated genes (Menkens et al., 1995; Ishige et al., 1999), upon interaction with the phoactivated Pfr form of phytochrome B (and also phyA; Ni et al., 1998; Martinez-Garcia et al., 2000). The light dependent, highly specific, reversible interaction of phyB with PIF3 has been shown to be maintained when PIF3 is bound to the G-box containing CCA-1 promoter, suggesting the existence of at least some very short signal transduction pathways controlled by phyB, in which phytochrome modulates directly the activity of some genes by forming complexes with their transcription factors (Martinez-Garcia et al., 2000).

1.1.2 Phototropins

In Arabidopsis, two UV-A (320-390 nm)/blue (390-500 nm) light receptors, denoted phototropins (phot1 and phot2), have been identified (Briggs et al., 2001; Liscum and Briggs, 1995; Jarillo, 1998). Phot1 and phot2 are Ser/Thr kinases (Reymond et al.,

1992; Huala et al., 1997). Two FMN (Flavin MonoNucleotide) molecules, which are responsible for the light sensitivity of phototropins, bind to two LOV (Light Oxygen Voltage) domains located at the N-termini of each phototropin (Huala et al., 1997). These domains belong to the superfamily of PAS-domains, which is known to mediate ligand binding and protein-protein interactions (Taylor and Zhulin, 1999). Phot1 has been found to be plasma membrane localized whereas phot2 localization is still unknown.

Phototropins have been demonstrated to mediate three responses that maximize photosynthetic apparatus potential in weak light and prevent its damage in excess light, namely, phototropism (bending, due to growth or cell turgor, of plant organs toward or away from the light source; Sakai et al., 2001), light-induced opening of stomata (that maximize gas exchange thus allowing full activity of the photosynthetic apparatus; Kinoshita et al., 2001) and chloroplast migration in response to changes in light intensity (Kagawa et al., 2001; Sakai et al., 2001; Jarillo et al., 2001). The two phototropins have overlapping functions in the control of stomatal opening and phototropism at high blue light intensities whereas, in low light levels, phot1 plays a major role (Briggs and Christie, 2002). Very little is known about their downstream regulators.

1.1.3 Cryptochromes

In Arabidopsis, two additional UV-A/blue light photoreceptors, denoted cryptochrome 1 and 2 (cry1 and cry2) and very recently a third one, cryptochrome 3, for which however the photoreceptor function has not yet been proven (Kleine et al., 2003), have been identified (Ahmad and Cashmore, 1993; Lin et al., 1998; Cashmore et al, 1999). Cryptochromes are flavoproteins showing sequence similarity to photolyases, proteins that mediate repair of UV-damaged DNA in a light-dependent manner (Sancar, 1994),

and are currently considered to be their evolutionary progenitors (Cashmore et al., 1999). However, cryptochromes lack photolyase activity and very often contain characteristic C-terminal extensions (Ahmad and Cashmore,1993; Lin et al., 1995).

Cryptochromes have been found to be nuclear localized both in dark and light conditions (Cashmore et al., 1999). They are involved in de-etiolation, flowering time control, and circadian rhythms (Quail, 2002). Cry2 mediates responses to low blue light intensities whereas cry1 has a major role in strong blue light responses (Ahmad et al., 1998b; Lin et al., 1998; Lin, 2002).

1.1.4 Downstream components

Beside positive regulators of photomorphogenesis such as HY5 (see below) and PIF3 (see 1.1.1.3), genetic screens primarily in Arabidopsis for mutants that are photomorphogenic in darkness (i.e., displaying phenotypes of light-grown plants) identified a group of eleven negative regulators of photomorphogenesis denoted the COP/DET/FUS family, that constitute a complex suppression system that represses photomorphogenesis in darkness.

The molecular mechanisms by which some of these downstream effectors act are now beginning to be understood. For example, COP1 is cytoplasmic in the light, but localizes to the nucleus in darkness (Ang and Deng, 1994; Ang et al., 1998) where it destabilizes the constitutively nuclear localized bZip transcriptional activator HY5, a positive regulator of photomorphogenesis (Oyama et al., 1997), by targeting it to the 26S proteasome (Osterlund et al., 2000a). Other observations, such as the presence of a ring finger domain at the N-terminus and a number of WD40 repeats at the C-terminus, infer that COP1 is probably an E3 ubiquitin-protein ligase which recruits the ubiquitin-conjugating enzyme E2 and mediates the transfer of polyubiquitin from E2 to target proteins (Hardtke and Deng, 2000; Hare et al., 2003). Moreover, a direct connection

between photoreceptors and the downstream effector COP1 has been shown in Arabidopsis where the photoactivated UV-A/blue light photoreceptors cryptochromes cry1 and cry2 have been shown to bind COP1 and, in so doing, appear to inhibit its degradation of HY5 in the light (Wang et al., 2001), providing a main pathway in the blue light regulation of photomorphogenesis in Arabidopsis. In contrast, the role of COP1 in regulating phytochrome-mediated photomorphogenic development is less clear.

Among the eleven COP/DET/FUS negative regulators of photomorphogenesis, five of them have been found to be subunits of the COP9 signalosome (CSN). CSN is an oligomer formed by eight subunits and has been found not only in plants but conserved also in yeast, Drosophila and mammals, indicating that it plays important functions in many eukaryotes (Wei and Deng, 1999). Evidence is accumulating to suggest that the CSN is involved in regulating protein degradation through modulation of activity of the ubiquitin-proteasome system (Schwechheimer et al., 2001). Two main findings supporting this role are the remarkable similarity between CSN and the "lid" of the proteasome (Wei et al., 1998), a subunit that is necessary for the recognition of the tag (a ubiquitin chain) of proteins targeted towards degradation, and a demonstrated role in regulating the activity of E3 ligases, which are required for the selective targeting of proteins to be degraded (Schwechheimer et al., 2001; Lyapina et al., 2001; Peng et al., 2001).

A picture has therefore emerged in which some key events controlling photomorphogenesis are phy translocation to the nucleus followed by binding to transcription factors that directly control light-regulated gene expression. Coupled with this, the degradation of positively acting intermediates appears to be an important process whereby photomorphogenesis is repressed in darkness.

The role of DET1 has remained unclear up until recently. Mutations in the *DET1* gene were first identified as being responsible for the constitutively de-etiolated phenotype of Arabidopsis *det1* mutants, which are essentially identical to *cop1* mutants (Chory et al., 1989; Pepper et al., 1994; Deng et al., 1991). Subsequently, mutations in the tomato homolog of *DET1* were found to be responsible for the light hypersensitive phenotype of tomato *high pigment-2* (*hp-2*) mutants (Mustilli et al., 1999). Although the mutant phenotypes are rather different in the two plant species, in both cases it appears that DET1 is a negative regulator of photomorphogenesis. The only clue to a precise function is that the protein is predominantly localised to the nucleus in both Arabidopsis and tomato (Pepper et al., 1994; Mustilli et al., 1999). Previous studies have ruled out that DET1 may directly bind to DNA or that it binds to the RNA polymerase holoenzyme (Malakhov and Bowler, Unpublished results), thus excluding two obvious mechanisms whereby DET1 could repress light-inducible genes.

In this thesis the role of DET1 has been investigated. The results indicate that DET1 is a novel chromatin interacting protein which binds to nucleosomes via interaction with unmodified H2B tails, inferring that chromatin remodelling could be involved in plant light signal transduction.

1.2 CHROMATIN REMODELLING

1.2.1 Chromatin structure

In eukaryotic cells, DNA has to be highly compacted in order to fit within the nucleus. This is achieved by packaging DNA into chromosomes, whereby its length is reduced around 10^4-fold (Wolffe, 1998; Pienta and Coffey, 1984). Chromosomes consist of chromatin, which comprises equal amounts of DNA and proteins, the most significant of which are the positively charged histones. Histones form a particle, termed the nucleosome, which is the basic unit of chromatin (Kornberg and Klug, 1981; Luger et

al., 1997). It has a core particle containing 145-147 bp of DNA, corresponding to 1.65 turns of the DNA superhelix. Adjacent core particles are separated by variable regions of "linker DNA" of 20-80 bp. This fundamental chromatin structure gives the characteristic 10 nm "beads-on-a-string" appearance when viewed in the electron microscope, in preparations of low ionic strength which relax higher-order folding (Olins and Olins, 1974). The core particle is disk-shaped and is formed by an octamer of two molecules of each of the four histones H2A, H2B, H3 and H4 (Fig.1). The "fold-domains" at the C-terminus of core histones mediate the interactions between histones and between histones and DNA. The core histone N-terminal tails are lysine rich and have relatively minor structural roles in the nucleosome context (Ausio et al.,1989). However, they have been found to be extremely well conserved between species, thus suggesting a major physiological role. Moreover, it has been demonstrated that histone tails are required for higher-order chromatin folding (see below; Carruthers and Hansen, 2000).

Structures with higher chromatin compaction are less well understood. For example, in interphase nuclei, a more condensed 30 nm fibre of chromatin is observed rather than the 10 nm fibre. This structure allows a total 40-fold compaction of linear DNA. The linker histone H1, which binds on the outside of the core particle and interacts with linker DNA, has been found to be associated with regions of increased chromatin compaction and seems to be required to stabilize the structure (Finch and Klug, 1976; Thoma et al., 1979; Graziano et al., 1994). For the 30 nm fibre, a solenoid structure has been proposed in which the 10 nm fibre is wrapped in a superhelix in which each turn is formed by 6 nucleosomes. However, this model has been shown not to fit with experimental data, for example, about the local concentrations of DNA in metaphase chromosomes (Daban, 2000). These results question the solenoid model and highlight the need for new studies to define the 30 nm fibre structure.

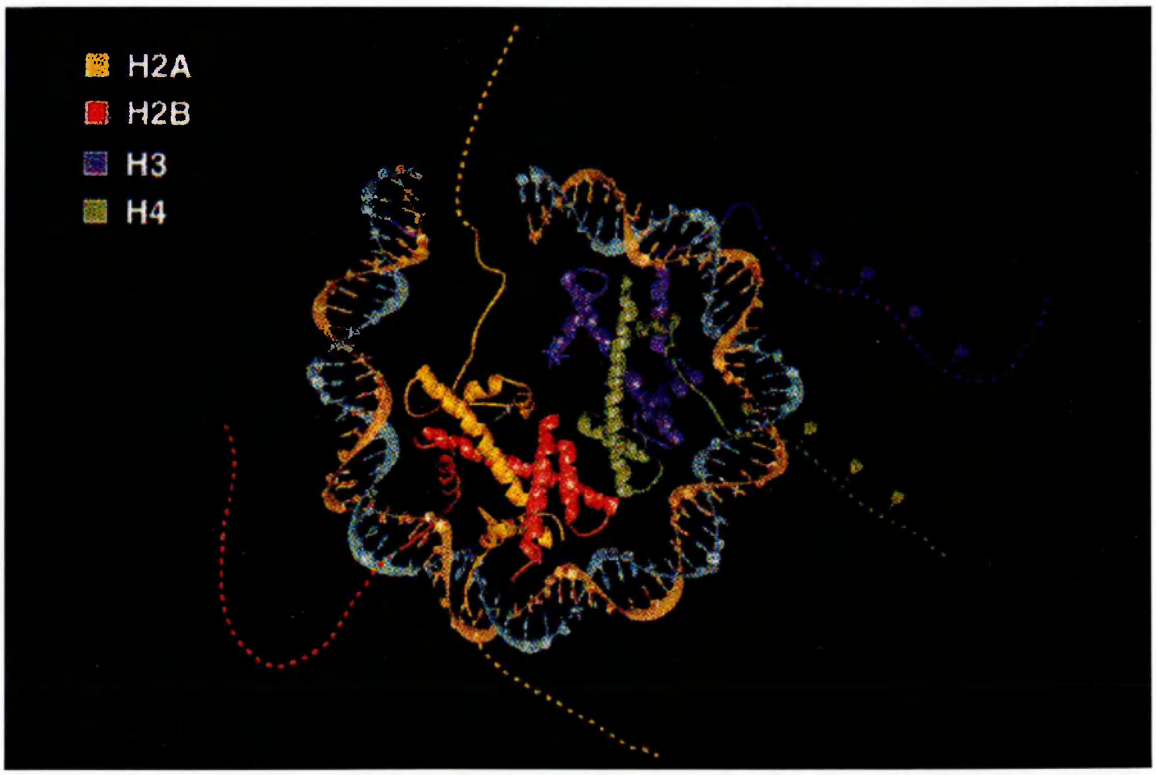

Fig.1 X-Ray structure of nucleosome core particle. Half the core particle, with four histones and 73 DNA basepairs, is shown. Histone tails are drawn as dashed lines, with lollipops to indicate acetylation sites. H2A tails are both N- (bottom) and C-terminal (top), while tails for the other histones are N-terminal. (Adapted from Kornberg and Lorch, 1999).

Higher-order chromatin folding is even less well understood. Electron microscopy preparations of human metaphase chromosomes show that DNA forms loops of 30-90 kb irradiating from a central scaffold, with a radial arrangement (Marsden and Laemmli, 1979; Paulson and Laemmli, 1977). The presence of such a structure has also been inferred from interphase nuclei, although with a looser scaffold (Razin and Gromova, 1995; Allen et al., 2000). Its significance is however not clear.

1.2.2 Chromatin structure and gene expression

Two forms of chromatin, denoted heterochromatin and euchromatin, were identified in interphase nuclei of plant and animal cells in the light microscope 75 years ago (Heitz, 1928). It is now known that heterochromatin is highly condensed and is transcriptionally inactive whereas euchromatin is less condensed and is the active form. Moreover, euchromatin exists in at least two forms: a less condensed transcriptionally active form and a more condensed form which is reversibly inactive (Alberts et al., 1994). These general observations correlating the transcriptional activity of chromatin and its compaction infer the importance of chromatin structure for the regulation of gene expression. Indeed, much evidence supports a connection between chromatin structure and transcription. Some examples follow: gene activation in interphase polytene chromosomes of *Drosophila* generates "chromosome puffs" at the sites of the gene, due to chromatin decondensation (Daneholt, 1975), which disappear upon gene downregulation (Ashburner, 1990). In amphibian lampbrush chromosomes, chromatin decondensation is associated with transcription (Callan, 1986). It has been shown that a heterochromatin context is inhibitory for gene expression (Iglesias et al., 1997). Naked reporter DNA inserted in cells by particle bombardment has been found to be more highly expressed than that integrated in the cellular genome and, therefore, in a

chromatin context (Chua et al., 2001). Finally, it has been argued that the default chromatin is per se inhibitory for transcription, because nucleosomes can interfere with the access of transcription factors (Struhl, 1999).

It emerges, therefore, that cells need specific systems to change dynamically their own chromatin structure in order to allow all the DNA-linked processes (not only transcription, but also, for example, mitosis, meiosis and DNA-repair), during their life-cycle.

Activities that change chromatin structure have been generically termed "chromatin remodelling". Chromatin remodelling involves the activity of ATP-dependent remodelling complexes, which have been shown to alter the association of DNA with the nucleosome core particle (Flaus and Owen-Hughes, 2001). Additionally the term is also used in a broader context to include processes such as the covalent modifications of histone tails, methylation, acetylation, phosphorylation and ubiquitination which are able to modify local gene activity, but for which the effects on chromatin structure remain unclear. These post-translational modifications target primarily specific residues within the N-terminal tails of histones (Luger et al., 1997) and in yeast and mammalian cells recent studies have revealed their importance for regulating transcription (Strahl and Allis, 2000; Jenuwein and Allis, 2001). Acetylation is the best studied example in the control of gene activation, and several histone acetyltransferases (HATs) and histone deacetylases (HDACs) have been described that can regulate acetylation on specific lysine residues within H3 and H4 tails (Strahl and Allis, 2000; Jenuwein and Allis, 2001).

An important characteristic of chromatin remodelling is that it is often associated with changes in gene expression that are particularly stable (but nonetheless reversible). Namely, they can persist after an initial stimulus has long since disappeared, therefore providing a "memory" of transient events. These changes have been denoted

"epigenetic" ("epi-", because they do not involve changes in the nucleotide sequence of DNA) because they have been shown to be heritable through mitosis and meiosis in animals (Cavalli and Paro, 1998; Cavalli and Paro, 1999; Nakayama et al., 2000) and plants (Cubas et al., 1999).

Chromatin remodelling is considered to be extremely important in animal development, where the term "epigenesis" has been coined to indicate the (epi) genetic changes that accompany the development and differentiation of different cell types from the zygote during embryogenesis. For example, during development in *Drosophila*, initial gradients of morphogenes are interpreted by the cells and result in changes in gene expression of different homeotic selector genes which are fixed by the cells and inherited through mitotic divisions. This memory determines cell fate during organism development, but because epigenetic determination is flexible, a further cell sub-differentiation may be nonetheless possible (Lawrence and Struhl, 1996). Chromatin remodelling can provide a means by which these changes occur, as inferred by the fact that in insect and vertebrates members of the trithorax and Polycomb-groups of genes are thought to confer, respectively, active or repressed chromatin structures which mediate the inheritance of the determined state.

1.2.3 Chromatin remodelling in plants

In plant development a similar picture has recently emerged (Jenik and Irish, 2001; Goodrich and Tweedie, 2002) although here the peculiarly high flexibility of cell fate would question an analogous role of chromatin remodelling in plant cell fate determination. However, it seems very probable that this flexibility is a consequence of a relatively easy reset of chromatin state rather than of a different mechanism for the regulation of gene expression. The following evidence supports the view that chromatin remodelling plays an important role in plants:

1. Genetic screens for developmental patterning mutants in plants have identified genes with predicted or established roles in chromatin remodelling.
2. Analysis of the complete genome sequence of Arabidopsis (Arabidopsis Genome Initiative, 2000) has revealed that plants also contain a range of genes encoding HATs, HDACs, and other chromatin remodelling proteins (Meyer, 2001; Verbsky and Richards, 2001).
3. The core histones are known to be reversibly acetylated in plants (Lusser et al., 2001), therefore suggesting that plants, like other eukaryotes, utilize histone tail modifications for the epigenetic control of gene expression.

Results presented in this thesis suggest that chromatin remodelling may also be an important aspect of plant responses to light signals. Furthermore, attempts have been made to develop a FRET-based microscopy system to visualize changes in chromatin structure in living plant cells (see below).

1.3 FRET AND FLUORESCENCE MICROSCOPY

1.3.1 Practical considerations

In the following paragraphs, I have attempted to highlight the major problems that must be faced when dealing with the establishment of a system for quantitative wide-field fluorescence microscopy, which underlies any system based on the quantification of FRET.

An appropriately equipped modern fluorescence microscope can be considered to be an imaging microfluorometer: a mercury or xenon lamp provides a versatile source of light spanning wavelengths from UV to the visible; excitation and emission filters can be used as monochromators for excitation and emission, and a CCD (Charged-Coupled Device) camera is an efficient light detector. The sample chamber is substituted by the microscope stage and the sample cell consists of a slide and

coverslip. Between the specimen and the light detector, the microscope optics are located. These allow the generation of a two-dimensional magnified fluorescence image of the specimen that can be focused in sequence, allowing the resolution and measurement of fine, microscopic details within the sample, in two and three dimensions. In particular, the use of the CCD camera as an imaging light detector, as opposed to a Photo Multiplier Tube (PMT)- based detector, allows the simultaneous measurement of the fluorescence deriving from each point of the image projected onto the light-sensitive chip of the CCD. From this point of view, each microscope field of view of the sample can be considered as an x, y array of microscopic fluorometer cells, the fluorescence of each being measured in the corresponding pixel of the CCD chip.

The main drawback of fluorescence microscopy applied to cell biology is that the specimen, constituted by cells, is highly heterogeneous. This generates several sources of "noise" which may degrade the quality of the acquired images to a variable extent. Strategies to deal with this issue are discussed below.

To study biomolecule localization, interaction or dynamics, the biomolecules can be tagged by fluorophores and introduced into the cells of interest. Each x, y point of this specimen (to continue the fluorometer cell analogy, each of the sample cells) contains a structured suspension of different substances (e.g., organelles, membranes, cytosol, etc.), some of which are autofluorescent, in which the fluorophore-labelled molecule is dispersed or differentially localized.

1.3.1.1 Autofluorescence

Autofluorescence can be a serious problem because the underlying principle of fluorescence microscopy is to selectively observe the structures or biomolecules of interest in an "empty" background. In contrast, the presence of autofluorescence can overlap with the fluorescence of interest, thereby masking it and, in a quantitative

respect, adding to it, thus modifying its intensity and generating artificial results. Autofluorescence can sometimes be excluded by carefully selecting the detection wavelengths; however, other methods are often required to deal with the autofluorescence problem (Billinton and Knight, 2001). One of these is based on the spectral characterization of cell autofluorescence to remove its contribution from the fluorescence of the exogenous fluorophore and, consequently, better performances are obtained when spectral imaging is used (Gadella et al., 1997). An alternative approach, although rather tedious and not always fruitful, consists of characterizing autofluorescence of the cells in order to identify conservative patterns. For example, during the present thesis work it was observed that the autofluorescence within the vacuoles of BY-2 cells is very much correlated to that within the nucleus, in the FRET and donor channels. This allowed estimation of autofluorescence within the nucleus by using that of the vacuoles as reference, which was used in cases where the tested proteins were exclusively nuclear localized. When such a strategy cannot be applied, it is sometimes possible to observe that the autofluorescence in a cell population is rather conserved among different cells and (in the best circumstance) is constant in the cell compartment of interest (this method has also been employed in the present thesis). If this is the case, the average value of autofluorescence calculated from a significant number of cells can be used to "extrapolate" autofluorescence of the tested cell. However, this method is less reliable especially when the cell population displays an unpredictable heterogeneity. Finally, fluorophore fluorescence is sometimes much higher than cell autofluorescence and so can be ignored (in the present thesis this was the case for the GFP-histone fusion fluorescence).

1.3.1.2 Cell thickness and ratio approach

Another source of "noise" derives from the variability of the thickness of living cells. It

is important to distinguish between the thickness of the sample, which is the distance between slide and coverslip and which is approximately constant, and what we could term the "effective thickness", to indicate that portion of the sample in the z direction, perpendicular to the sample plane, where the fluorophore can diffuse. For example, many fluorescent dyes can diffuse only in the cytosol, but if one observes a point through which a portion of a chloroplast is present, then only the thickness of the cytosol constitutes the effective thickness in that region. In fluorescence microscopy, the effective thickness of the sample in each point corresponds to the optical path of the fluorometer sample cell. Because fluorescence is directly proportional to the optical path of the sample cell, its variability in fluorescence microscopy strongly affects the fluorescence intensity of each point of the specimen and can generate ambiguity in interpreting the fluorescence images. The question is: are the regions with different fluorescence intensity due to differences in fluorophore concentration (i.e., to different affinity of the fluorophore tagged molecule for those regions) or to differences in the effective thickness (i.e., just a consequence of imaging a heterogeneous sample)?

Consider the following example: in plant cells GFP can freely diffuse in the cytosol and in the nucleoplasm (von Arnim et al., 1998). It is, however, excluded from the vacuoles, that occupy a large fraction of the cellular volume and leave thin "cytoplasmic streams" between the nucleus and the plasma membrane, delimiting a thin layer of cytosol. In such a complex structure, if one observes a plant cell labelled with GFP in two points, one point through the nucleus and one through the cytosol, the impression is that GFP has a preferred nuclear localization because the fluorescence in the nucleus is higher than in the cytosol. The experimenter could then infer that there is a mechanism of retention of GFP in the nucleus or a preferential GFP localization in the nucleus. However, considering the effective thickness of the specimen in the two points, it is immediately clear that the nuclear region has a thickness much greater than

that of the cytosol. This could easily explain the differences in fluorescence and the apparent preferential GFP localization to the nucleus.

A general approach to overcome the limit of the undetermined effective thickness in fluorescence microscopy is based upon calculating ratio images, i.e., dividing the fluorescence image of the fluorophore-tagged molecule of interest by a normalizing fluorescence image of the same specimen, that takes into account the differences in thickness (Specific software allows to do easily operations between images. This is equivalent to do operations between the value of each $pixel_{(x,y)}$ in an image and the value of each pixel $_{(x,y)}$ in a second image for all the image pixels, in order to generate an "operation"-image whose pixels have the calculated value). In this way, the effective thickness is cancelled out by the ratio and the resulting image reflects only differences in concentration. One way of normalizing the fluorescence image is to introduce a spectrally distinct tracing fluorophore which is known (both theoretically and experimentally) to not be preferentially localized in the cellular compartments of interest. In the above example of cytoplasmic- and nuclear- localized GFP signals, the tracing fluorophore should be homogeneously distributed in the cytosol and in the nucleus. The fluorescence of this fluorophore would therefore be a direct expression of the effective thickness in each point, and it could be used in the ratio to cancel the thickness-derived heterogeneity. In the GFP example, this operation would produce a flat ratio image showing that GFP is not preferentially localized between cytosol and nucleoplasm.

The same concept applies for concentration-normalizing fluorescence images. For example, fluorescent probes sensitive to small molecules ("analytes"), such as calcium (Minta and Tsien, 1989; Grynkiewicz et al., 1985; Tsien, 1989; Haugland, 2002), produce images in which the fluorescence in each point is related to the concentration of the molecule in that point. We already know that the effective

thickness can be misleading for interpretation of the images. Another source of variability could arise from different probe concentrations in different cell compartments. In this case, one would need a normalizing fluorophore (image) whose fluorescence depends on effective thickness and probe concentration. This last prerequisite necessitates the choice of a fluorophore that is chemically very similar to the probe and whose cellular distribution is the same. Because this is very difficult to ascertain, this approach is called "pseudoratio". Many efforts have consequently been made to generate "ratiometric" dyes. These dyes are characterized by a shift of their fluorescence spectrum when bound to their analyte. In general, ratiometric-dye quantum yield and/or extinction coefficient at a certain wavelength increase upon binding of the analyte, resulting in an increase of dye fluorescence. On the contrary, at a different wavelength, fluorescence remains constant (or decreases) upon binding of the analyte and therefore constitutes a constant reference of probe concentration and sample thickness. Consequently, the ratio between the two fluorescences at the two wavelengths allows correction for thickness and probe concentration, without any need to use a second dye.

1.3.1.3 Out of focus blur and scatter

The limitations of fluorescence microscopy described above are due to the nature of the material (i.e., cells) under observation. Other limitations derive from the microscope optics. Considering again a point x, y in a microscope specimen, the fluorescence measured in this point derives from a corresponding specimen cylinder x, y, z, where z, the depth of the cylinder, is the effective thickness. In the microscope, for well known optical reasons (Inoué, 1997), only the portion of the cylinder contained in the objective depth of field is in focus. All the fluorescence coming from the regions above and below the focal plane is out of focus and determines the "out of focus blur" of the

image. From the point of view of the "fluorometer sample cell" in a quantitative respect this means that the measured fluorescence contains a contribution from the points in the optical planes delimiting that which is in-focus, within the same z axis and paraxial. This is a critical limit of fluorescence microscopy which reduces the resolution of thick samples in two and three dimensions. One way to overcome this is to apply advanced deconvolution algorithms that are based upon the mathematical description (the Point Spread Function) of the spatial distribution in three dimensions of the light coming from a point source, and which allow to reassign the out of focus contributions to the in-focus points (Wallace et al., 2001).

A supplementary noise due to the thickness and heterogeneity of cells is scatter, which is the random disturbance of light caused by its passage through regions of heterogeneous refractive index within the specimen. Scatter produces a random disarrangement of image details which is difficult to model and consequently cannot be corrected with the same accuracy obtainable for out of focus blur (Kam et al., 2001).

The above discussion reveals some of the problems of obtaining reliable quantitative data in fluorescence microscopy. For the exploitation of FRET in fluorescence microscopy the same limits apply, as well as the ratio concept. Moreover, although when applied to fluorescence microscopy new complexities emerge, the basic methods are essentially identical. FRET determination is discussed below.

1.3.2 FRET theory

FRET is the transfer of energy that can occur between two fluorophores, denoted donor and acceptor, if they are in close proximity, in a permissive orientation and if there is spectral overlap between acceptor excitation and donor emission spectra. After excitation of the donor molecule, the acquired excitation energy can be transferred in a

non-radiative way (i.e., without photon emission) to the acceptor molecule (that could be only an absorbing chromophore, denoted, in this case, a "quencher") that will be excited and will be able to emit its own fluorescence.

E, the efficiency of FRET, which is related to the fraction of excitation energy absorbed by the donor that is transferred to the acceptor, is defined in the *Förster equation* (Förster, 1948):

1) $E = Ro^6/(R^6+Ro^6)$

where R is the distance between donor and acceptor and Ro is the distance at which E is 50% (usually between 30 and 60 Angstroms). In this equation, because E depends on the distance R between the FRET partners, it is a measurement of their proximity. Moreover, Ro in the Förster equation must take into account the other two conditions required for FRET occurrence, donor and acceptor orientation, and spectral overlap. Consequently:

2) $Ro = 9.79 \times 10^{3}(\kappa^2 Q J n^{-4})^{1/6}$

where

κ is the "orientation factor", which is related to the relative orientation of the donor and acceptor dipoles. The square of its value κ^2 ranges from 0 to 4. The minimum value 0 corresponds to perpendicular donor and acceptor dipoles, where FRET is not possible. For parallel dipoles, κ^2 has the maximum value of 4. For random orientation, κ^2 is equal to 2/3. **Q** is the donor quantum yield (number photons emitted/number photons absorbed) in the absence of acceptor. **J** is the "overlap integral". J expresses the degree of spectral overlap between donor emission and acceptor absorption and is given by $J = \int_{\infty}^{o} F_D(\lambda)\varepsilon_A(\lambda)\lambda^4 d\lambda$, where F_D is the normalized donor emission fluorescence with respect to the area under the donor fluorescence spectrum and ε_A is the acceptor extinction coefficient. The symbol **n** represents the refractive index of the

intervening medium. Ro is established for a particular donor-acceptor pair, in a certain orientation, and can be calculated from eq. 2. However, most often it is experimentally measured using model systems and is then assumed to apply to the FRET measurements in question. For practical purposes, tables of Ro values for useful donor-acceptor pairs are available in the literature.

Interest in using FRET in applications with biomolecules has existed since the first theoretical studies of FRET. Indeed, energy by FRET can be transferred over distances on the order of common macromolecular dimensions (1-10 nm). Consequently, if the donor and acceptor are tagged to two proteins (or other biomolecules) of interest then it is possible to study protein-protein interactions by FRET. Moreover, transfer of energy by FRET is almost exclusively due to a real interaction between molecules, rather than to transient colocalization of freely diffusible molecules, because in the latter case FRET can occur only when local donor-acceptor concentrations are in the millimolar range (Lakowicz, 1999b), which usually exceeds those reached under normal experimental conditions. Interestingly, if using a high enough resolution (i.e., accuracy) to detect FRET, it is possible to reveal interactions between biomolecules or, at higher resolution still, the geometry of the interaction as can be inferred from the dependence of FRET from proximity and orientation of the fluorescent tags (Lakowicz, 1999b).

1.3.3 FRET quantification

The efficiency of FRET, E, corresponds to the quantum yield of energy transfer Φ_{FRET} (Clegg, 1992). The quantum yield of any spectroscopic process $\Phi_{process}$ is the ratio of the rate **k** away from some selected state by way of this process, divided by the total rate of escape from this state (which is the sum of the rate of escape due to each of the operating escape processes). This is equivalent to defining $\Phi_{process}$ as a number equal to

the quanta lost from some particular molecular state through this process, divided by the total quanta absorbed to create this particular state. We can write a basic definition of E, in which the molecular state and process of interest are the excited donor and FRET:

$$\mathbf{E = \Phi_{FRET} = k_{FRET} / k_{TOT}}$$

From this equation we can derive equations that show the relationship to the most important measurable quantities used to experimentally quantify FRET:

1. Lifetime of the donor excited state, τ (Clegg, 1992; Clegg, 1996; Gadella, 1999). Given that the lifetime τ of a certain molecular state is the reciprocal of its total rate of escape (k_{TOT}) from it, i.e., $\tau = 1/ k_{TOT}$, we have:

$$E = k_{FRET}\, \tau_{DA}$$

where τ_{DA} is the lifetime of the excited donor in the presence of the acceptor. Considering that

$$k_{FRET} = k_{TOT} - k_{TOT(D)} = \tau_{DA}^{-1} - \tau_{D}^{-1}$$

where τ_D is the lifetime of the excited donor without acceptor (and analogously $k_{TOT(D)}$ is the total rate of escape of the donor without acceptor), we have

$$E = (\tau_{DA}^{-1} - \tau_{D}^{-1})\, \tau_{DA} = 1 - \tau_{DA}/\tau_{D}$$

which is the desired expression. If FRET occurs, $\tau_{DA} < \tau_D$ (the excited donor state has a supplementary way to escape from it so its lifetime is shorter).

2. Donor fluorescence quantum yield (Clegg, 1992).

Using the definitions given above about quantum yield and the rate of a process, together with the previous equation, we can derive:

$$E = 1 - \Phi_f^{DA}/\Phi_f^{D}$$

where Φ_f means fluorescence quantum yield and the DA and D superscripts refer, as above, to the presence or absence of acceptor. Measuring the donor fluorescence **D** (per

unit time) of a donor population interacting with an acceptor and of the same donor population without acceptor, and assuming that the number of photons absorbed in both cases is the same, we can also infer that:

$$E = 1 - D_{DA}/D_D$$

If FRET occurs, $\Phi_f^{DA} < \Phi_f^D$ or $D_{DA} < D_D$ (because the donor is partially quenched by the acceptor, absorbing a fraction of its quanta of energy). Another option is to apply the following equation:

$$E = netF'/netF'_{100\%\ FRET}$$

in which **netF'** is the enhanced acceptor emission due to FRET (see below) in the donor+acceptor sample and $netF'_{100\%\ FRET}$ is the acceptor emission that would occur if E was 100%.

3. Photobleaching donor-fluorescence decay time constant, τ^{bl} (Gadella and Jovin, 1995).

Donor photobleaching is the photochemical process that depletes the total pool of donor molecules (via the donor excited state), when illuminated, characterized by the decay time constant τ^{bl}. In this case, we have:

$$E = 1 - \tau^{bl}_D/\tau^{bl}_{DA}$$

where τ^{bl}_D and τ^{bl}_{DA} refer to the time constants measured without and with the acceptor, respectively. If FRET occurs, $\tau^{bl}_{DA} > \tau^{bl}_D$ (because the lifetime of the excited donor is shorter, the probability that photodestruction can occur is less and the process becomes slower).

The present thesis deals with the quantification of FRET by determination of donor fluorescence quantum yield and photobleaching donor-fluorescence decay time constant.

Measurement of the lifetime of the donor excited state is one of the most

powerful approaches to reveal FRET between interacting fluorescent molecules. However, this technique requires a complex instrumentation that was not available during the present thesis (Gadella, 1999; Lakowicz, 1999a).

A discussion concerning the experimental treatment of one of the major complications in the measurement of FRET efficiency by donor fluorescence quantum yield determination follows. Subsequently, in Materials and Methods (see *2.7.1* and *2.7.2*), each of the two methods will be described as it was used in the present thesis.

1.3.4 Decomposition of measured fluorescence

To measure the efficiency of FRET in a sample containing donor and acceptor by the donor fluorescence quantum yield determination, one of the major experimental complications is the decomposition of the measured fluorescence signal in terms of its components:

1) enhanced emission from the acceptor due to FRET (we can call this "donor-sensitized acceptor emission")
2) acceptor emission from direct excitation of the acceptor
3) donor emission from direct excitation of the donor.

This problem can be overcome most accurately by detecting emission and excitation spectra of the sample containing donor and acceptor, and of two standards, deriving from donor-only and acceptor-only samples (Clegg, 1992). Emission spectra are acquired by a donor excitation wavelength and excitation spectra, and by an acceptor emission wavelength (both usually correspond, respectively, to the donor and acceptor λ_{max}). Either type of spectrum must be broad enough to include the emission of both the donor and the acceptor. Once these data have been obtained they can be used to decompose the donor+acceptor sample spectra into its components, fitting the donor-only emission spectrum to the donor+acceptor emission spectrum, both detected at the

same donor excitation wavelength, in a region where only the donor emits. This fitted curve is then subtracted over the entire donor+acceptor sample emission spectrum, to isolate the remaining fluorescence component due only to the acceptor, which is made up of two components: fluorescence from the acceptor directly excited at the donor excitation wavelength, and the donor-sensitized acceptor emission. By repeating the procedure with excitation spectra, i.e., fitting the acceptor-only excitation spectrum to the donor+acceptor excitation spectrum, both detected at the same acceptor emission wavelength, in a region where only the acceptor emits, allows extrapolation of the fluorescence component (at the emission wavelength used to acquire the excitation spectrum) of the donor+acceptor sample due to the acceptor directly excited at the donor excitation wavelength, from the fitting curve in the region of donor excitation. By subtracting this quantity (at the excitation wavelength used to acquire the emission spectrum) from the previous one (at the emission wavelength used to acquire the excitation spectrum), the desired donor-sensitized acceptor emission, indicated above by netF', can be generated. With less accuracy, it would also have been possible to use single wavelength pairs (or fluorescence integrated over wavelength ranges) instead of spectra to perform the fluorescence decomposition (Gordon et al., 1998). This approach is the preferred one in fluorescence microscopy applications where it is difficult to detect whole spectra, and will be described below in Materials and Methods.

The donor-sensitized acceptor emission of a sample is proportional to the efficiency of FRET. This quantity is however directly proportional to the concentration of the donor:acceptor complex, so it should be normalized for this concentration to compare it to other samples and to calculate E. In the best case, the donor:acceptor concentration is known by other means, so it is very easy to calculate E, for example, by measuring the donor emission in a sample without acceptor at the known donor concentration and then converting this fluorescence into the $netF'_{100\% FRET}$ (essentially

by multiplying by $\Phi_{A(\lambda emA)}/\Phi_{D(\lambda emD)}$ the donor fluorescence) to apply the equation 2 in section *1.3.3.* In particular cases, calculating suitable ratios between the obtained fluorescence components allows some unknowns to be cancelled (Clegg, 1992). However, also in this case, a preliminary knowledge of certain data such as the percentage of donor/acceptor labelling or a step of donor:acceptor purification are necessary to obtain E.

It is not always necessary to calculate E. E is usually desired if one wants to measure distances between interacting donor and acceptor molecules, whereas FRET is often exploited only to reveal interactions. However, also in this case, normalization for at least total donor and/or total acceptor fluorescence is very important because it allows comparison between different samples. Consequently, the normalized quantity FRETN, netF'/D (Gordon et al., 1998), N_{FRET} and $netF'_A$ are often used in fluorescence microscopy. The last two were used in the present thesis and are defined subsequently (see Materials and Methods).

One final general note concerns the determination of the photobleaching decay constant (and fluorescence lifetime). Also in this case one usually deals with composite samples. Although only the donor fluorescence is detected, and usually donor selective wavelength pairs do exist, one has to bear in mind that the measured donor fluorescence comes from donor:acceptor complexes and free donor molecules. This produces more complex decay curves in which the fraction of each species appears as a factor of the multi-exponential functions that have to be used to fit the experimental data (Lakowicz, 1999d).

1.4 GREEN FLUORESCENT PROTEINS

The green fluorescent proteins (GFPs) have been chosen as fluorescent tags for all the fusions tested in the present thesis. Below, a brief summary of the characteristics of the

GFP progenitor is reported together with the advantages deriving from its use. The GFP spectral variants differ from the progenitor by their spectral features, being differently coloured, but they retain the main characteristics. Moreover, some of them (independently from their colours) have been improved with regard to level of expression, stability, etc.

The Green Fluorescent Protein (GFP) was discovered by Morin and Hastings as a component of the bioluminescence of some marine coelenterates in 1971 (Morin and Hastings, 1971). Subsequently, the two proteins responsible for the green bioluminescence of the jellyfish *Aequorea victoria*, aequorin and GFP, were characterized (Shimomura and Johnson, 1975; Blinks et al, 1976). In vivo, these two small proteins interact: the aequorin, a calcium-activated photoprotein, emits blue light which is converted by energy transfer into green light by GFP, a fluorescent protein that is excited by blue light and which emits green light.

1.4.1 Structure

GFP is an "autofluorescent" protein of 238 amino acids (MW 26 kDa) whose native structure is essentially an 11-stranded β-barrel ("β-lantern") which wraps the imidazolinone chromophore, guarding it very efficiently (Fig. 2; Ormo et al, 1996). The chromophore is formed in the presence of oxygen by a slow (approximately 4 hours) reaction of autocatalytic cyclization (Cody et al., 1993) of the three amino acids Ser 65, Tyr 66, and Gly 67 (Cubitt et al., 1995) lying within a central helical segment. These features explain some fundamental characteristics of GFP:

(a) No external cofactors, except for oxygen, are required for fluorescence (Cubitt et al., 1999)

(b) Very high stability with respect to the effects of denaturants, proteases, temperature (Tm=78°C) and pH (Ward, 1982).

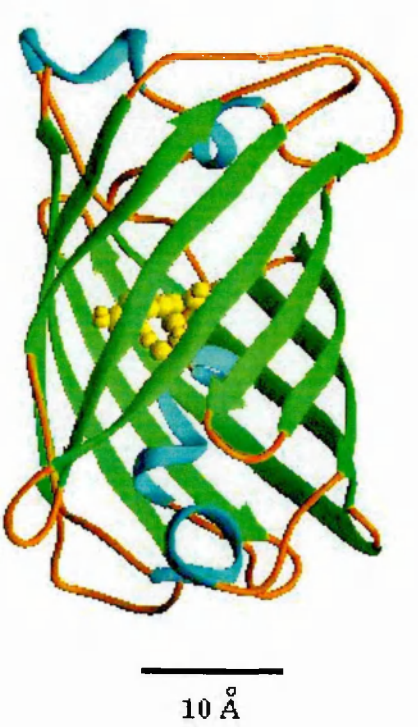

Fig. 2 The structure of the GFP protein. Eleven strands of β-sheet (green) form the walls of a cylinder. Short segments of α-helices (blue) cap the top and bottom of the 'β-can' (β-lantern) and also provide a scaffold for the fluorophore, which is near the geometric center of the can (Image from Yang et al., 1996).

1.4.2 Applications

Immediately following isolation of the GFP cDNA from *Aequorea victoria* (Prasher, 1995) the potential uses of the protein became clear. Indeed, GFP has now been used as a fluorescent marker of many proteins *in vivo* to follow their cellular fate. Furthermore, it has been possible to study the interaction between different proteins and other structures (e.g., membranes) by exploiting fluorescence resonance energy transfer (see FRET). In all these applications, the GFP cDNA is fused to the cDNA of the protein of interest to obtain a labelled fusion protein which often retains all the features of both the constituting proteins. These hybrid cDNAs can be expressed potentially in any cells, if carried by a suitable expression vector.

GFP is a very good fluorescent molecule thanks to its high stability and quantum yield, and relatively low photobleaching rate. These features allow one to easily study GFP-tagged protein localization at the subcellular level, in a normal epifluorescence microscope. Moreover, GFP-based applications offer some advantages with respect to enzymatic- or antibody-based assays. In the latter cases the administration of specific substrates or antibodies to the cells is required; this is often accompanied by some step of cell fixation and/or permeabilization which can lead to some artefacts. Furthermore, these compounds can be quite expensive. On the contrary, GFP fluorescence requires only an inexpensive excitation light that is relatively non-toxic and which is usually capable of "permeating" the cells easily without any perturbation. As a consequence, GFP allows reliable *in vivo* real-time experiments to be performed in single cells or whole organisms. GFP is easy to use because it involves only the application of standard recombinant DNA techniques to place the GFP cDNA into the desired expression vector. Other methodologies, e.g., those involving labelling of proteins with detectable groups, require extensive use of biochemical techniques and

consequently are both money- and time-consuming.

1.4.3 GFP spectral variants

Wild-type GFP (wtGFP) is excited by blue light. Its excitation spectrum is characterized by two peaks at 395 nm (major peak) and at 475 nm (minor peak). On the contrary, there is only one emission peak with a maximum at 507 nm (corresponding to green light). Several GFP spectral variants have been obtained by introducing mutations in and around the chromophore. These alter the spectral features of wtGFP by shifting its excitation and/or emission peaks. Moreover, different mutations have been introduced into the sequences of the GFP variants in order to obtain GFPs with an enhanced overall fluorescence, in different conditions or living hosts. These mutations change codon usage, eliminate intron splicing sites or enhance GFP folding, without altering the GFP spectra.

Roger Tsien has grouped all the GFP mutants into seven classes with similar excitation and emission spectra (Tsien, 1998). Essentially, both blue- and red- shifted mutants with respect to the spectra of wtGFP are available and, in addition, the excitation spectra are simplified because only one peak is present (Fig. 3). Given the wide availability (e.g., from Clontech Laboratories Inc., Palo Alto, USA) of so many different mutants that are selectively detectable by using suitable monochromators or optical filters (Omega Optical Inc., Brattleboro, VT, USA www.omegafilters.com, or Chroma Technology corp. Brattleboro, VT, USA, www.chroma.com), it is now possible to choose GFP variants which allow multiple labelling applications. For example, labelling different proteins with different GFPs having different light excitation/emission characteristics, it is possible to follow their behaviour simultaneously in the same cell and to study their interactions.

In the present thesis, the two fluorescent proteins ECFP (*Enhanced Cyan Fluorescent Protein*), maximally absorbing at 433 nm and emitting at 475 nm, and

EYFP (*Enhanced Yellow Fluorescent Protein*), maximally absorbing at 513 nm and emitting at 527 nm have been chosen (Fig. 3).

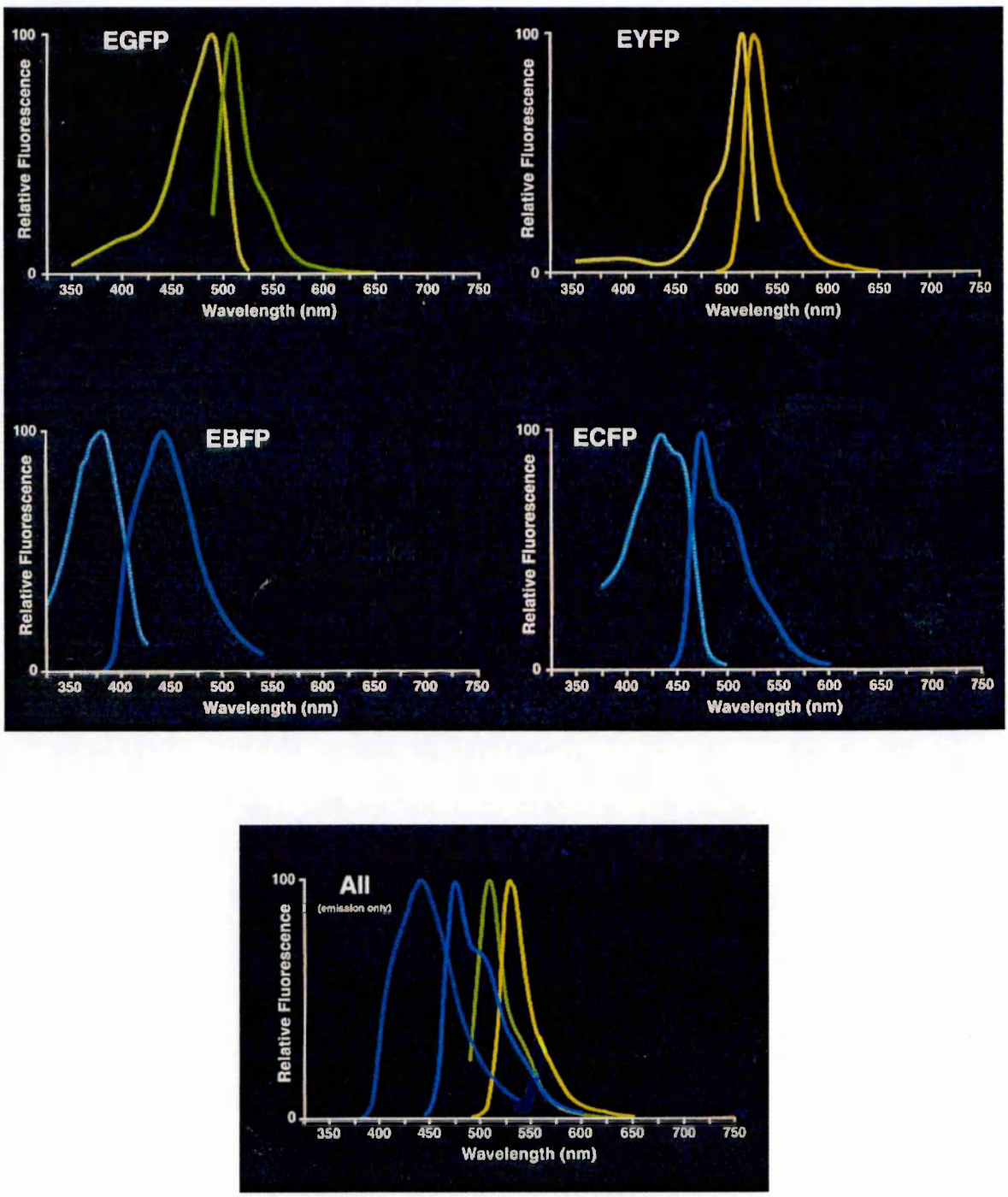

Fig. 3 Spectra of GFP variants. Excitation and emission spectra of EBFP, ECFP, EGFP and EYFP. These fluorescent proteins form a series of progressively higher excitation and emission wavelengths, by which multiple labelling of samples is possible (Adapted from Patterson et al., 2001).

1.5 SCOPE OF THE THESIS

Part of this thesis was devoted to investigating whether the influence on photoregulated gene expression of DET1 might be mediated by an epigenetic mechanism involving binding to histone tails. In a series of in vitro and in vivo experiments, evidence is presented that this is indeed the case, specifically, that DET1 binds to non-acetylated H2B tails within a nucleosome context. This study infers that chromatin remodelling may play an important role in mediating photoregulated gene expression.

The main goal of this thesis was to establish an effective system for studying interactions between biomolecules, in vivo, by FRET detection in a fluorescence microscope. These advanced microscopy techniques were used to demonstrate the interaction between DET1 and histone H2B in living cells. Furthermore, considering the emerging importance of chromatin remodelling in plants, considerable efforts were made to attempt to establish a reliable FRET-based assay to monitor changes in chromatin architecture at a subnuclear resolution in plant cells *in vivo*.

Finally, FRET technology was used to study in vivo interactions between proteins involved in light signal transduction, such as phytochrome and PIF3. Moreover, a preliminary characterization of GFP fusions to the negative regulator of photomorphogenesis COP1 and to the positive regulator HY5 in cultured BY-2 cells is presented.

MATERIALS AND METHODS

2.1 In vitro Translation and Binding Assays

^{35}S-labelled DET1 and lamin proteins were generated by the TNT Quick in vitro transcription-coupled translation system from Promega. For histone-agarose binding assays 3µl of in vitro-translated DET1 proteins were incubated with 10 µl of histone-agarose beads (Sigma) in 50 µl of PBS. After overnight incubation at 4°C, beads were washed three times in PBS. Subsequently the beads were resuspended in 20 µl of Laemmli buffer and resolved on 10% or 12% SDS-PAGE. Following electrophoresis, the gels were fixed in 40% (v/v) MeOH/10% (v/v) HOAc for 30 min, with agitation, followed by further 30 min incubation in ENLIGHTENING solution (NEN Life Sciences). The treated gels were dried on Whatman 3 MM paper using a gel dryer (Bio-Rad) and exposed to X-ray film in the presence of intensifying screens, at -80°C.

For GST pull-down assays, 2 µg of GST-H2B fusion proteins (Lorain et al., 1998) immobilized on glutathione-Sepharose 4B beads were mixed with in vitro-translated DET1 proteins in 0.3 ml PBS/0.1% Triton X-100. After 2 hours incubation at 18°C on a rotary incubator, beads were washed three times with the same buffer and treated as described above.

Binding of DET1 and lamin to the synthetic H2B peptides were performed using the same conditions described for the GST pull-down assay. The peptides corresponding to the first 32 amino acids of human H2B, unmodified and modified, were synthesized, purified and coupled to amino hexyl-agarose (Department of Biochemistry, Kentucky, USA). Lysines at positions 5, 12, 15 and 20 were acetylated in the modified peptide.

For competition experiments competitors were incubated with in vitro-translated DET1 proteins for 30 min before performing the binding assay. Purified histones were

purchased from Boehringer Mannheim. 200 μg of each histone (a 20-fold excess) were used in the competition assays. All binding reactions were performed at least three times.

2.2 GST Fusion Proteins

The construction of GST-H2B and derivatives was described previously (Lorain et al., 1998). Plasmids encoding GST-H2B fusion proteins were introduced into competent *E. coli* BL21 cells and GST fusion protein expression was induced by adding 1 mM IPTG overnight at 18°C. Cells were lysed by sonication and Triton X-100 was added to a final concentration of 1% and incubated for 30 min on ice. Cellular debris was removed by centrifugation at 14000 rpm for 45 min. Supernatants were incubated with 0.5 ml of a 50% slurry of glutathione-Sepharose 4B beads (Amersham Pharmacia Biotech) for 1 hr at 4°C. Subsequently the beads were washed three times with ice-cold PBS. Overexpressed proteins were eluted with 2 mM reduced glutathione (Boehringer Mannheim) and quantified on SDS-PAGE using purified BSA as standard.

2.3 Nucleosome Preparation

Chicken blood containing Alsever anticoagulant was purchased from Charles River. Nuclei were extracted from chicken erythrocytes according to Greyling et al. (Greyling et al., 1983). Batches of nuclei were stored as 50% (v/v) glycerol suspensions at –20°C until ready for further processing. Histone H1-depleted oligonucleosomes were prepared according to Schnitzler (Schnitzler, 2000) and separated by ultracentrifugation using a 10% to 40% linear glycerol gradient layered with 4 ml of quenched micrococcal nuclease digestion reaction. Centrifugation was carried out for 16 hr at 45000 *g* at 4°C in a Beckman SW28 rotor. The DNA concentration of the gradient-harvested fractions was determined and the sizes of the oligonucleosomes were measured by electrophoresis on 1.5% (w/v) agarose/TAE gels. Mononucleosome fractions were

pooled and concentrated using Centricon-10 concentrators (Amicon). The concentrated samples were then dialyzed overnight and the dialysates stored at 4°C. The dialysates were verified for the absence of histone H1 by SDS-PAGE on 15% precast acrylamide gels (Bio-Rad). Approximately 1 mg of mononucleosomes were immobilized to 500 µl CNBr-activated Sepharose 4B (Amersham Pharmacia Biotech) according to the manufacturer's instructions. As a negative control, 10 mg of BSA (Sigma) were immobilized to 500 µl CNBr-activated Sepharose 4B in a similar manner. In both cases, immobilization and blocking were carried out overnight at 4°C. In vitro-translated tomato and Arabidopsis DET1 proteins (3 µl) were incubated together with 10 µl of nucleosome resin in the presence of PBS + 1 mg/ml BSA, in a final volume of 50 µl, overnight at 4°C with agitation. After binding the resin was washed three times and resuspended in 15 µl 2X Laemmli buffer. The bound proteins were resolved on 10% SDS-PAGE. Gels were then treated as previously described.

2.4 FPLC Analysis of DET1 Binding

In vitro-translated DET1 was incubated with histone-agarose or nucleosome-sepharose as described above. The incubation mix was then poured into an empty HR 5/2 glass column (Amersham Pharmacia Biotech) resulting in a bed height of 10 mm. The column was connected to an FPLC system (Amersham Pharmacia Biotech) and the resin was washed with PBS, with a flow rate of 0.5 ml/min, until the A280 nm reading was stabilized and had attained a zero baseline reading. Elution of radioactive DET1 was carried out using a 10 ml linear salt gradient (0 to 550 mM NaCl in PBS), with a flow rate of 0.5 ml/min, and 500 µl fractions were collected. A 100 µl aliquot of each fraction was counted for ^{35}S content in 5 ml ULTIMA GOLD scintillation cocktail (Packard Bioscience) using an LS 6500 Multi-purpose scintillation counter (Beckman

Coulter), while the remaining aliquots were TCA/DOC precipitated, resuspended in 15 µl 1x Laemmli buffer and subjected to SDS-PAGE on 10% pre-cast acrylamide gels (Bio-Rad). Following electrophoresis, the gels were treated as previously described.

2.5 myc-TDET1 expressing plants

A 6xMyc epitope tag sequence (corresponding to amino acids 408-439 of human c-Myc) was added to the N-terminus of tomato *DET1* by PCR and the resulting fusion was transferred into a pBI121-based vector for plant expression (Jefferson et al., 1987). Tomato cotyledons were transformed with an *Agrobacterium tumefaciens* strain containing this construct as previously described (McCormick, 1991). Primary transformants (T1) were selected on kanamycin.

Transgenic plants (T2 generation) were screened for the presence of the myc-TDET1 protein using a modified version of the EZ method (Martinez-Garcia et al., 1999). Young leaf tissue (250–300 mg) was ground in a mortar and pestle in the presence of liquid nitrogen and the homogenates were resuspended in 2 vol (w/v) 2 X Laemmli buffer. Following electrophoresis on 10% SDS PAGE (Bio-Rad), the proteins were transferred to PVDF membranes for western blotting. Western blots were revealed using a monoclonal anti-c-Myc (9E10) antibody (Santa Cruz) and the ECL detection kit (Amersham Pharmacia Biotech).

Nuclear proteins from myc-TDET1 positive plants were extracted according to Foster et al. (Foster et al., 1992) with the following modifications. NLB and NEB buffers were prepared with 5 µg/ml pepstatin and 5 µg/ml leupeptin. Tissue was ground to a fine powder in the presence of liquid nitrogen and the homogenate was resuspended in NGB at a ratio of 1:4 (w/v) followed by filtration through 5 layers of Miracloth (CalBiochem). The nuclear pellets were resuspended in NWB at a ratio of 1:2 (v/w)

following centrifugation at 2000 *g*, and at a ratio of 1:1 (w/v) with NLB following centrifugation at 3000 *g*. Ammonium sulfate was added dropwise to a final concentration of 400 mM to the resuspended nuclear pellets, post-centrifugation at 3000 *g*. Protein concentration was determined according to the method of Bradford (Bradford 1976). Protein precipitates following centrifugation at 10000 *g* were resuspended with a minimal volume (200–500 µl) of NEB and dialyzed for 2 hr in 1 l of NEB containing 5 mM β-mercaptoethanol using slide-a-lyzers with a molecular weight cut off of 10 kDa (Pierce). The dialysates were stored at – 20°C until ready for use.

Approximately 100 µg of total nuclear protein extract were incubated with either 10 µl of nucleosome resin, 20 µl of histone resin, or 20 µl of histone H2B N-terminal tail resin, in a final volume of 50 µl NEB, overnight at 4° C with agitation. The resins were resuspended with 18 µl 2X Laemmli buffer, after washing 3 times with NEB and the bound proteins were resolved by SDS-PAGE on a 12% pre-cast polyacrylamide gel (Bio Rad). The gel was then treated as previously described.

2.6 CONSTRUCTION OF PLASMIDS FOR IMAGING

For all the FRET-based studies described in this thesis, I generated fusion proteins containing one or both the two GFP spectral variants ECFP and EYFP, which have been previously shown to be an optimal pair for FRET-based studies (Tsien and Prasher, 1998). Four "recipient" constructs containing ECFP or EYFP were first generated in order to clone genes of interest either downstream or upstream as N-terminal or C-terminal fusions. The fusion proteins obtained are shown schematically in Fig. 4.

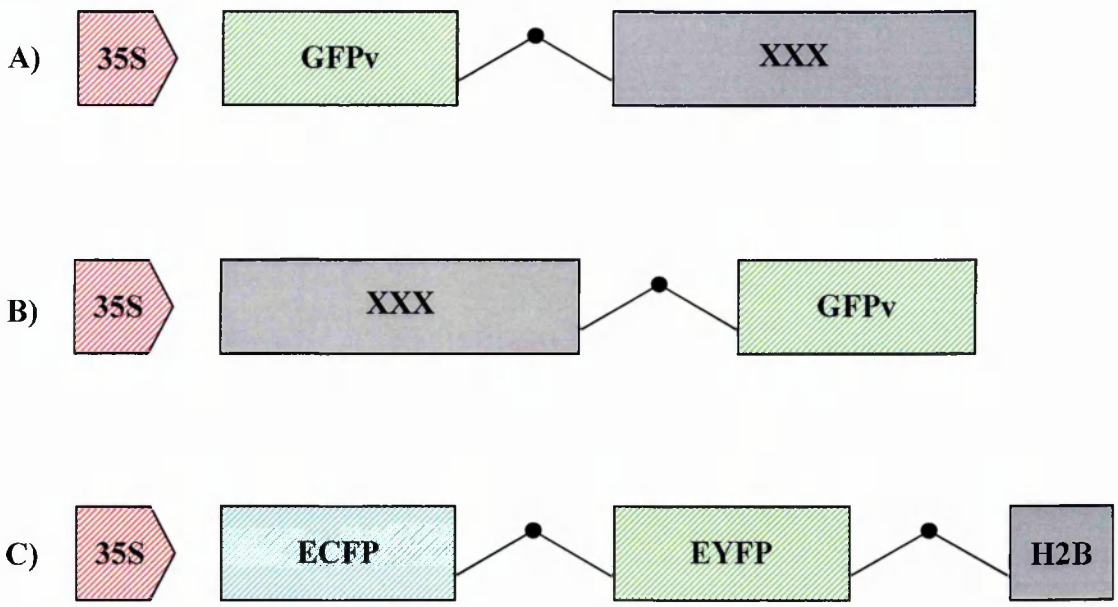

Fig. 4. Scheme of the GFP fusion proteins used in this thesis. A and B represent, respectively, the N-terminal and C-terminal fusions to ECFP or EYFP (which are indicated as "GFPv") of each of the proteins (which are indicated as "XXX") that were studied (i.e., TDET1, PIF3, phyB2, THY5, TCOP1, histone H2A and H2B). In C, the "triple" fusion of ECFP to EYFP and to H2B is represented. Note that in all the constructs a flexible linker joins the fused proteins. This should, in principle, increase the chances of each of the two proteins to be functional and able to interact. Note also that in the construct in C, an additional linker was positioned between histone H2B and EYFP to obtain the highest "malleability" of the resulting fusion protein. This characteristic makes the protein particularly suitable to study chromatin dynamics in living cells (see later in the text). For all the constructs, gene expression was driven by the constitutive 35S cauliflower mosaic virus promoter.

All PCR amplifications were made using the high fidelity Pfu polymerase enzyme (Stratagene) and all constructs were verified by DNA sequencing. PCR conditions were the following:

1. Denaturating 95 °C, 3 min.
2. Denaturating 94 °C, 1 min.
3. Annealing 55 °C, 1 min. When both primers were longer than 25 bp, for the first 5 cycles (steps 2-4) the annealing temperature was set to 55 °C, and for the following cycles, it was set to 65 °C.
4. Elongation 72 °C, 1 min (Pfu rate of elongation is 1 kb/min. For fragments longer than 1 kb, a time equal to [basepair number/1000] min was used).
5. Repeat steps 2-4 25 times.
6. Elongation 72°C, 15 min.
7. End, 4°C.

The construct containing tomato phyB2-EYFP was kindly provided by Ferenc Nagy (Sreged, Hungary).

2.6.1 N-terminal fusions

In order to generate the recipient construct containing EYFP for constructing N-terminal fusions, the EYFP-coding sequence was first PCR amplified from pEYFP-N1 (Clontech, Palo Alto, USA) using primers 5'-GGGGGGTACCGGATCCAACAATGGTGAGCAAGGGCG-3' (forward) and 5'-GGGGTCGACTCCTCCTAAGCTTGCATAATCAGGAACATCATACTTGTACA GCTCGTCC-3' (reverse) to amplify a *Kpn*I-*Sal*I fragment containing the full length coding region of EYFP with a *BamH*I site inserted immediately upstream of the ATG,

the stop codon removed and an HA1 epitope tag-Gly-Gly flexible linker added at the C-terminus (Fig. 4). This fragment was then cloned into the *Kpn*I-*Sal*I sites of plasmid pKS and sequenced. An analogous strategy was used to generate the recipient construct containing ECFP, using plasmid pECFP (Clontech). The two primers used to amplify the ECFP-coding sequence were identical to those used to amplify EYFP, because the ECFP ends are identical to those of the EYFP gene. The *genes* of interest *DET1*, *HY5*, *PIF3* and *COP1* (see below) were then inserted into the *Sal*I-*Not*I sites of the recipient constructs to obtain N-terminal EYFP or ECFP fusions between a 5'*BamH*I and a 3'*Sac*I site in plasmid pKS.

The tomato *DET1* (*TDET1*) cDNA (Mustilli et al., 1999) was cloned as a *Spe*I fragment in plasmid pSK+ (Stratagene). The region containing the coding sequence was then PCR amplified using primers to introduce a new *Sal*I restriction site at the N-terminus, immediately upstream of the ATG, and a *Not*I site at the C-terminus, immediately downstream of the stop codon. Two primer pairs were used to amplify separately the N- and C-terminal portions of *DET1*; these two fragments, after complete sequencing, were ligated together with the *Eco*RI-*Nde*I central fragment obtained by digestion of the above mentioned pSK-DET1, and *Sal*I-*Not*I digested pKS+ plasmid (Stratagene), to build the desired full length tomato *DET1* sequence cloned in plasmid pKS. The primer pair 5'-GGGGGTCGACATGTTCAAAACTAACAATGT-3' (forward) and 5'-GGGGGAATTCCCCAATTGCTC-3' (reverse) was used to amplify the *Sal*I-*Eco*RI N-terminal fragment containing the *TDET1* ATG, and the primer pair 5'-GGGGCATATGAACTTCATGTCC-3' (forward) and 5'-GGGGGCGGCCGCTTATCGACGAAAATGGATA-3' (reverse) was used to amplify the *Nde*I-*Not*I C-terminal fragment containing the stop codon.

The tomato *HY5* (*THY5*) coding region was amplified from a parent plasmid containing the full-length *THY5* cDNA derived from screening of a tomato cDNA

library (Lambda Zap II, Stratagene). The specific primer pair 5'-GGGGGTCGACATGCAAGAGCAAGCGACG-3' (forward) and 5'-GGGGGCGGCCGCCTACTTCCTCCCTTCCTGTGC-3' (reverse) was used to PCR amplify a *Sal*I-*Not*I fragment containing the full length coding region, including the ATG and the stop codon. This fragment was cloned into the *Sal*I-*Not*I sites of pKS and completely sequenced. An identical strategy was used for cloning the full length coding region of *PIF3* and *COP1* into the *Sal*I-*Not*I sites of pKS. For *PIF3*, the Arabidopsis *PIF3* (*APIF3*) coding region was amplified from a plasmid containing the full length cDNA kindly provided by Jaime Martinez-Garcia (Barcelona, Spain). The specific primer pair 5'-GGGGGTCGACATGCCTCTGTTTGAGCTTTTCAG-3' (forward) and 5'-GGGGGCGGCCGCTCACGACGATCCACAAAACTG-3' (reverse) was used. For *COP1*, the tomato *COP1 (TCOP1)* gene was cloned from a parent plasmid already available in our laboratory and the specific primer pair 5'-GGGGGTCGACATGGTGGAAAGTTCAGTTGG-3' (forward) and 5'-GGGGGCGGCCGCTCAAGCTGCAAGGACTAACAC-3' (reverse) was used.

For construction of the ECFP-EYFP and ECFP-EYFP-H2B constructs, the recipient construct containing ECFP, which was built for generating N-terminal fusions, was used with the only modification being that a *Not*I-*Sac*I linker containing stop codons in all three reading frames was first added in the *Not*I-*Sac*I sites of plasmid pKS. The EYFP-coding sequence was PCR amplified from pEYFP-N1 using the specific primer pair 5'-GGGGCTCGAGGTGAGCAAGGGCGAGGA-3' (forward) and 5'-GGGGACTAGTGTCGACTCCTCCCTTGTACAGCTCGTCCAT-3' (reverse)

to amplify an *Xho*I-*Spe*I fragment containing the full length coding region of *EYFP* with an *Xho*I site inserted immediately upstream of the ATG, which was removed. The stop codon was also removed and a Gly-Gly dipeptide was added at the C-terminus,

followed by a *Sal*I site. This fragment was then cloned into the *Xho*I-*Spe*I sites of plasmid pKS and sequenced. The cloned EYFP was then inserted as an *Xho*I-*Spe*I fragment into the *Sal*I-*Spe*I sites of the recipient construct to obtain the ECFP-EYFP fusion, comprised between a 5'*BamH*I and a 3'*Sac*I site in plasmid pKS.

The histone H2B-coding sequence was PCR amplified from plasmid pKS-H2B (that was used to generate C-terminal fusion constructs; see below), using the specific primer pair 5'-GGGGGTCGACATGGCACCAAAGGCAGG-3' (forward) and 5'-GGGGGCGGCCGCTTAATTGCTAGTAAACTTGGTG-3' (reverse) to amplify a *Sal*I-*Not*I fragment containing the full length coding region of *H2B* containing a *Sal*I site inserted immediately upstream of the ATG. This fragment was then cloned into the *Sal*I-*Not*I sites of plasmid pKS and sequenced. The cloned H2B fragment was subsequently inserted into the *Sal*I-*Not*I sites of the ECFP-EYFP construct to obtain the ECFP-EYFP-H2B fusion, comprised between a 5'*BamH*I and a 3'*Sac*I site in plasmid pKS.

2.6.2 C-terminal fusions

In order to construct recipient plasmids containing EYFP to be used for generating C-terminal fusions to genes of interest, the EYFP-coding sequence was PCR amplified from pEYFP-N1 (Clontech) using primers 5'-GGGGCGGCCGGGAGGATATGATGTTCCTGATTATGCAAGCCTAATGGTG AGCAAGGGCG-3' (forward) and 5'-GGGGCCGCGGTTACTTGTACAGCTCGTCC-3' (reverse) to amplify an *Eag*I-*Sac*II fragment, containing the full length coding region of *EYFP* and an HA1 epitope tag-Gly-Gly flexible linker inserted at the N-terminus. This fragment was cloned into the *Eag*I-*Sac*II sites of plasmid pKS and sequenced. An analogous strategy was used to generate the recipient constructs containing ECFP. In this case, plasmid pECFP

(Clontech) was used as template. Genes of interest *TDET1*, *TH2B* and *TH2A* (see below) were then inserted into the *BamHI-EagI* sites of the plasmid to obtain C-terminal EYFP/ECFP fusions, comprised between a 5'*BamHI* and a 3'*SacI* site in plasmid pKS.

For the *TDET1* C-terminal construct, the specific primer pair 5'-GGGGCATATGAACTTCATGTCC-3' (forward) and 5'-GGGGCGGCCGTGGTCGACGAAAATGGATATTT-3' (reverse) was used to amplify a 3' *NdeI-EagI* fragment, which lacked the stop codon, from the above mentioned plasmid pTDET1. This fragment was cloned into the *NdeI-EagI* sites of pKS+ and sequenced. A 5' *SalI-NdeI DET1* fragment was obtained by restriction enzyme digestion from the TDET1 construct that was used to generate the N-terminal construct (see above). The 5' *SalI-NdeI* and the 3' *NdeI-EagI* fragments were then ligated together in a *SalI-EagI* digested pKS+ plasmid to generate the desired full length *TDET1* sequence cloned in plasmid pKS.

A full-length cDNA encoding tomato histone H2B (accession number AJ224934) was amplified from a lambda ZAP tomato cDNA library (Wilkinson et al., 1995) using specific primers. The following primer pair 5'-GGGGGGATCCAACAATGGCACCAAAGGCAGGAA-3' (forward) and 5'-GGGGCGGCCGTGGATTGCTAGTAAACTTGGTG-3' (reverse) was then used to amplify a *BamHI-EagI* fragment containing the full length coding region of tomato *H2B*, without the stop codon. The fragment was cloned into the *BamHI-EagI* sites of pKS (pKS-H2B) and sequenced. An analogous strategy was used to amplify a tomato histone *H2A* (tomato cDNA clone *H2A-1*; Koning et al., 1991). The following specific primer pair 5'-GGGGGGATCCAACAATGGATGCTACTAAGACAACCA-3' (forward) and 5'-GGGGCGGCCGTGGTGCCTTCTTCGGTGACT-3' (reverse) was used.

The resulting chimeric constructs, EYFP-TDET1, ECFP-THY5, ECFP-APIF3, ECFP-TCOP1, ECFP-EYFP, ECFP-EYFP-H2B, TDET1-EYFP, TH2B-ECFP, TH2B-EYFP and TH2A-EYFP were subcloned into a pBI121-based vector (Jefferson et al., 1987) for expression in plant cells as *BamHI-SacI* fragments. These vectors, in which expression is driven by the 35S cauliflower mosaic virus promoter, were used in all subsequent transfections.

2.7 BY-2 CELL CULTURES

2.7.1 Plant Cell Transfection

For all experiments, BY-2 cells (Nagata et al., 1992) were used. This tobacco cell line, which was derived from a callus induced on a seedling of *Nicotiana tabacum* L. cv. Bright Yellow No. 2 (Kato et al., 1972), was chosen because of its inherent low autofluorescence at the wavelengths used, and for its high rate of growth (generation time 13 hours; Nagata et al., 1992).

BY-2 cell cultures kindly provided by Gunther Neuhaus (Freiburg, Germany) were grown in liquid medium at 24°C, 120 rpm in dim light (see below) conditions with a 16 hour light/8 hour dark photoperiod in the following medium: 4.3 g/l MS salt mixture (Gibco BRL), 30 g/l sucrose, 0.2 g/l KH_2PO_4, pH 5.8. Subcultures were made each week by inoculating 2 ml of the old culture in 100 ml of fresh medium supplemented with 100 mg/l myoinositol, 1 mg/l thiamine and 0.2 mg/l 2,4-dichlorophenoxyacetic acid. This medium, supplemented with hormones and vitamins, is denoted "BY-2 medium".

All the constructs in pBI121-based vector were introduced into BY-2 plant cells by helium-accelerated microparticle bombardment using a Bio-Rad PDS 1000 device (Bio-Rad Laboratories, Hercules, California, USA) with 1.5-3.0 μm spherical gold

particles (Aldrich Chem. Co, Milw. WI 53201) following standard procedures, at a pressure of 1550 psi and 24 inches of vacuum. After 18-24 hours incubation in dim light (10^{-4} $\mu mol \cdot s^{-1} \cdot cm^{-2}$), light ($10^{-1}$ $\mu mol \cdot s^{-1} \cdot cm^{-2}$) or darkness, 50 µl of cells were placed on microscope slides (Lab-Tek, Chambered Coverglass, 1 chamber 25 x 56 mm, Nunc Inc. US), covered with coverslips (squared, 18 mm sides) and observed by fluorescence microscopy (this procedure was followed for all the microscope observations).

In order to isolate clones stably expressing the fusions of interest, cells were plated on BY-2 medium containing 0.8% agar supplemented with 100 mg/l kanamycin, 2 days after transfection. After one month, single colonies were transferred into liquid medium and subcultured each week by inoculating 4 ml of the old culture into 100 ml of fresh BY-2 medium supplemented with 10 mg/l kanamycin.

2.7.2 BY-2 aphidicolin synchronization

Stable cell lines expressing ECFP-EYFP and ECFP-EYFP-H2B were synchronized with the DNA polymerase inhibitor aphidicolin according to Combettes et al. (Combettes et al., 1999) with minor variations. Briefly, 20 ml of 7 day-old BY-2 cultures were diluted in 100 ml fresh BY-2 medium supplemented with 5mg/l aphidicolin. After 24 hours incubation in normal growth conditions (see *2.7.1*) the cells were washed 4 times with fresh BY-2 medium. The last two washes were performed by incubating the cells for 10 min with gentle shaking, following addition of the fresh medium, to ensure that all the inhibitor had been removed. The cells were then resuspended in fresh BY-2 medium and incubated in normal growth conditions. An aliquot of cells was then tested every 45 min in the microscope to monitor cell stage before initiating FRET assays.

2.8 FLUORESCENCE RESONANCE ENERGY TRANSFER (FRET)

2.8.1 Methods

2.8.1.1 Three-channel FRET

The method of FRET measurement discussed here (see Figs. 5A,B and 6A,B for detailed procedures) uses three filter sets or "channels" which are termed donor, acceptor and FRET filter sets (channels). These filter sets were designed to select and maximize, respectively, the donor fluorescence, the directly excited acceptor fluorescence and the acceptor fluorescence due to FRET. The acceptor, donor and FRET fluorescence channels were set at the following wavelengths (see *2.9.1* for filters used): acceptor excitation 500 nm, emission 535 nm; donor excitation 440 (or 430) nm, emission 480 (or 470) nm; FRET excitation 440 (or 430) nm, emission 535 nm.

In the present thesis all the fluorescently-labelled proteins contained ECFP or EYFP. These two fluorophores were, respectively, the donor and the acceptor in FRET experiments.

To isolate the different components (see *1.3.4*) of fluorescence F, acquired in the FRET channel, of a sample co-expressing the donor and acceptor fusions, the following α_m and δ_m "cross-talk" coefficients (see *1.3.4* and *3.1.2*), were calculated in cells expressing, respectively, only the EYFP or the ECFP fusion:

$$\alpha = (\Sigma_{ROIpixels}\, \alpha_{(x,y)})/N_{ROIpixels}$$

$$\delta = (\Sigma_{ROIpixels}\, \delta_{(x,y)})/N_{ROIpixels}$$

$$\alpha_m = (\Sigma_i^N \alpha_i)/N$$

$$\delta_m = (\Sigma_i^N \delta_i)/N$$

where

$$\alpha_{(x,y)} = \mathrm{netF}_{(x,y)}/\mathrm{netA}_{(x,y)}$$

$$\delta_{(x,y)} = \mathrm{netF}_{(x,y)}/\mathrm{netD}_{(x,y)}$$

and

$$netA_{(x,y)} = A_{(x,y)} - A_{bg} - A_{au}$$

$$netF_{(x,y)} = F_{(x,y)} - F_{bg} - F_{au}$$

$$netD_{(x,y)} = D_{(x,y)} - D_{bg} - D_{au}$$

in which $A_{(x,y)}$, $F_{(x,y)}$, $D_{(x,y)}$ are the fluorescence of the pixel at coordinate x,y of the selected ROI, A_{bg}, F_{bg}, D_{bg} are the average background fluorescence, and A_{au}, F_{au}, D_{au} are the average autofluorescence (estimated in each experiment in around 20 different cells), through, respectively, the acceptor (A), FRET (F) and donor (D) channels. The quantities netA, netF and netD are therefore the background-corrected fluorescences (*net* quantities) measured through the three channels. The $\sum_{ROIpixels}$ symbol in the α and δ equations means that the sum is extended to all the pixels in the ROI selected in each cell; $N_{ROIpixels}$ is the total number of pixels in each ROI. The α_m and δ_m equations express the average value of α and δ. N is the number of cells analysed. All the fluorescence values were first normalized for the exposure time actually used and, consequently, each value is expressed as fluorescence per unit of time (1 msec).

The equation used to isolate the donor-sensitized acceptor fluorescence ($netF'_{(x,y)}$; see *1.3.3*) was according to Gordon et al. (Gordon et al., 1998):

$$netF'_{(x,y)} = netF_{(x,y)} - \alpha_m\, netA_{(x,y)} - \delta_m\, netD_{(x,y)}$$

The following quantities (Xia and Liu, 2001) were used to normalize the donor-sensitized acceptor fluorescence for the total acceptor and/or total donor concentration (fluorescence):

$$N_{FRET(x,y)} = netF'_{(x,y)}/[netA_{(x,y)}\, netD_{(x,y)}]^{1/2}$$

$$netF'_{A(x,y)} = netF'_{(x,y)}/netA_{(x,y)}$$

When dealing with FRET experiments, two models are considered (Lakowicz, 1983):

1. the interaction-sensitive model

2. the single-distance model.

In the interaction-sensitive model, donor and acceptor are attached to two distinct molecules. They are free to diffuse independently of each other and interact according to their specific K_{eq} for interaction, bringing the donor and the acceptor closer together. Moreover, in general donor and acceptor labelled species do not have the same concentration.

In the single-distance model, donor and acceptor are covalently bound and, consequently, the two molecules are assumed to be at a fixed distance (however, this may not be true if the structure is flexible). Moreover, the concentration of the donor is equal to the concentration of acceptor (and to the concentration of the complex itself).

N_{FRET}, in the interaction-sensitive model, is a function of FRET efficiency and percentage of the complex exhibiting FRET to total donors and acceptors (Xia and Liu, 2001), which can be expressed as P = 2 x [donor - acceptor] / ([acceptor] + [donor]). P depends on the donor- and acceptor-labelled species concentrations and on their affinity (i.e., the affinity of the molecules to which acceptor and donor are attached). This quantity has been used to quantify FRET in all the experiments except for those with the ECFP-EYFP-H2B histone fusion (see below).

$netF'_A$, in a single-distance model based experiment, is a function of FRET efficiency per unit of complex concentration (being expressed as acceptor fluorescence). This quantity has been used to quantify FRET in the experiments with the ECFP-EYFP-H2B histone fusion ("unimolecular approach"), which can be assumed to follow a single-distance model.

2.8.1.2 Donor photobleaching FRET

This technique reveals FRET by measurement of the time constant of the fluorescence decay due to photobleaching of a donor fluorophore, and is commonly referred to as

"donor photobleaching FRET" (dpFRET).

In dpFRET only the donor channel (see *2.8.1.2*) is used (except at the beginning, when also the acceptor channel is used to ascertain the presence of the acceptor in the co-transfected cells).

To determine the exponential decay constant τ^{bl}, the kinetics of photodestruction of the donor is followed, measuring the donor fluorescence D under continuous illumination for 2 minutes and collecting images approximately every 4 sec (see Figs. 7A,B and 8A,B for the detailed procedure). Data are extracted from the temporal series of images to construct the experimental curves depicting the fluorescence decay (see *2.8.2.4*), to which the function $D(t) = D(t_0)\, e^{-t/\tau bl}$ is fit (more precisely, instead of D, $netD_{(x,y)}$ is used; see *2.8.1.1*). The constant τ^{bl} is then extrapolated from the obtained functions.

In the presence of FRET, the decay process gets slower and τ^{bl} increases (Clegg, 1996). Consequently, the constant τ^{bl}, measured in a sample containing donor and acceptor, compared to that derived from a sample containing only the donor, allows a determination of whether FRET is occurring. Moreover, by applying the equation $E = 1 - \tau^{bl}_{D}/\tau^{bl}_{DA}$ (see *1.3.3*), it is possible to calculate the efficiency of FRET.

2.8.2 Image Acquisition and Analysis

2.8.2.1 Introduction

Image acquisition and analysis were performed using the system described below (see *2.9*). The four flow charts of Figs. 5A, B - 8A, B (I and II part each) describe schematically the whole procedure.

Prior to image acquisition, particular care was taken to minimize exposure of the sample to excitation light in order to avoid photodamage of the cells and to standardize

the length of time of light exposure for all cells in each experiment. This was achieved by:

1. Skilled use of the excitation shutter, to limit light exposure to the time required to acquire an image or to observe the sample.
2. Channel A visual observation, to allow examination of samples at longer light wavelengths, which are less damaging to the cells.
3. Use of automations to allow light exposure for a fixed time, so that all cells are treated equally in any single experiment and throughout different experiments.
4. Exploitation of the sensitivity of the digital camera, coupled with suitable automations, to monitor samples using a minimal excitation light intensity.

All experiments were repeated at least 3 times and the results presented are derived from all the repetitions.

2.8.2.2 Data extraction and analysis, general considerations

The analysis of images (see flow charts) was performed on a pixel by pixel basis. Signal intensity was extracted from each pixel of the analysed image in order to generate an initial output list of x, y coordinates with corresponding intensity data. The pixel intensity value with its spatial coordinates was denoted by I(x, y). The symbol I is substituted by A, D or F depending on the fluorescence channel used to acquire the image. For extension, also the calculated variables are represented by the I(x, y) notation using the proper symbols instead of I, keeping the same meaning, i.e., pixel of coordinates x and y has the (calculated) value I. The images were first treated with a 3x3 median filter ("*Median filter*" Openlab tool), which calculates the average value of nine pixels (3 x 3) of a square array of 3 x 3 pixels, assigning this value to the central pixel of the array. The resulting images were subsequently considered as being constituted by an ordered array of 3 pixel-side square macro-pixels (therefore, each

macro-pixel is formed by 9 pixels: one central pixel surrounded by eight pixels) from which only the central pixel values were extracted and used in the following analyses. This simplification was admitted because these values are indeed representative of the surrounding 8 pixels of the original image, being their average. The resulting calculated images, i.e., the images derived from the proper calculations applied (central-) pixel by pixel, were subsequently built with "macro-pixels" of 9 pixels (3x3), each containing the same value, which was equal to the values calculated from the central pixel values (see flow chart 6A). This approach allowed to reduce pixel noise (because an average value was considered) and to accelerate the analysis procedure (because for each image, values were extracted from a number of pixels equal to its original number divided by 9, therefore obtaining a reduction of the number of data that had to be elaborated by approximately 10 times), although the space resolution of the original image was sacrificed. All the analyses were done on macro-pixels, and the term "pixel" is always used to refer to them.

Data were extracted from ROIs (Regions Of Interest) within each image (selected by "*Make binary layer*" Openlab tool), and most often corresponded to the nuclear region of the cell. ROIs were also selected in cell-free regions to detect fluorescence background, and in regions (mostly nuclear) of non-transfected cells, to detect autofluorescence.

2.8.2.3 Three-channel FRET

Data were extracted from the images acquired in the three fluorescence channels by the procedure depicted in Figs. 6A and 6B and were used to calculate net-Data$_{(x, y)}$, N_{FRET} and netF'$_{A\,(x, y)}$ (defined in *2.8.1.1*). The "*Single-cell based excel-worksheet*" (see flow chart) was used to perform all the cell-based calculations and to perform statistical tests for data significance.

N_{FRET} and $netF'_A$ average values (generically "FRET value") of each cell containing the two tested fusions were used as inputs for the statistical *t-test* against corresponding data from cells containing negative control fusions. The t-test output is given by the *p-value*, expressing the probability that the two groups of cells have the same average value (*null-hypothesis*). The p-value threshold for inferring that the two sets of values derive from two different cell populations characterized by different mean values is 5% (or 0.05). Therefore a p-value of ≤5% from a t-test means it is likely that a difference between the average values derived from the two tested cell populations does exist. When the p-value is equal to 5% (or to 0.05) the difference is said to be "*significant*". When the p-value is lower or equal to 1% (or to 0.01), the difference is said to be "*highly significant*" to indicate the higher probability that the null-hypothesis has to be rejected.

The "*Cell pool based excel work-sheet*" (see flow chart) performs the same calculations as the single cell work-sheet but on the entire set of pixels derived from sets of cells. This was used to build histograms of FRET values vs pixel frequency (or, more precisely, because a defined range of values was used instead of single values, the mid range value vs frequency of pixels falling in the range of values), thereby providing a global view of all the data. These histograms were used for a comparison of pixel data extracted from the whole sets of cells under examination and from the whole set of negative control cells, which reveal whether there is a global shift of tested cell FRET quantities toward higher values, and which visualizes unique peaks of distribution of N_{FRET} and $netF'_A$ in the tested cell population.

Maps of fluorescence and FRET values in pseudocolor- or grey-scale were made using the Surfer software (see *2.9.2*), employing as source data-sheet the s*ingle-cell based excel-worksheet* (see flowchart). These were used to visualize regions of

determined N_{FRET} and $netF'_A$ values and for making overlays with the channel A and D fluorescence images.

2.8.2.4 Donor photobleaching FRET

The $netD_{(x, y)}$ values derived from data extracted from the photobleaching FRET series of images by the procedure depicted in Figs. 8A and 8B have been used to calculate the $\tau^{bl}_{(x, y)}$ values (see *2.8.1.2*) using the *"Donor photobleaching" excel work-sheet* on a single cell basis (see Figs. 8A and 8B). Average τ^{bl} values from sets of cells transfected with two gene fusions of interest were used as inputs for statistical t-tests against values from cells transfected with negative control constructs. Moreover, histograms of $\tau^{bl}_{(x, y)}$ values vs pixel frequency were made on a single cell basis with the aim of identifying distribution peaks of interest and to show τ^{bl} shifts toward higher values for cells expressing interacting fusion proteins.

Finally, netD(t) values deriving from the temporal series of images were used to build representative I/Io (relative fluorescence) vs time photobleaching-decay curves.

FIG. 5A

THREE –CHANNEL FRET ACQUISITION FLOW CHART (I)

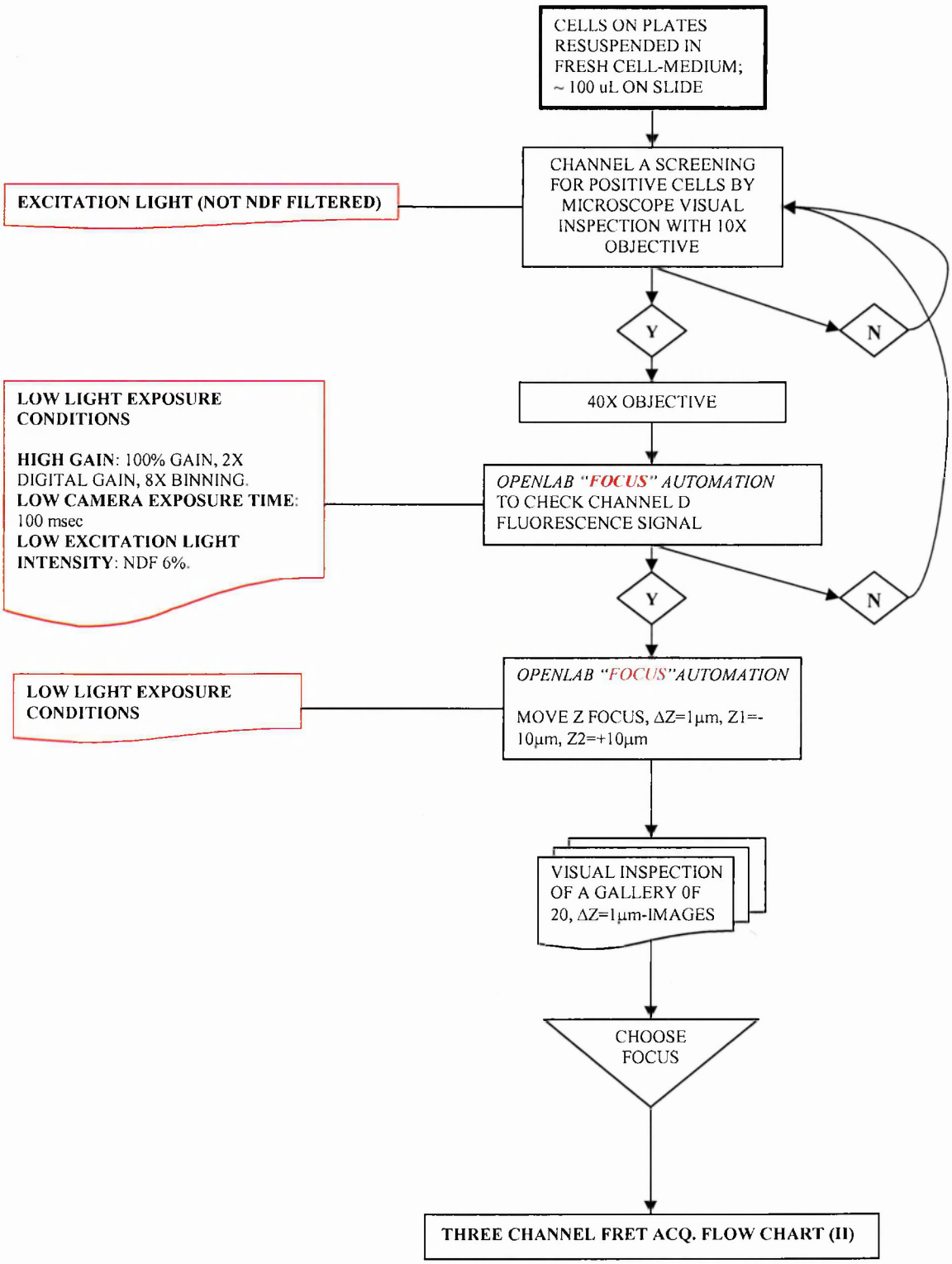

NDF: Neutral Density Filter
Y: Yes
N: No

FIG. 5B

THREE–CHANNEL FRET ACQUISITION FLOW CHART (II)

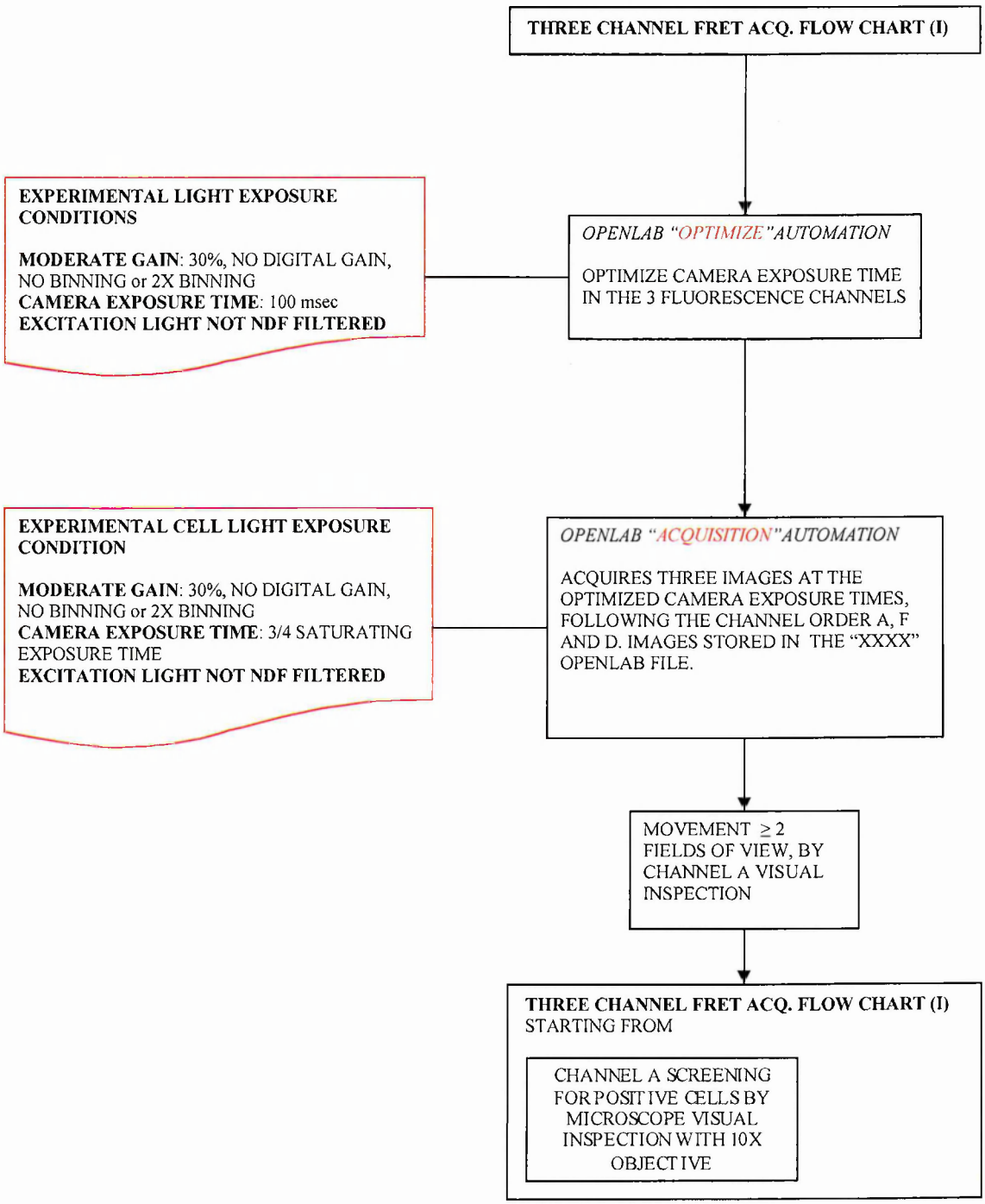

FIG. 6A

THREE–CHANNEL FRET ANALYSIS FLOW CHART (I)

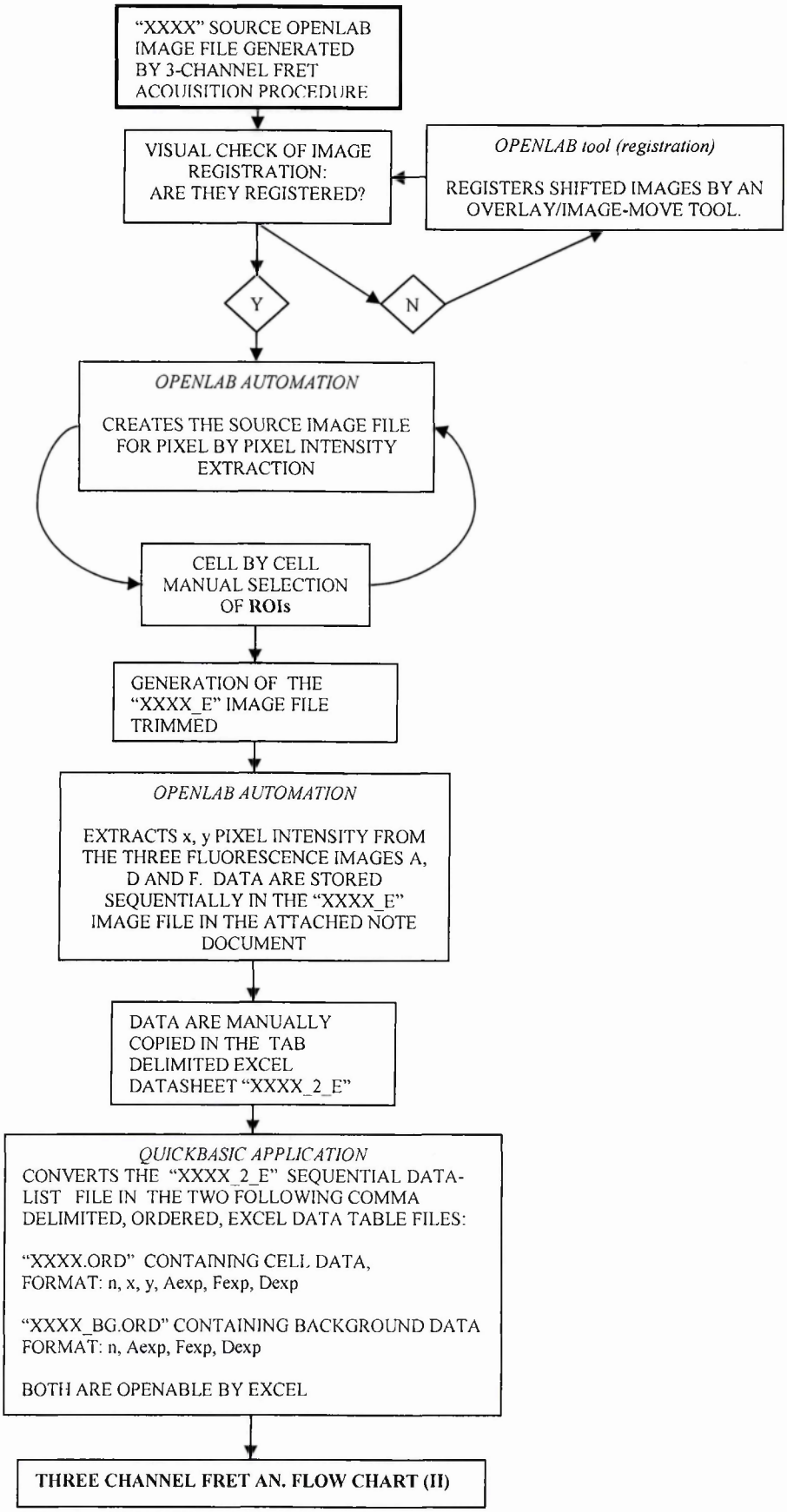

FIG. 6B

THREE–CHANNEL FRET ANALYSIS FLOW CHART (II)

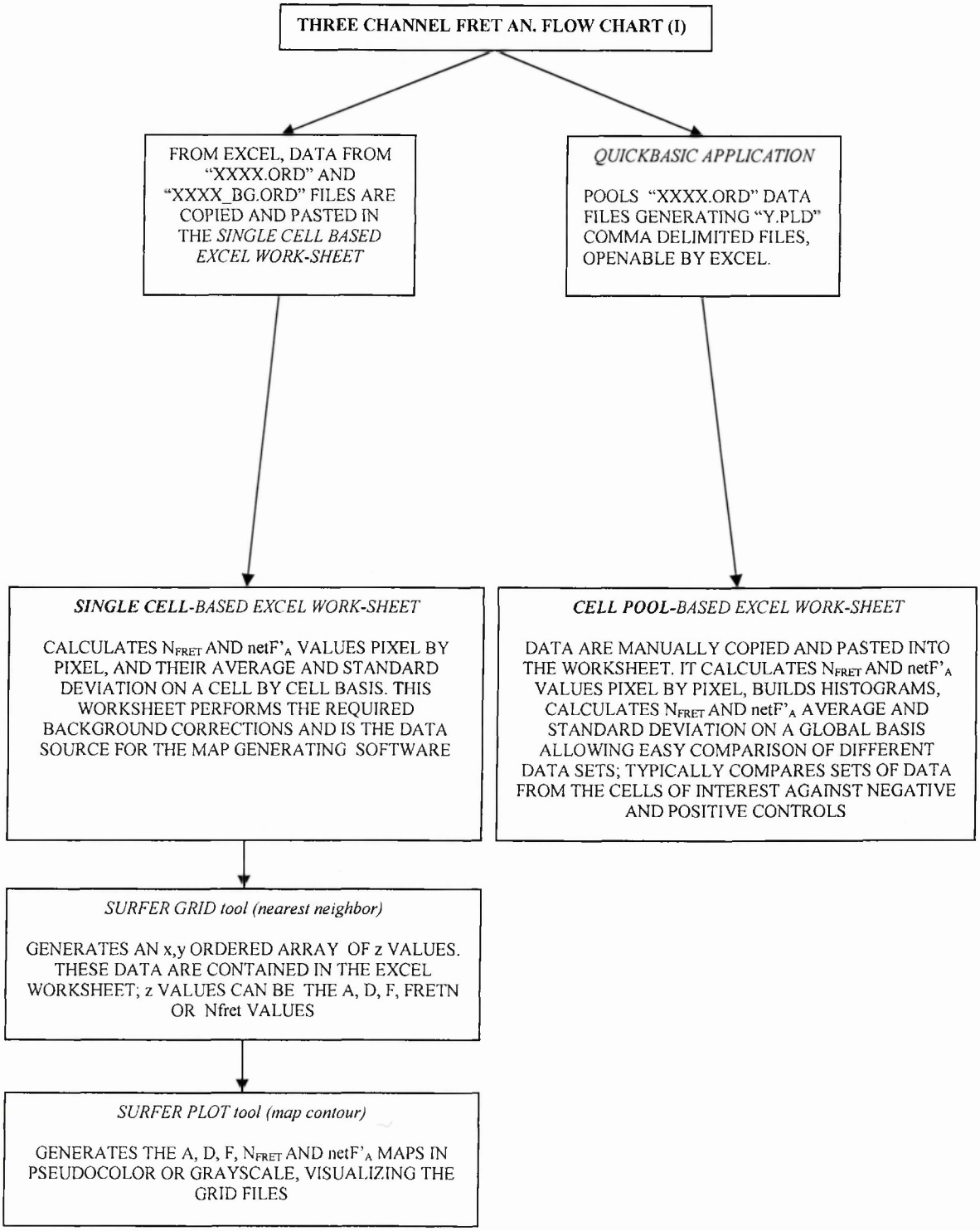

FIG. 7A

DONOR PHOTOBLEACHING FRET ACQUISITION FLOW CHART (I)

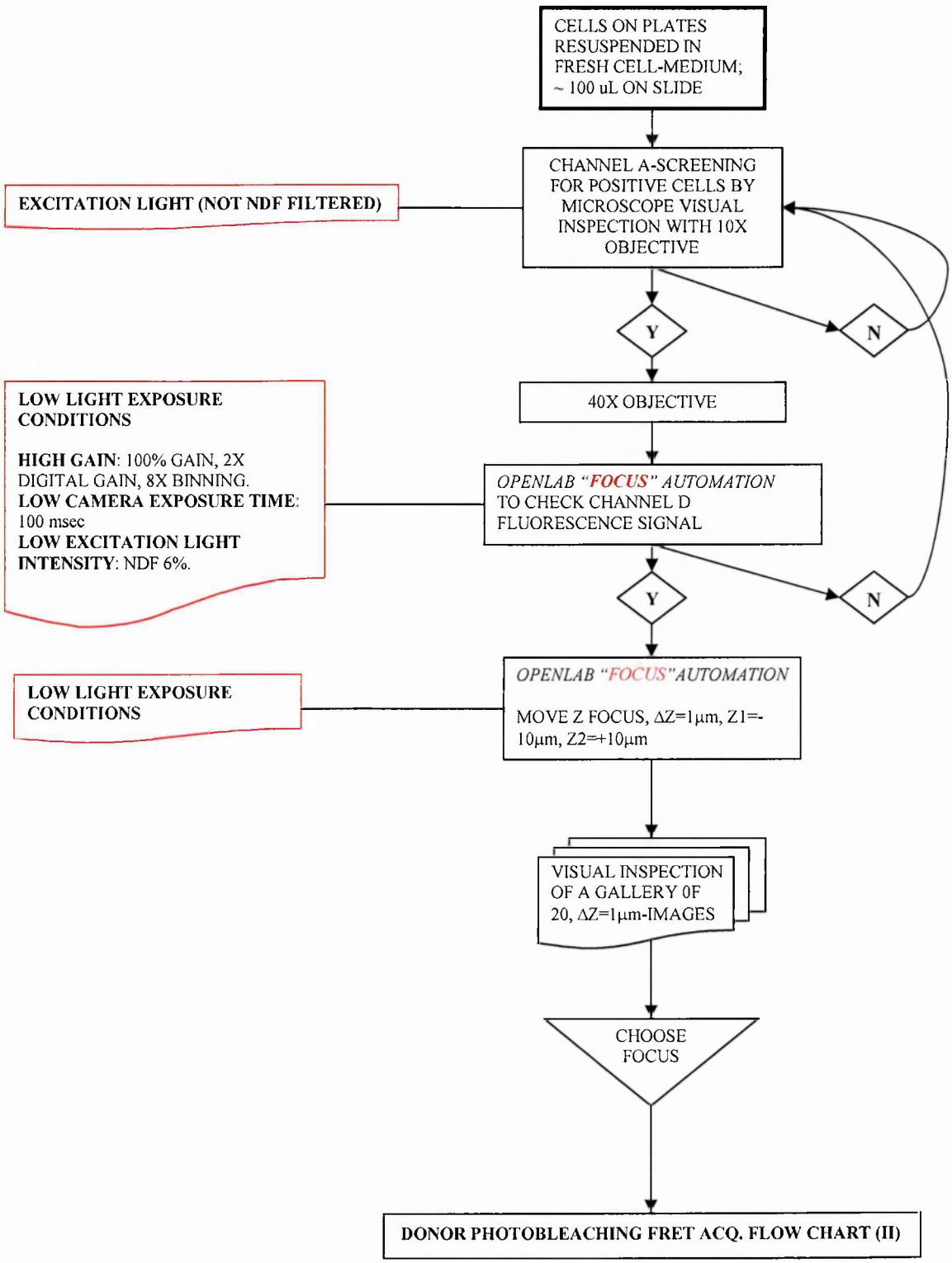

FIG. 7B

DONOR PHOTOBLEACHING FRET ACQUISITION FLOW CHART (II)

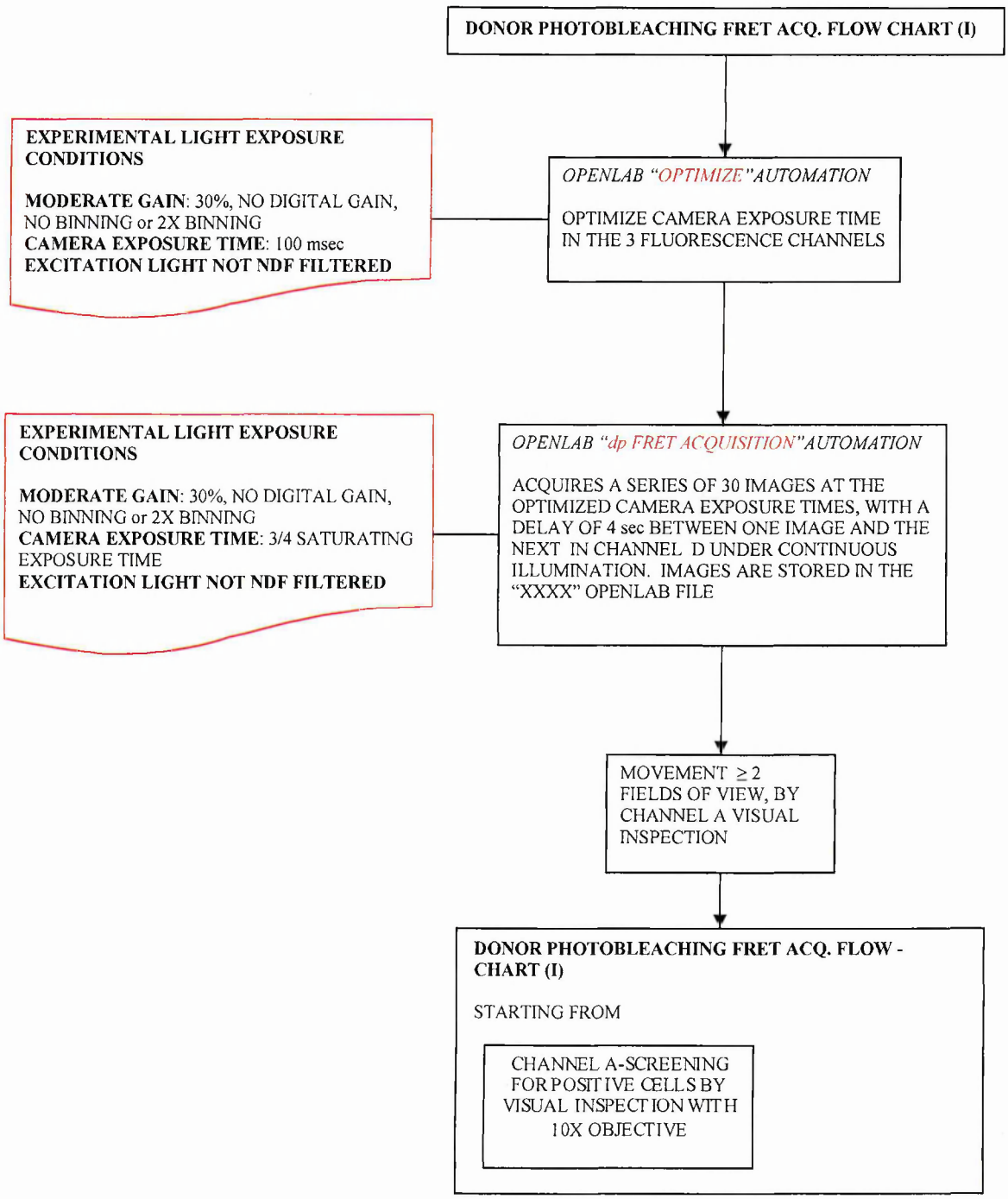

FIG. 8A

DONOR PHOTOBLEACHING FRET ANALYSIS FLOW CHART (I)

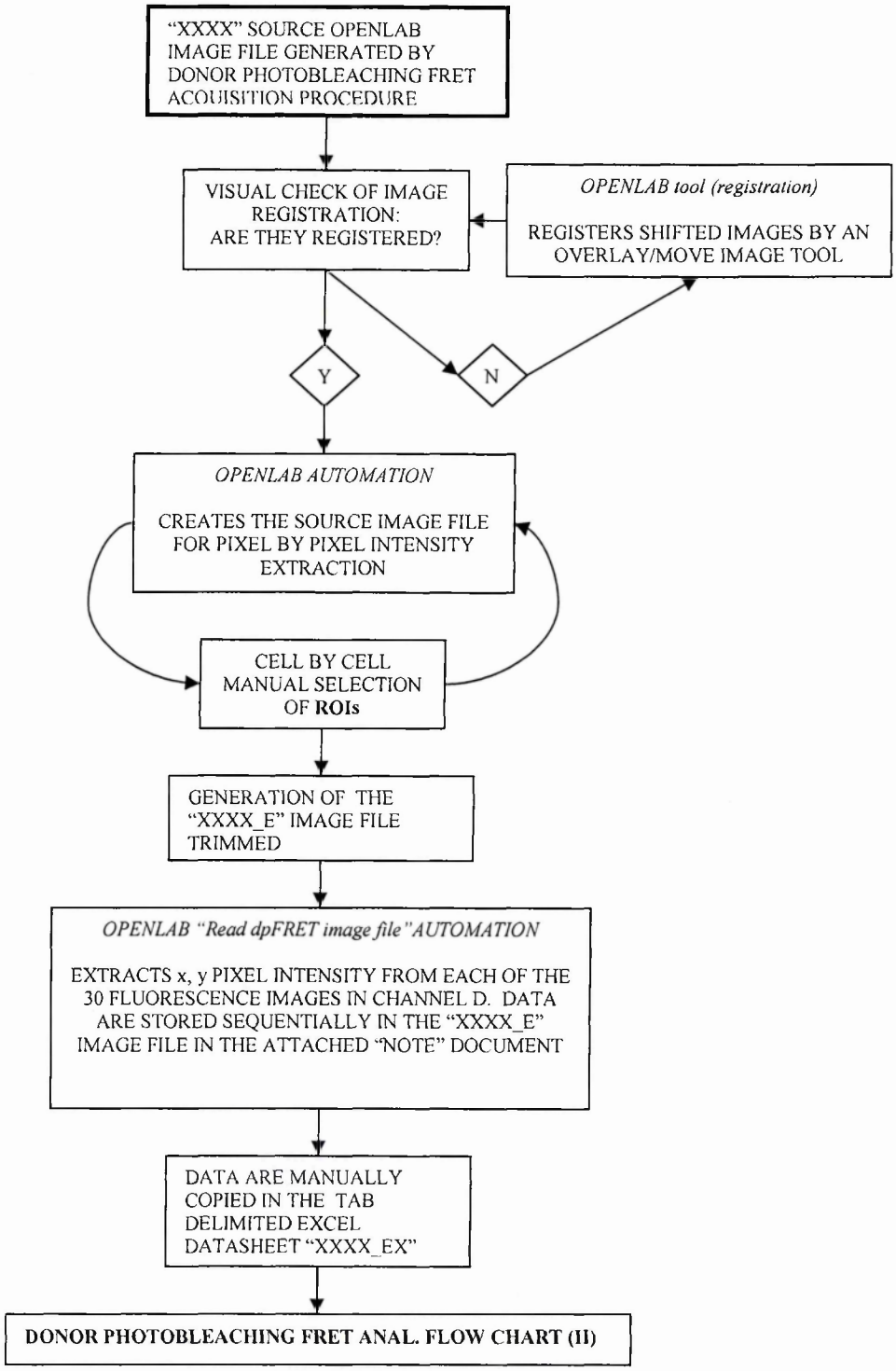

FIG. 8B

DONOR PHOTOBLEACHING FRET ANALYSIS FLOW CHART (II)

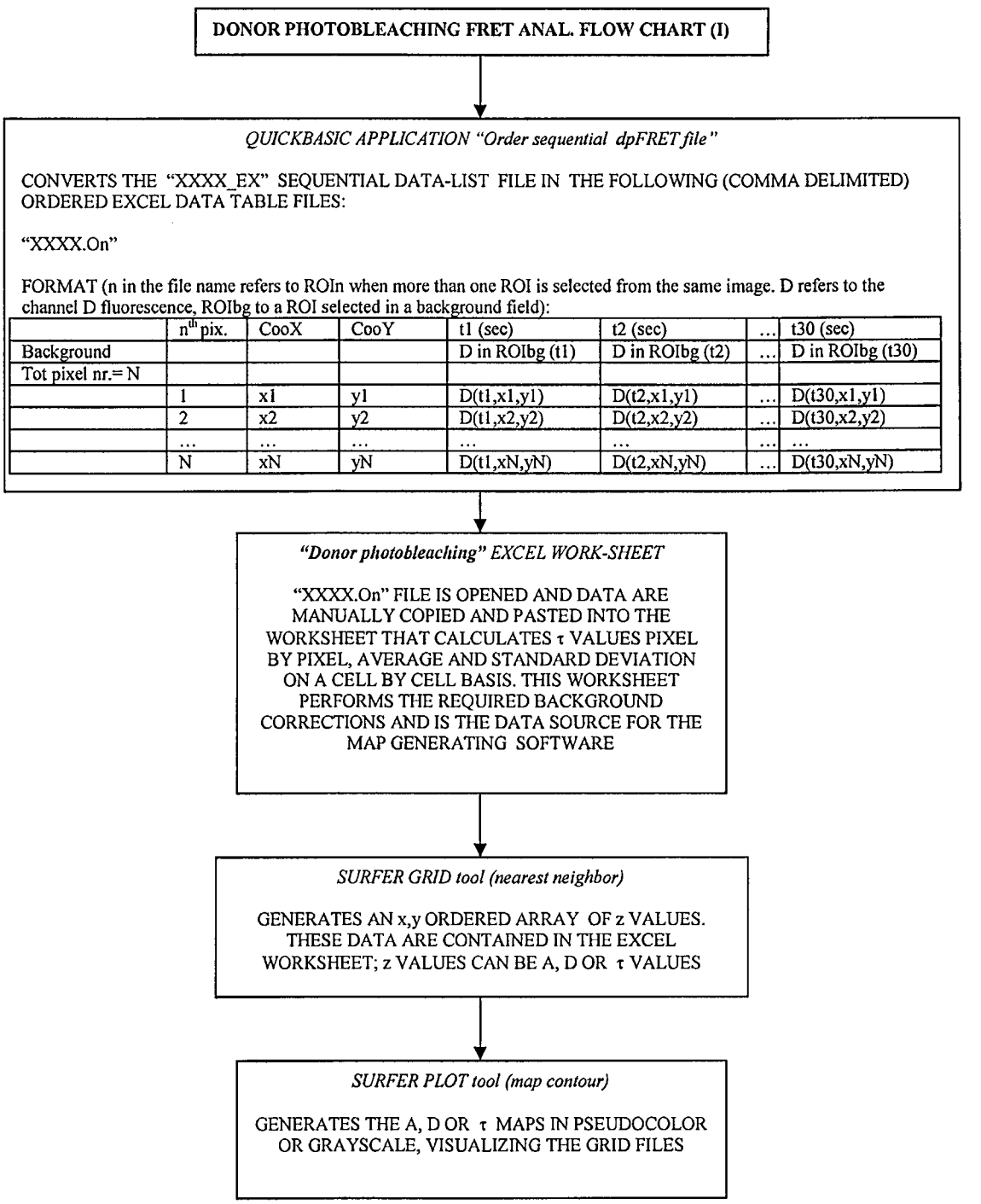

2.9 SYSTEM

2.9.1 Hardware

The core of the microscopy system was an epi-fluorescence inverted microscope Zeiss Axiovert 135 VT equipped with a 100 W Osram mercury lamp (HBO 100W/2) stabilized by an FR power supply Antel s.n.c. (Teramo, Italy), implemented with:

1. "ORCA-100" C4742-95 cooled CCD camera (Hamamatsu, Hamamatsu city, Japan)
    a. Cooling method: Peltier cooling with air
    b. Bit depth: 12 bit
    c. Cell (pixel) size: 6.7 μm x 6.7 μm (square format)
    d. Effective number of pixels: 1280 (H) x 1024 (V).
2. Excitation filter wheel LEP (Ludl Electronic Products Ltd., Hawthorne, USA)
3. Emission filter wheel LEP
4. Excitation shutter LEP
5. Transmission shutter LEP
6. Automated z-focus LEP.

The following optical filter sets were used:

- Selective for ECFP, donor channel:

    From filter set "86002v2 JP4 – CFP and YFP", Chroma Technology Corp. (Brattleboro, USA; www.chroma.com):

    a. Excitation filter S430/25
    b. Dichroic mirror "86002bs v2 beamsplitter" (dual band)
    c. Emission filter S470/30

Filter set "XF114", Omega Optical Inc. (Brattleboro, USA; www.omegafilters.com):

d. Excitation filter 440AF21
e. Dichroic mirror 455DRLP
f. Emission filter 480AF30

- Selective for EYFP, acceptor channel

From filter set "86002v2 JP4 – CFP and YFP" (Chroma, see above):

a. Excitation filter S500/20
b. Dichroic mirror "86002bs v2 beamsplitter" (dual band)
c. Emission filter S535/30

Filter set "XF104", Omega Optical Inc.

d. Excitation filter 500AF25
e. Dichroic mirror 525DRLP
f. Emission filter 545AF35 (or 535AF26)

- Selective for donor-sensitized acceptor emission, FRET channel

From filter set "86002v2 JP4 – CFP and YFP" (Chroma, see above):

a. Excitation filter S430/25
b. Dichroic mirror "86002bs v2 beamsplitter" (dual band)
c. Emission filter S535/30.

From filter set "XF104" and "XF114" (Omega, see above):

d. Excitation filter 440AF21
e. Dichroic mirror 455DRLP

f. Emission filter 535AF26.

The three filter sets formed by the a, b and c filters selective for ECFP (donor channel), for EYFP (acceptor channel) and for donor-sensitized acceptor emission (FRET channel), were used later ("filter upgrade") to increase the efficiency of detection of FRET.

The images were acquired using a non-immersion Zeiss PH2 Achroplan 40X objective with numerical aperture equal to 0.65.

2.9.2 Software

The Openlab 3 (Improvision, UK) software controlled all automated parts of the digital microscopy system, i.e., filter wheels, CCD camera, shutters and z-focus. This software was used to optimize the acquisition conditions, to acquire the images and to control the required flow of hardware operations, to visualize and organize the initial images, to perform some image elaborations, such as background correction, application of the median filter, image overlay and registration of images, and to extract the numerical data from the images for the subsequent analysis (see *2.8.2*).

The Microsoft Excel software was used to elaborate all the numerical data. It was used to calculate, from the raw data, the values N_{FRET}, $netF'_A$ and τ^{bl} used for quantifying FRET pixel by pixel, and to produce all the graphs and the statistical t-tests (see *2.8.2.3* and *2.8.2.4*).

The Surfer 7.0 (Golden Software Inc., USA) software was used to create all the FRET maps using the data elaborated by the Excel software as input, applying the "nearest-neighbour gridding" algorithm and then using the "Contour map" tool for visualizing the maps in pseudocolor- or grey-scale.

SwissPdbViewer 3.5 (Swiss Institute of Bioinformatics, Basel, Switzerland; www.expasy.org/spdbv/; Guex and Peitsch, 1997) was used to calculate distances

between C-termini of histones H2A and H2B. RasMol 2.6 (University of Massachusetts, Amherst MA, USA) was used to represent nucleosome structures (Fig. 21), using the PDB ID 1AOI (Luger et al., 1997) crystallographic data of the nucleosome from the RCSB PDB (Protein Data Bank; www.pdb.org; Berman et al., 2000).

RESULTS

3.1 FRET CALIBRATION EXPERIMENTS

3.1.1 Fluorescence of GFP variants

The two green fluorescent protein (GFP) variants ECFP and EYFP were used to label all the studied proteins. These variants comprise a well studied FRET pair in which the ECFP molecule is the donor and the EYFP molecule is the acceptor (Tsien and Prasher, 1998; Heim, 1999). The Förster distance (see *1.3.2*) Ro for this pair is equal to 5.3 nm, calculated assuming that donors and acceptors can randomize by rotational diffusion prior to energy transfer (Heim, 1999). The value 2 x Ro defines the upper limit for the distance R between ECFP and EYFP, for which they can generate a reliably measurable energy transfer (Lakowicz, 1999c).

All the GFP fusions used were generated in plant expression vectors and transfected into cultured BY-2 cells by helium-accelerated particle bombardment. The transfected BY-2 cells were then used either for transient expression experiments after 18 hours or were subcultured on selective medium after 48 hours in order to isolate stable cell lines.

EYFP and ECFP were transfected first into BY-2 cells to characterize their fluorescence characteristics within the experimental system used. Eighteen hours after transfection, the two fluorescent proteins displayed very good fluorescence levels only slightly below those of mGFP4, which is a variant very commonly used in plant studies (data not shown). Moreover, fluorescence was found localized in both the cytosol and the nucleus of the cells, as previously reported (see, for example, Fig. 18D; Haseloff et al., 1997, von Arnim et al., 1998).

3.1.2 Filter cross-talk

In section *1.3.4* I discussed that when two fluorophores coexist in a sample, especially if they form a FRET pair, the fluorescences measured at some wavelengths are often compounded by the fluorescence deriving from both fluorophores. Corrections are consequently necessary to isolate the fluorescence deriving from each of the fluorophores or which is due to FRET (i.e., the donor-sensitized acceptor emission). The term "cross-talk" or also "filter cross-talk" (maybe inappropriate) is sometimes referred to this because optical filters sometimes do not allow the selective visualization of the fluorescence of a single fluorophore.

In the case of ECFP and EYFP, Fig. 9 shows that the overlap between their excitation end emission spectra generates cross-talk in some regions. For example, it would be clearly impossible to measure selectively the emission of EYFP (acceptor) due to FRET under ECFP (donor) excitation wavelengths without also measuring the ECFP fluorescence, because every EYFP emission wavelength is contained within the ECFP emission spectrum, thus excluding the possibility to find an emission wavelength selective for EYFP (or of identifying an appropriately selective optical filter).

The fluorescence channels (or filter sets) used were tested for cross-talk by measuring the fluorescence of ECFP- transfected cells, in the donor and acceptor channels, and by calculating the ratio between the two values. The same was done for acceptor fluorescence in EYFP-transfected cells. The ratios obtained, representing the donor/acceptor filter cross-talk, showed that no more than 0.5% of each fluorophore fluorescence detected by each selective fluorescence channel could bleed through the fluorescence channel selective for the other fluorophore of the FRET pair (data not shown). These values were very likely overestimated because the fluorescence of ECFP or EYFP that is expected to be detected by the non-specific filters is very low and consequently it is relatively highly affected by cellular autofluorescence, which cannot

be completely corrected. However, even disregarding this aspect, donor/acceptor filter cross-talk was so small that it was considered, in practice, negligible.

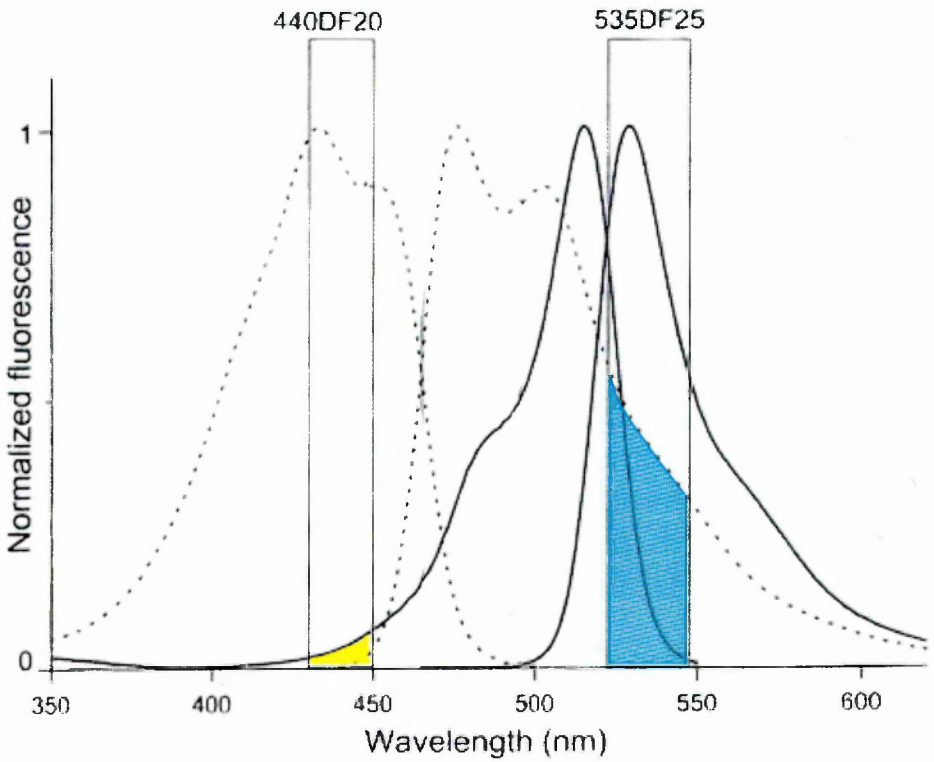

Fig. 9. Normalized excitation and emission spectra of ECFP and EYFP. Excitation and emission spectra of ECFP (dotted line) and EYFP (continuous line) are indicated. Boxes indicate wavelength bands selected by the donor excitation filter (440AF21) and the acceptor emission filter (535AF26) which have been used in the present thesis as FRET channel. Note that in the filter-selected regions, EYFP and ECFP spectra are overlapped (highlighted by the yellow and blue coloured areas). This prevents the selective detection of the donor-sensitized acceptor emission due to FRET (see text; Adapted from Miyawaki and Tsien, 2000).

The same procedure was repeated for the FRET channel filters by measuring the fluorescence of ECFP in the donor and FRET channels, and by measuring the fluorescence of EYFP in the acceptor and FRET channels. The ratios between the fluorescence in the FRET channel and that in the donor channel or in the acceptor channel were then calculated. These ratios, representing the two cross-talk coefficients α and δ (see *2.8.1.1*), were equal to 0.22 and 0.33 (data not shown) and were re-calculated in each experiment of this thesis, in 5 different cells. A final observation was that these two coefficients were remarkably robust because their values always remained constant, when the same filter sets were used. Subsequently, during the course of this thesis some of the filters used for the different fluorescence channels were upgraded (see *2.9.1* in Materials and Methods) and the new δ value became 0.60.

3.1.3 Photo-stability of EYFP and ECFP

Every fluorophore has a defined stability to light irradiation. The term "photobleaching" is used to indicate the irreversible process of photodestruction to which a fluorophore is subjected when it is irradiated with its excitation wavelengths. GFP variants display a different stability with respect to photobleaching. EYFP, in particular, is expected to be more stable than ECFP (Clontech information). This results in an underestimation of the fluorescence measurements, which is even more significant when longer exposure times are used to acquire images and for molecules that are less stable, e.g., for ECFP as compared to EYFP. Because this phenomenon could in principle limit the reproducibility of measurements, the stability of EYFP and ECFP was tested in BY-2 cells.

EYFP and ECFP were transfected in BY-2 cells and after eighteen hours in dim light fluorescent cells were assayed. The assay consisted of continuously irradiating

cells with the excitation wavelengths selective for the transfected GFP variant or with those selective for the other variant, and acquiring images at intervals of approximately 4 seconds for 2 minutes. In some assays, it was necessary to periodically and briefly interrupt the bleaching irradiation to allow acquisition of the images with the selective filters, but this was assumed to have a negligible effect on the determinations. These series of images were then used by a data extraction/analysis protocol similar to that discussed in Materials and Methods for the donor photobleaching method (see *2.8.2* and *2.8.4*), to plot the kinetic decay of ECFP and EYFP fluorescence under the excitation wavelengths used in the subsequent experiments of this thesis (Fig. 10). ECFP under selective excitation wavelengths showed a fluorescence decay that was 2-fold faster than EYFP while ECFP fluorescence decay under EYFP excitation wavelengths was negligible (data not shown). Conversely, a different and unexpected result was obtained for EYFP in ECFP excitation wavelengths. In fact, in these conditions EYFP fluorescence showed the fastest decay and, moreover, following 2 min of ECFP irradiation, EYFP fluorescence recovered almost completely after approximately 2 min in darkness. This result was probably linked to the known reversible instability of EYFP, which is termed photochromism (Dickson et al., 1997).

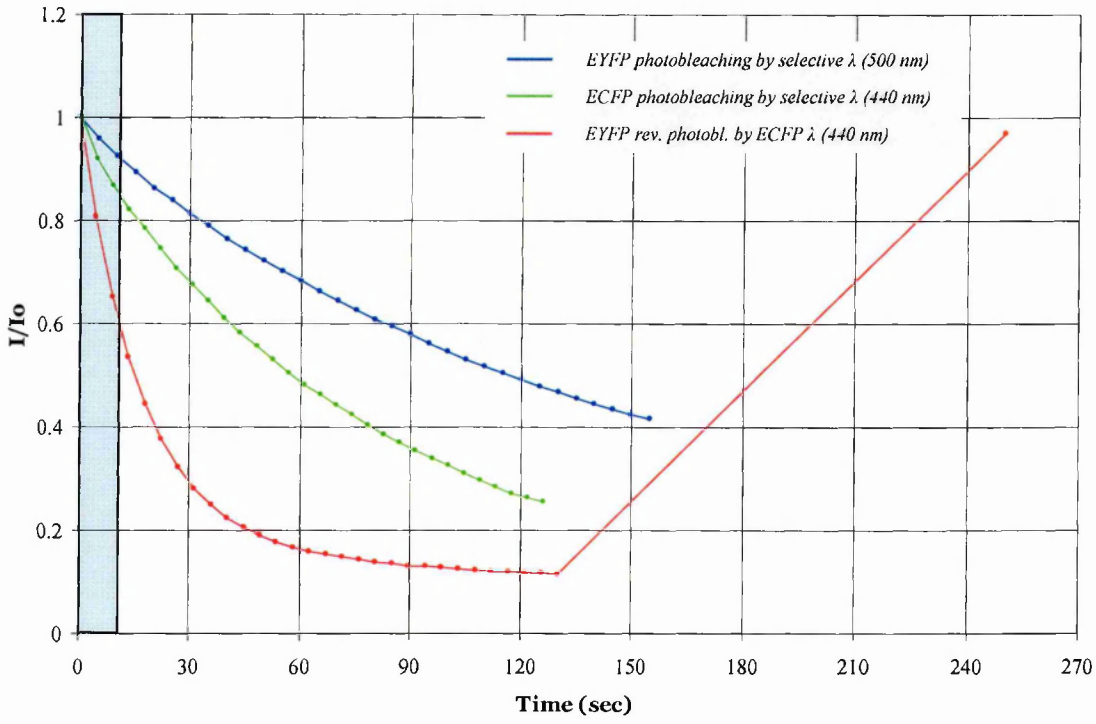

Fig. 10. ECFP and EYFP photo-stability. ECFP is less photo-stable than EYFP under selective excitation wavelengths. However, EYFP is the least stable under ECFP excitation wavelengths. The kinetics of photodestruction of ECFP and EYFP, irradiated with light of their selective excitation wavelengths, are shown. Moreover, for EYFP the kinetics of reversible photobleaching due to irradiation with light of ECFP excitation wavelengths, is shown. On the y axis is reported the intensity of fluorescence normalized by the intensity at time zero. A grey box indicates the temporal window in which all the subsequent FRET assays were performed.

In order to minimize the impact of photochemical instability of EYFP and ECFP on the precision of our fluorescence measurements, the three channel FRET method applied in the present thesis was designed to reduce inter and intra-experimental variability of time exposure of the samples to light irradiation and to minimize sample exposure to ECFP excitation wavelengths, which caused the biggest problems (see *2.8.2.1*). In addition, the global effect of EYFP and ECFP instability on FRET quantification was experimentally tested by examining the effect of a prolonged light irradiation on N_{FRET} measurements in 20 cells transfected with an ECFP-EYFP construct (see *2.6.1*). This construct contained the two GFP variants fused to each other and was thus expected to be a very efficient positive control for FRET. A total of 10 cells were first assayed using camera exposure times no higher than 1 sec, which was possible because of the high expression levels of the ECFP-EYFP fusion. Subsequently, another set of 10 cells was assayed analogously but by reducing the emission fluorescence reaching the CCD camera by 10-fold using a neutral density filter with transmittance equal to 10%. This allowed increasing CCD camera exposure time 10-fold, i.e., up to 10 seconds, without saturating the detector. Comparison of N_{FRET} values obtained with and without the neutral density filter, i.e., with camera exposure times equal to 10 sec and lower than 1 sec, respectively, revealed a decrease in N_{FRET} for the higher exposure time of around 10%. Analogous calculations were performed for $netF'_A$ for which the same underestimation of approximately 10% was found. This was therefore assumed to be the maximal fraction by which the N_{FRET} and $netF'_A$ measurements made in the present thesis could be underestimated as a consequence of EYFP photochromism and ECFP photobleaching.

3.1.4 Donor photobleaching FRET (dpFRET)

In an attempt to increase the accuracy of FRET measurements (albeit sacrificing real-time applications), the donor photobleaching FRET technique was used on cells transfected with ECFP-EYFP. With this technique, the photobleaching decay constant, τ_b, for the process of bleaching of a fluorescent molecule by irradiation at its specific excitation wavelength, is measured. When the fluorescent molecule acts as donor for another molecule which is the acceptor of a FRET process, the process of bleaching becomes slower and the τ_b constant increases.

The efficiency of FRET can also be calculated by the equation $E = 1 - \tau_b^D/\tau_b^{AD}$, where the superscripts D and AD refer, respectively, to the sample containing only the donor and the donor plus the acceptor (see FRET). The main advantages of the donor photobleaching FRET method with respect to the three channel FRET approach are that the photobleaching decay constant depends only on the nature of the donor/acceptor complex, being independent of the donor, acceptor and donor/acceptor complex concentrations, and that the extensive measurements of fluorescence required in the three channel method are not necessary. In principle, both aspects make the constant τ_b much more accurate as a measure of FRET efficiency than that obtainable by the three channel FRET method.

BY-2 cells stably expressing ECFP-EYFP were assayed by donor photobleaching FRET following the procedure described in detail in Materials and Methods. Analysis of donor (ECFP) fluorescence decay curves (time vs donor fluorescence) revealed an unexpectedly "aberrant" behaviour in which an initial rapid increase of donor fluorescence was observed during the initial 20 seconds prior to the expected fluorescence decrease (Fig. 11A). This behaviour could be explained by the previous observation that EYFP fluorescence can be reversibly bleached by ECFP irradiation (see *3.1.3*). If this was the case, the EYFP acceptor of the donor energy

would have been removed by the irradiation wavelength used to bleach the ECFP in the experiment, producing a kind of fluorescence donor unmask, that could explain the initial fast increase of donor fluorescence. Subsequently, once this effect was worn (or reduced), the decrease in donor fluorescence due to ECFP bleaching could prevail.

Nevertheless, the exponential fitting procedure was applied to the experimental curves derived from 10 cells expressing ECFP-EYFP, but without including the "aberrant" points from the initial 20 seconds and the mean τ_b was calculated to be approximately 80 sec (Fig. 11B). The experiment was done in parallel on cells expressing only ECFP. These cells, for which FRET cannot occur, were expected to give the reference value of τ_b. Indeed, the time vs donor fluorescence experimental curves did not show the aberrant trend (Fig. 11A). By the fitting procedure, the calculated mean τ_b value over 10 cells was approximately 80 sec (Fig. 11B), i.e., the same that was found for ECFP-EYFP (t-test p-value >>5%), for which a high efficiency of FRET was expected (as confirmed by the three-channel FRET assay, data not shown). These results suggested that the donor photobleaching method, as implemented in the system used, was not reliable for detecting FRET and so was not used further.

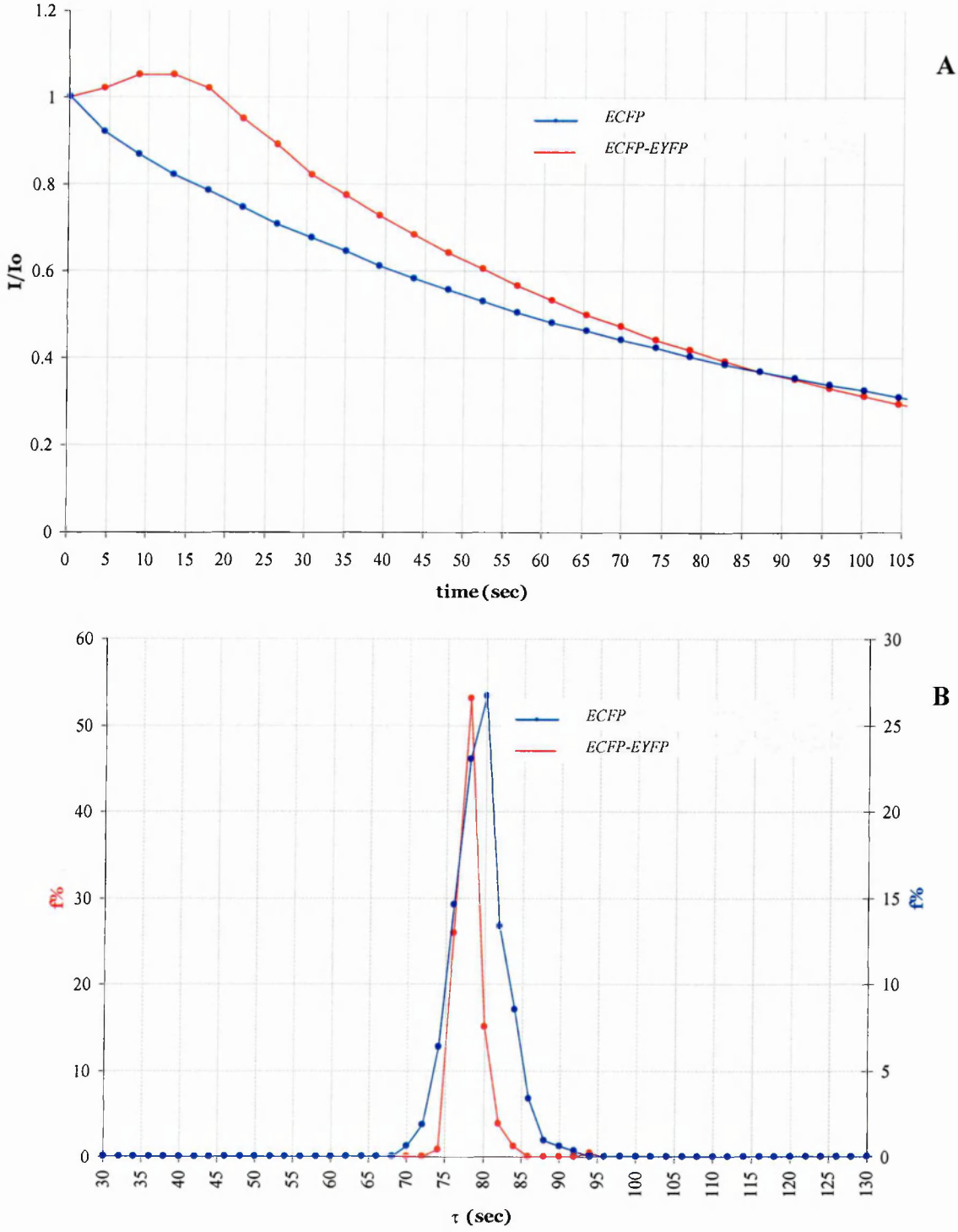

Fig. 11. Donor photobleaching FRET was not able to distinguish an ECFP (donor-only) negative control from an ECFP-EYFP strong unimolecular positive control. BY-2 cells were transfected with ECFP or ECFP-EYFP and assayed by donor photobleaching FRET (dpFRET) eighteen hours after transfection. Reported data derives from two representative cells. A) kinetics of the decay of donor fluorescence under irradiation with ECFP excitation wavelengths. Cells containing ECFP-EYFP display an "aberrant" trend in the first 20 sec of the curve, which consists of an increase of donor fluorescence followed by a decrease. On the contrary ECFP containing control cells show the expected trend. B) Pixel frequency distribution of τ values for the same cells reported in A, in ROIs corresponding to the nucleus of cells: both negative and positive control cells display single overlapping peaks. These results suggested that dpFRET cannot be used with our wide-field microscopy system.

3.1.5 Acceptor photobleaching FRET

A method to detect and quantify FRET by acceptor photobleaching was also tested on cells expressing the ECFP-EYFP fusion. By selective photobleaching of EYFP (acceptor) it should be possible to measure donor fluorescence in the presence, before photobleaching, and in the absence, after photobleaching, of the acceptor. These two values were used to calculate directly the efficiency of FRET (see *1.3.2* and *1.3.3*) as 0.30. This value is related (by the Forster equation) with an estimated distance between ECFP and EYFP in the ECFP-EYFP fusion of around 6 nm, employing the Forster distance Ro equal to 5.3 nm (see *3.1.1*). This distance is a reasonable estimate considering that the diameter of GFP is around 3 nm. Consequently, the method of acceptor photobleaching, consisting of acquiring an image of the donor before and after the selective bleaching of the acceptor, could be an alternative (albeit without real-time applications) to the methods used and described in this thesis. However, some limitations arose from the fact that the sample had to be irradiated for 15 minutes in order to bleach completely the acceptor using the arc lamp implemented in our system. Within this time, the sample was very likely subjected to heating caused by the prolonged light irradiation, which produced movement of the cells over the x, y and even the z axis. Thus, at the end of the experiment, the images acquired before and after irradiation often did not overlap. Due to the complexity of these movements, registration of the images was not possible and, consequently, only the mean fluorescence value over ROI reliably corresponding in the two images could be used for FRET efficiency calculations. This decreased dramatically the resolution obtainable by the acceptor photobleaching method (in practice, the smallest ROI whose FRET was determined was the entire nucleus of the examined cells).

In conclusion, the acceptor photobleaching method implemented in our widefield microscopy system to detect FRET did not provide sufficient subcellular imaging resolution. For other applications, the method could nonetheless be used to detect the efficiency of FRET with remarkable accuracy because only two fluorescence measurements in one fluorescence channel (donor channel) are required.

3.2 STUDY OF THE INTERACTION BETWEEN TDET1 AND HISTONE H2B

3.2.1 DET1 binds histones

To investigate whether DET1 may repress photoregulated gene expression by a mechanism involving chromatin remodelling, it was first examined whether it could bind to histones, the core units of the nucleosome. Binding assays were performed with a histone-agarose resin, which contains all the histone proteins covalently bound to agarose beads. In vitro translated ^{35}S-labelled tomato and Arabidopsis DET1 proteins were incubated with the resin and after several washes the bound fraction was separated by SDS-PAGE. Both proteins were found to be retained on the resin (Fig. 12A).

To further characterize the interaction an FPLC analysis of tomato DET1 binding to histone-agarose was performed. Fig. 12B shows the elution profile of tomato DET1 with increasing concentrations of NaCl. The majority of the DET1 protein was eluted from the resin at a concentration of close to 400 mM NaCl, suggesting a fairly strong affinity between DET1 and histones.

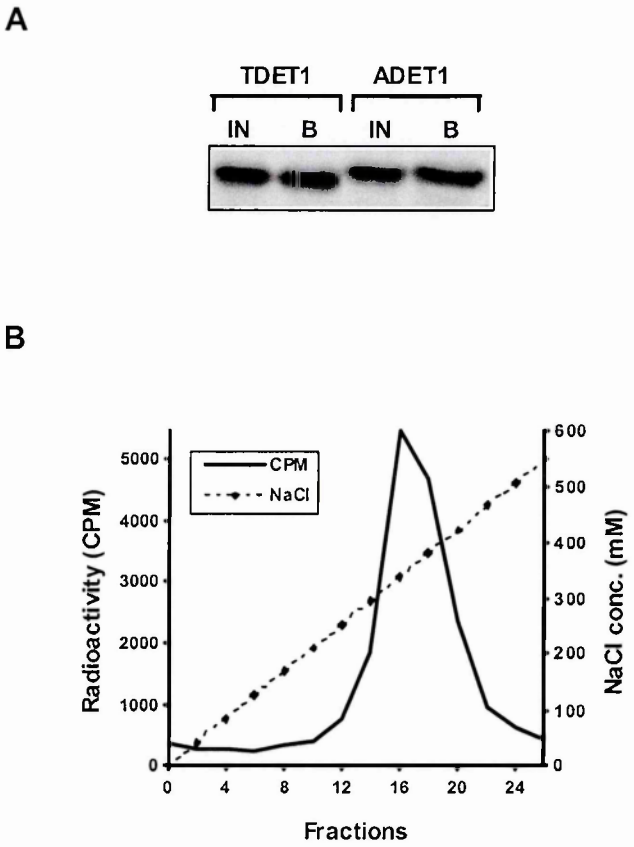

Fig. 12. DET1 Binds Histones

(A) Binding assay of in vitro-translated DET1 proteins to histone-agarose. Equal amounts of ^{35}S-labelled tomato DET1 (TDET1) and Arabidopsis DET1 (ADET1) were incubated with 10 µl of histone-agarose in 50 µl PBS overnight at 4°C. After several washes the bound fractions (B) were resolved on 10% SDS-PAGE and visualized by fluorography. One third of each in vitro-translated product (IN) was loaded as a control of the relative binding.

(B) Chromatogram of in vitro-translated tomato DET1 following elution from histone-agarose using a linear 0 to 550 mM NaCl gradient in PBS with a flow rate of 0.5 ml/min. The 25 fractions collected were analyzed for radioactivity content (CPM) and the obtained results were plotted with the relative salt concentration values.

3.2.2 DET1 binds to the amino-terminal tail of histone H2B

The histone-agarose resin used in the previous experiments contains equimolar concentrations of all five histones. To determine whether DET1 binds to a specific histone, competition assays were performed by incubating a 20-fold excess of each purified histone with DET1 prior to binding on histone-agarose. Fig. 13A shows that only histone H2B was able to compete the binding of DET1 to histone-agarose. Because H2A and H2B are present in the nucleosome core as dimers it was tested whether the dimer was a better competitor than the monomer. However, no difference was detected in competition capability with respect to H2B alone (Fig 13A).

To define the domains of H2B that DET1 is able to interact with, binding to GST-fusion constructs containing different regions of human H2B (Lorain et al., 1998) was tested. Human H2B was used at this stage because its domains have been much better defined than have plant H2B proteins. Equal concentrations of purified recombinant proteins were immobilized on glutathione-sepharose and used in in vitro binding assays. As shown in Fig. 13B DET1 binds only to the N-terminal 32 amino acids of H2B. This corresponds exactly to the N-terminal tail of human H2B, which extrudes from the core nucleosome structure (see Fig. 1; Luger et al., 1997) and is the site for post-translational modifications that control chromatin remodelling (see later). To confirm the significance of this binding it was verified that both tomato and Arabidopsis DET1 could bind to the amino-terminal tail of plant H2B (data not shown).

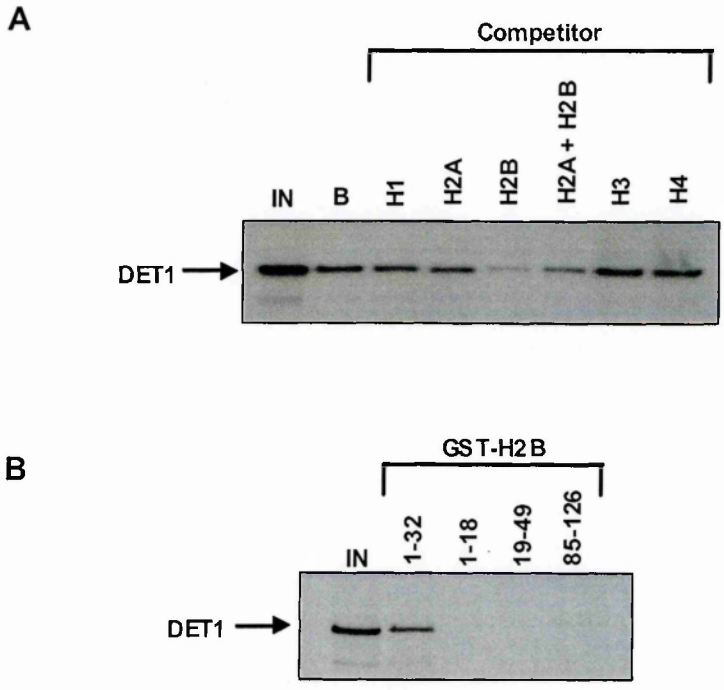

FIG 13. DET1 Binds the Amino-Terminal Tail of H2B

(A) 200 μg of each purified histone protein (20-fold excess) were incubated with in vitro-translated tomato DET1 for 30 min before performing the binding assay to histone-agarose. The different histones used as competitors of binding are indicated on top of each lane. In the lane indicated as H2A+H2B, 100 μg of each histone were used. As control one third of the total input (IN) and the bound fraction without competitors (B) were also included.

(B) GST pull-down assays were performed using different GST-H2B deletion constructs as matrices for binding. 3 μl of in vitro-translated tomato DET1 were incubated with 2 μg of each of the different GST-H2B fusion proteins immobilized on glutathione-Sepharose 4B. The bound material was then loaded on 10% SDS-PAGE and visualized by fluorography.

3.2.3 DET1 binds the H2B N-terminal tail in a nucleosome context

Although the results described demonstrate a specific interaction of DET1 with the N-terminal tail of H2B, they do not define at what level this interaction is occurring. To test the hypothesis that DET1 interacts with histone H2B that is integrated in the chromatin, binding of DET1 to isolated nucleosomes was examined.

Mononucleosomes were purified from chicken blood erythrocytes and bound to CNBr-activated sepharose and used for binding assays with in vitro-translated tomato DET1. After several washes the resin was resuspended in Laemmli buffer and bound fractions were separated on 10% SDS-PAGE. Fig. 14A shows that tomato DET1 was selectively retained on this resin, as was Arabidopsis DET1 (data not shown). An FPLC analysis to determine the affinity of nucleosome binding was then performed. As with the histone-agarose resin, DET1 was found to be eluted from mononucleosomes at a concentration of approximately 400 mM NaCl (Fig. 14B).

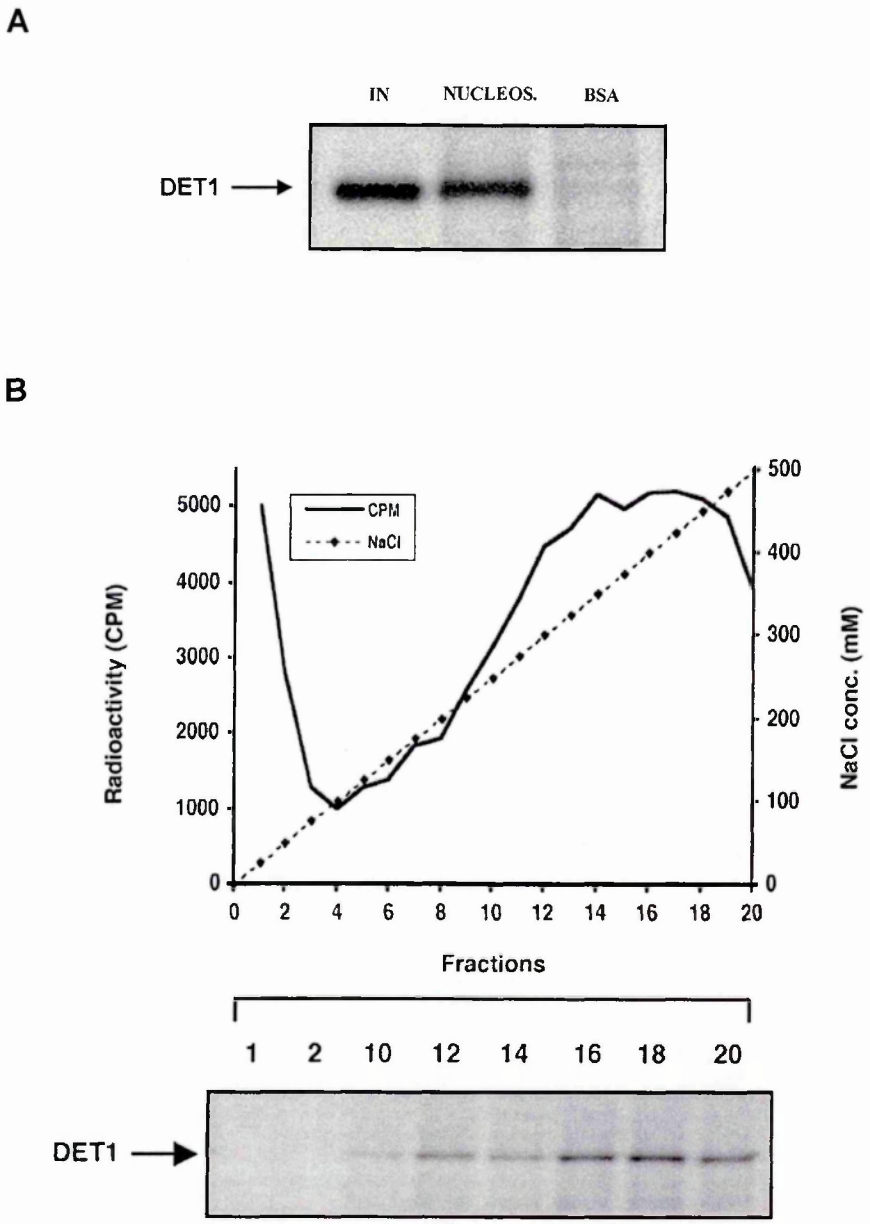

FIG. 14. DET1 Binds Histones in a Nucleosome Context. (A) Autoradiogram of binding assays of in vitro-translated tomato DET1 to nucleosome-sepharose or BSA-sepharose. In vitro-translated DET1 (3 µl) was incubated with 10 µl of nucleosome- or BSA-resin in a final volume of 50 µl PBS + 1mg/ml BSA overnight at 4° C with gentle agitation. The resins were resuspended in 15 µl 2x Laemmli buffer after washing 3 times with PBS. Bound proteins were resolved on 10% SDS-PAGE and gels were then treated as previously described. Input (IN) is equivalent to 1/3 of the amount used in the binding reaction. (B) Chromatogram and autoradiogram of ^{35}S-labelled in vitro-translated tomato DET1 following elution from nucleosome-sepharose using a 10 ml linear 0 to 500 mM NaCl gradient in PBS. A nucleosome-sepharose column (5mm i.d. x 10 mm) was connected to a FPLC unit and run at a flow rate of 0.5 ml/min. Fractions (0.5 ml) were collected and 100 µl was used for liquid scintillation counting while the remaining fraction was TCA/DOC precipitated, resuspended in 15 µl 1x Laemmli buffer and subjected to SDS-PAGE. Following electrophoresis, the gels were treated as previously described.

3.2.4 DET1 purified from plants can interact with histones

The results presented so far show clearly that DET1 binds histone H2B within the context of the nucleosome. However, all the experiments have been performed using in vitro-obtained products. To verify that DET1 in planta could behave in the same manner, binding assays using extracts prepared from transgenic tomato plants expressing epitope-tagged tomato DET1 (Myc-TDET1) were performed. Young leaves were used to purify nuclei from which a nuclear lysate was prepared. This lysate was then used as starting material for binding assays with nucleosome-sepharose, histone-agarose, and GST-coupled H2B N-terminal tails. After separation by 12% SDS-PAGE, the bound fractions were transferred to a PVDF membrane and subjected to western blot analysis using a mouse monoclonal antibody against the Myc epitope (Fig. 15). The results demonstrated clearly that plant-purified DET1 behaves in exactly the same way as the in vitro-translated protein, thus excluding an artefact due to the use of an in vitro translated DET1 protein in the previous experiments.

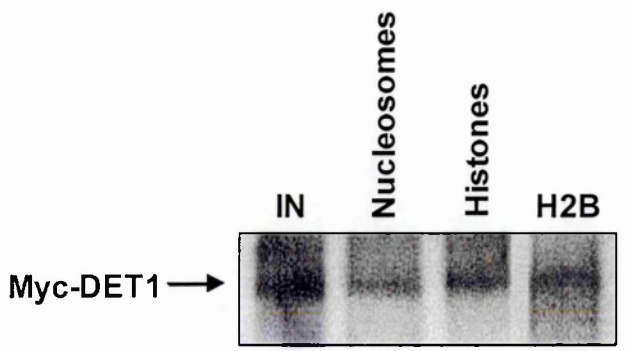

Fig. 15. DET1 Purified from Plants Interacts with Histones.
Autoradiogram of binding assays of nuclear protein extracts from myc-TDET1 overexpressing tomato plants to nucleosomes, histones, and the N-terminal tail of histone H2B. Approximately 100 µg of total nuclear protein extract were incubated with 10 µl of nucleosome-sepaharose, 20 µl of histone-agarose, or 20 µl of GST-H2B (amino acids 1-32)-sepharose, in a final volume of 50 µl NEB, overnight at 4° C with gentle agitation. After washing 3 times with NEB the resins were resuspended in 18 µl 2X Laemmli buffer. Bound proteins were resolved by 12% SDS-PAGE. The gel was then treated as previously described. Input (IN) is equivalent to one third of the amount used in the binding reaction.

3.2.5 DET1 binds preferentially to non-acetylated H2B tails

Emerging correlations between gene expression and post-translational modifications of the histone N-terminal tails has provided strong evidence that these modifications play an essential role in modulating the transcriptional activity within different chromatin domains (Strahl and Allis, 2000; Jenuwein and Allis, 2001). For example, acetylation of histone tails correlates with the activation of transcription. Because DET1 is a negative regulator of light-inducible gene expression it was of interest to test whether its binding to H2B tails could be influenced by acetylation. Resin-immobilized synthetic peptides corresponding to the first 32 amino acids of human H2B, in which the lysine residues had either been acetylated or not, were used (Fig. 16A). These experiments revealed that DET1 binds preferentially to the unmodified form of H2B (Fig. 16B). As a control, a Drosophila lamin construct (Goldberg et al., 1999), whose binding to H2B was not affected by acetylation, was used (Fig. 16C). Furthermore, it was confirmed that the plant-derived Myc-DET1 protein also displayed preferential binding to non-acetylated H2B tails (data not shown).

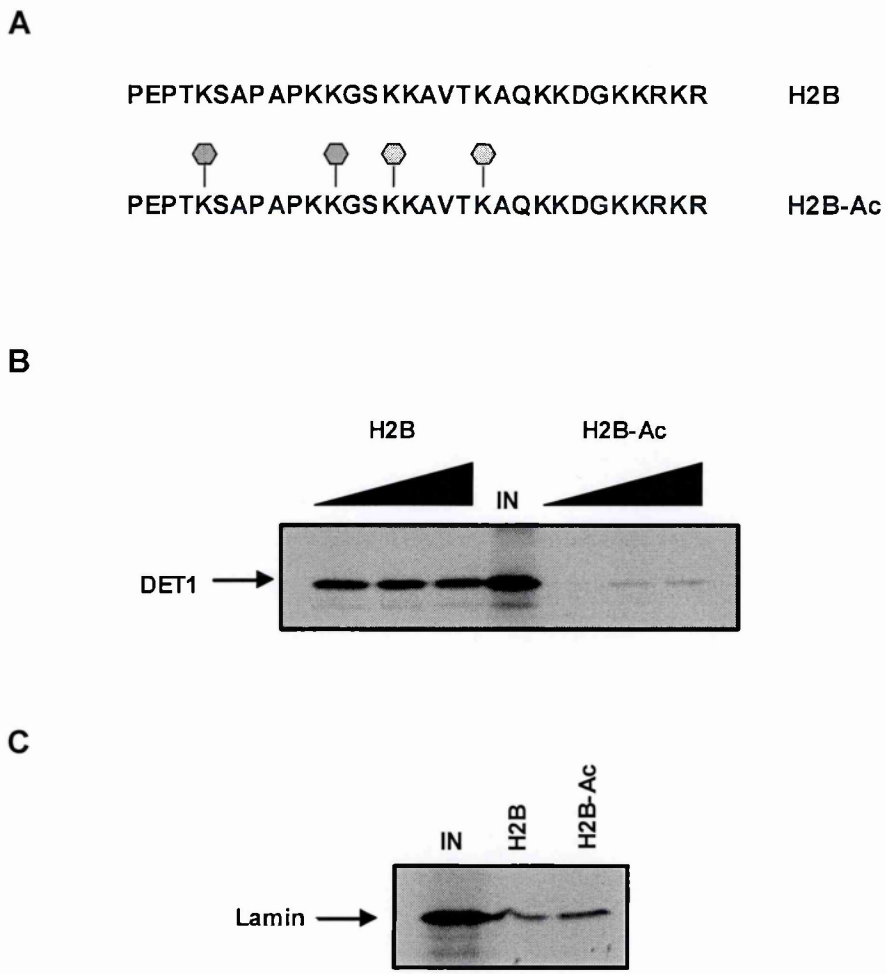

FIG. 16. DET1 Binds Preferentially to Unmodified H2B N-Terminal Tails
(A) Peptides corresponding to the first 32 amino acids of H2B were synthesized either in the unmodified form (H2B) or acetylated at the indicated lysines (H2B-Ac).

(B) Increasing amounts of H2B N-terminal peptides coupled to amino hexyl-agarose were used as matrices for binding assays with 3 µl of in vitro-translated tomato DET1. 1 µl of the in vitro reaction mix (IN) was loaded to indicate the relative binding.

(C) 3 µl of in vitro-translated Drosophila lamin was bound to the unmodified (H2B) and acetylated (H2B-Ac) peptides. After several washes the bound material was resolved on 10% SDS-PAGE and visualized by fluorography. IN corresponds to one third of the total in vitro-translated product used in the binding assays.

3.2.6 In vivo TDET1/H2B interaction. Transient assay

In order to study DET1-histone H2B interactions in living cells, the green fluorescent protein variant EYFP was fused to TDET1 either at its N-terminus or at its C-terminus to generate, respectively, EYFP-TDET1 and TDET1-EYFP (see *2.5.2*). Both constructs were transfected into BY-2 cells and observed after eighteen hours. EYFP-TDET1 was found localized predominantly in the nucleus (as reported previously with other DET1 fusion proteins; Pepper et al., 1994; see Fig. 18A and compare to 18B) whereas TDET1-EYFP was nuclear excluded and often formed bright fluorescent patches in the cytoplasm (data not shown), indicating most likely that it was inactive. Consequently, only the EYFP-TDET1 fusion was used in the subsequent experiments.

No differences in localization were found if transfected cells were incubated in complete darkness or in constant light conditions (as reported previously; Pepper et al., 1994), indicating that light/dark dependent nuclear-cytoplasmic shuttling is unlikely to be involved in regulating DET1 activity, in contrast to other negative regulators of photomorphogenesis such as COP1 (von Arnim and Deng, 1994).

To assess whether TDET1 could interact with histone H2B in live cells and to localize this interaction at the sub-nuclear level using FRET, BY-2 cells were co-transfected with EYFP-TDET1 and a C-terminal fusion of a tomato histone H2B with the GFP variant ECFP, denoted H2B-ECFP. As a negative control, H2B-ECFP and EYFP constructs were co-transfected.

Fluorescent cells were assayed eighteen hours after transfection by three-channel FRET following the procedures described in detail in Materials and Methods. N_{FRET} was calculated to quantify FRET in ROIs corresponding to the nuclear regions of the cells.

A comparison between the mean N_{FRET} value for the cells co-transfected with H2B-ECFP/EYFP-TDET1 and that of the negative control revealed a statistically

significant three-fold increase in the experimental cells over the negative control (Table 1), indicating the occurrence of a specific interaction between H2B and TDET1.

The further analysis of $N_{FRET\ (x,y)}$ pixel frequency histograms (Fig. 17) did not reveal any clear peaks. Nonetheless, a clear difference was found between data from test and control cells. In particular, only 5% of the pixels of the negative control had $N_{FRET\ (x,y)}$ values equal or higher than 0.11 and no pixel at all had $N_{FRET\ (x,y)}$ values equal or higher than 0.26. On the contrary, around 50% and 20% of the pixels derived from images of cells co-transfected with H2B-ECFP/EYFP-TDET1 had $N_{FRET\ (x,y)}$ values equal or higher than, respectively, 0.11 and 0.26. These values constituted therefore two cut-offs. Assuming that the more stringent value of 0.26 was the most reliable for identifying pixels in which a specific interaction between H2B-ECFP and EYFP-TDET1 was occurring, our results would indicate that H2B-ECFP and EYFP-TDET1 interacted in at least 20% of the nuclear interior in these transiently transfected cells. However, analysis of the $N_{FRET\ (x,y)}$ images did not reveal any clear sub-nuclear localization pattern in cells co-transfected with H2B-ECFP and EYFP-TDET1 (Fig. 18C).

Table 1 Statistical analysis of results shown in Fig. 17 and 18.		
	H2B-ECFP+EYFP-TDET1	***H2B-ECFP+EYFP***
Mean N_{FRET}	**0.153**	**0.042**
σ (standard dev.)	0.108	0.045
No. of Observed Cells	13	13
t-test P value	**< 1%**	

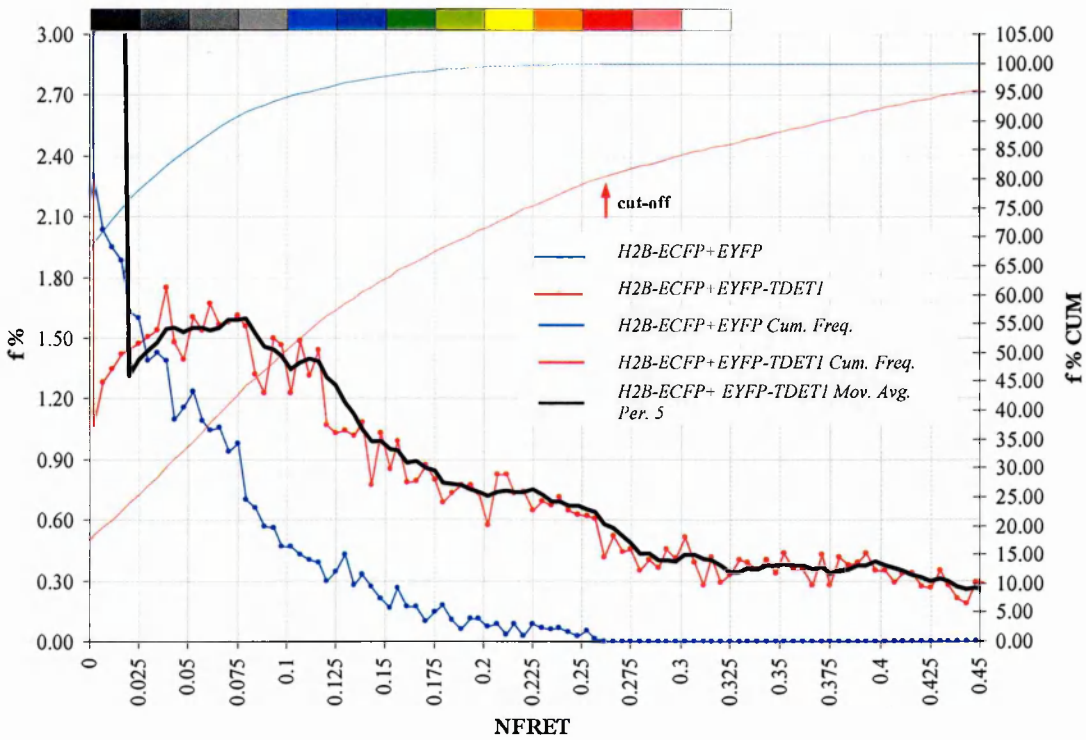

Fig. 17. Cells transiently expressing H2B-ECFP and EYFP-TDET1 show a frequency distribution of N_{FRET} values without any clear peak but which is characterized by a shift towards higher values with respect to the frequency distribution obtained from H2B-ECFP/EYFP expressing cells. Pixel frequency distributions of N_{FRET} values from all cells of a "transient" experiment from which the images in Fig. 18 were selected are shown. N_{FRET} values were calculated in the nuclei. Note that although no clear peak is present, cumulative frequency curves highlight clearly a shift towards a higher N_{FRET} value of DET1 containing cells, with respect to the control. Note that no pixel in control cells (H2B-ECFP/EYFP) has N_{FRET} values higher than 0.26, whereas 20% of pixels from H2B-ECFP/EYFP-TDET1 cells do so. This is highlighted with a cut-off arrow in the graph. Compare this result with that in Fig. 22 for cells stably expressing these fusions.

Remarks: f% indicates the percent fraction (frequency) of pixels having each N_{FRET} value. f% CUM indicates the percent fraction (frequency) of pixels having each N_{FRET} value or less. Mov. Avg. Per. 5 indicates a Moving Average (Period 5) trendline through the data points, calculated using 5 adjacent points.

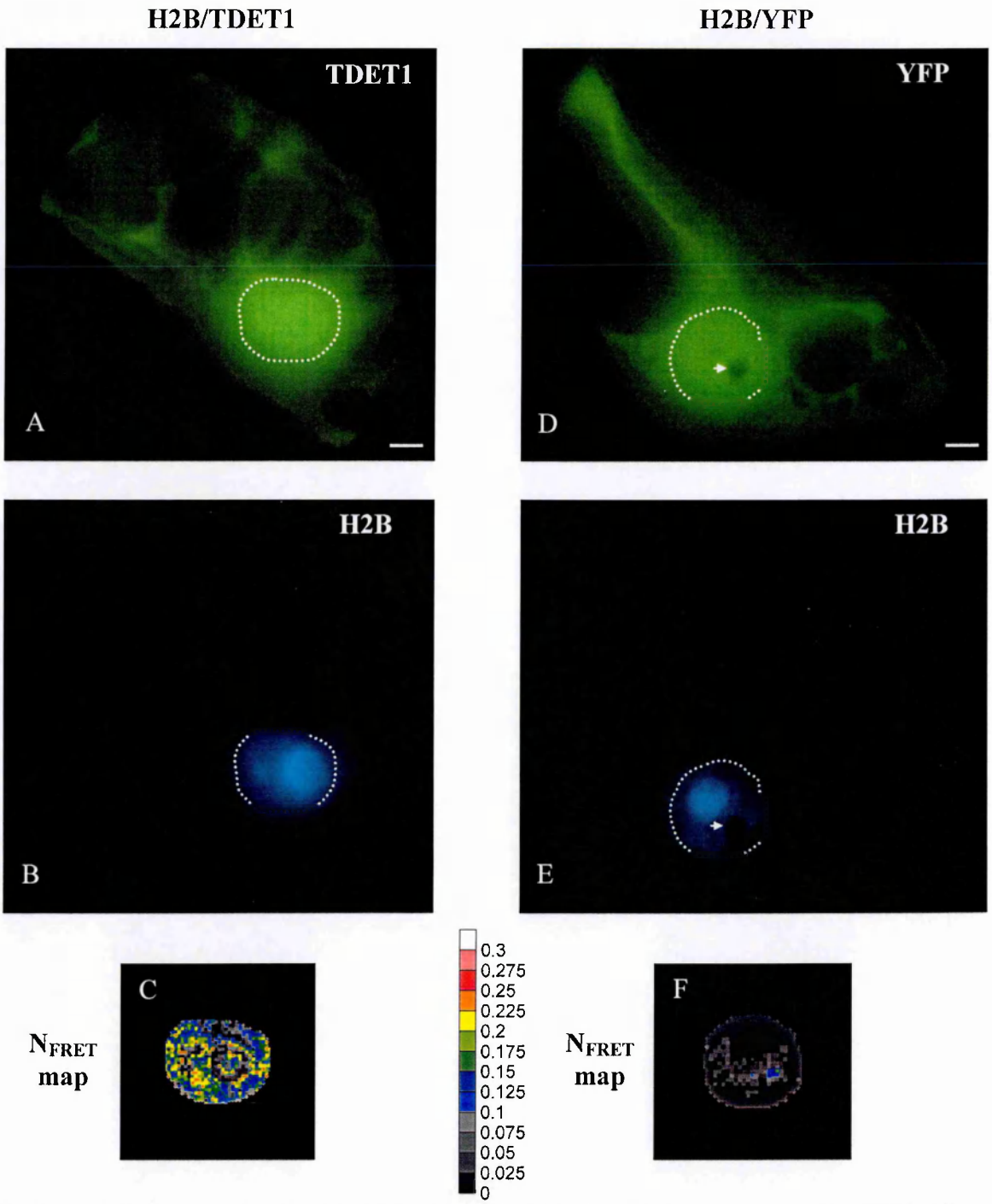

Fig. 18. TDET1 is nuclear localized and interacts with histone H2B in heterogeneous sites. BY-2 cells co-transfected with H2B-ECFP and EYFP-TDET1 or EYFP were imaged and assayed by three-channel FRET 18 hours after transfection. One representative cell for each transfection is reported. A-C) refers to a cell co-transfected with H2B-ECFP and EYFP-TDET1. A) TDET1 is both nuclear and cytoplasm localized. B) Histone H2B is exclusively nuclear localized. C) N_{FRET} map in pseudocolor scale of the nucleus which is highlighted by a white-dotted circle in A and B: TDET1 interacts with histone H2B but without any clear sub-nuclear localization. D-F) refers to a cell co-transfected with H2B-ECFP/EYFP (negative control). D) EYFP is nuclear and cytoplasm localized. E) Histone H2B is exclusively nuclear localized. F) N_{FRET} map in pseudocolor scale of the nucleus which is highlighted by a white-dotted circle in D and E: EYFP does not interact with histone H2B-ECFP. Note that in F there is a region of higher N_{FRET} values. However, this is not an interaction site but an artifact due to the presence of a "hole" (arrow) of very low fluorescence in images D and E, in which background is artifactually amplified. The normalization procedure applied to generate the N_{FRET} values was responsible for this kind of noise. Colour scale key: grey tones indicate low values characterizing the negative control. The scale bars are 5 μm.

3.2.7 In vivo TDET1/H2B interaction. Assays in stable cell lines.

In transient transfection experiments, epigenetic modifications such as acetylation or methylation of the N-terminal tails of the GFP-tagged histones are unlikely to be comparable to those of endogenous histones in non-transfected cells. BY-2 cell lines stably expressing the H2B-ECFP and EYFP-TDET1 fusions, together with negative controls expressing H2B-ECFP and EYFP, were therefore generated, in order to study the H2B/DET1 interaction under more physiological conditions. A clear difference with results obtained in the transient experiments was that EYFP-TDET1 was localized exclusively within the nucleus of these cells (Fig. 19A, D, and compare with Fig. 19B, E). On the contrary H2B-ECFP was always found exclusively in the nuclei in both types of experiments.

Cells were assayed by three-channel FRET in the regions corresponding to the nucleus. Comparison of mean N_{FRET} values of H2B-ECFP/EYFP-TDET1-expressing cells showed a three-fold statistically significant increase with respect to the mean values of control cells expressing H2B-ECFP and EYFP (Table 2). From $N_{FRET(x,y)}$ pixel frequency histograms (Fig. 19), no clear peak could be observed, although a remarkable fraction, approximately 90% of the pixel population, had an $N_{FRET(x,y)}$ value equal to 0 for both test and control cells. Interestingly, an $N_{FRET(x,y)}$ value higher or equal to 0.05 was observed in 5% of the pixels in images derived from H2B-ECFP/EYFP-TDET1 expressing cells, whereas only 0.4% of the pixels in negative control cells had these values. Furthermore, no pixels in control cells had values higher than 0.1, in contrast to 2% of the pixels found in experimental cells. On this basis, an $N_{FRET(x,y)}$ value of 0.1 was considered to be a selective cut-off value for visualizing a physiologically relevant H2B/TDET1 interaction.

Analysis of $N_{FRET(x,y)}$ images from stable H2B-ECFP/EYFP-TDET1 cells showed that the nuclear region in which N_{FRET} values were greater than 0.1 was localized mainly at the periphery of the nucleus (Fig. 20C, F). This fraction, equal to 2% of the nuclear area, could be roughly indicative of the fraction of the genome whose activity is modulated by the DET1 protein. Moreover, this result is in agreement with the in vitro results showing that DET1 binds hypoacetylated H2B tails, because this is the typical state of heterochromatin, which is commonly localized at the nuclear periphery.

Table 2 Statistical analysis of results shown in Fig. 19 and 20.		
	H2B-ECFP+EYFP-TDET1	***H2B-ECFP+EYFP***
Mean N_{FRET}	**0.006**	**0.002**
σ (standard dev.)	0.007	0.003
No. of Observed Cells	25	24
t-test P value	**< 1%**	

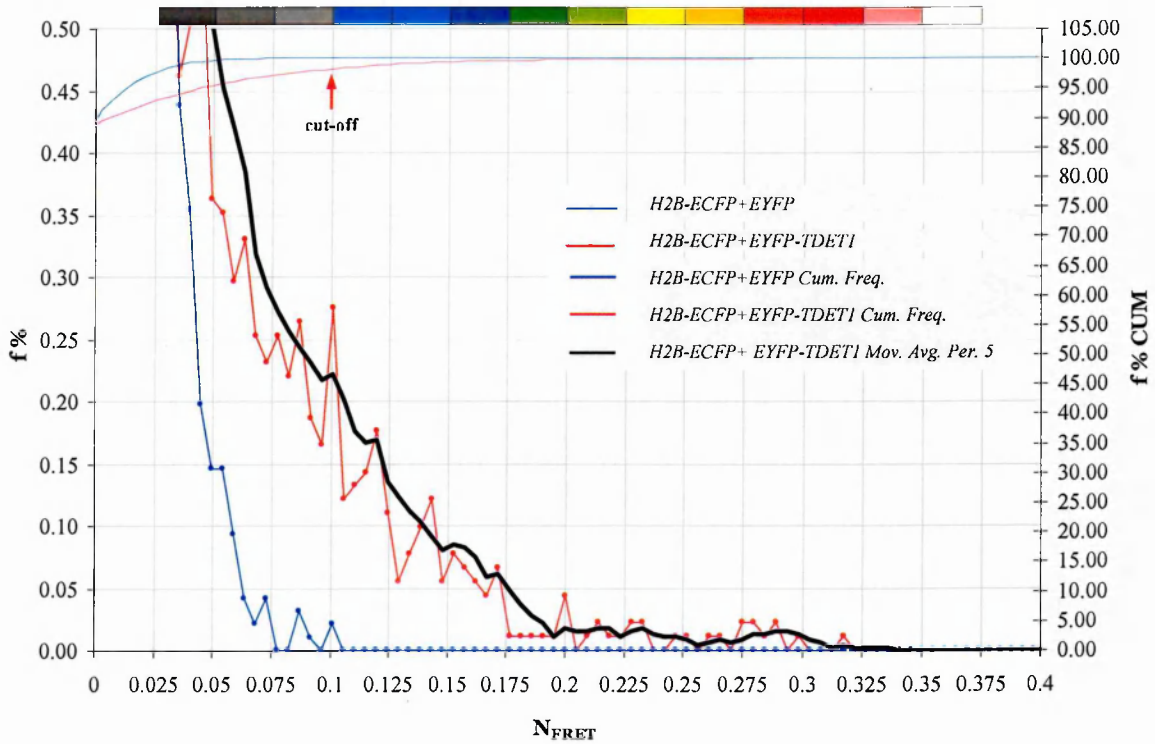

Fig. 19. Cells stably expressing H2B-ECFP and EYFP-TDET1 show a frequency distribution of N_{FRET} values without any clear peak but which is characterized by a shift towards higher values with respect to the frequency distribution obtained from H2B-ECFP/EYFP expressing control cells. Pixel frequency distributions of N_{FRET} values from all the cells of the experiment from which images of Fig. 20 were selected are reported. N_{FRET} values were calculated in the nuclei. Note that although no clear peak is present, cumulative frequency curves show a shift towards higher N_{FRET} values of DET1 containing cells with respect to the control. Note that no pixel in the control cells (H2B-ECFP/EYFP) has N_{FRET} values higher than 0.1, against 2% of pixels from H2B-ECFP/EYFP-TDET1 cells. This is highlighted with a cut-off arrow in the graph. A comparison of the percentages of pixels which pass through the cut-offs in this experiment and in the transient experiment of Fig. 20, shows a remarkable reduction of the total nuclear area of TDET1/H2B interaction in stable lines with respect to TDET1/H2B interaction in transiently expressing cells. For f%, f% CUM and Mov. Avg. Per. 5 meaning, see remarks in legend of Fig. 17.

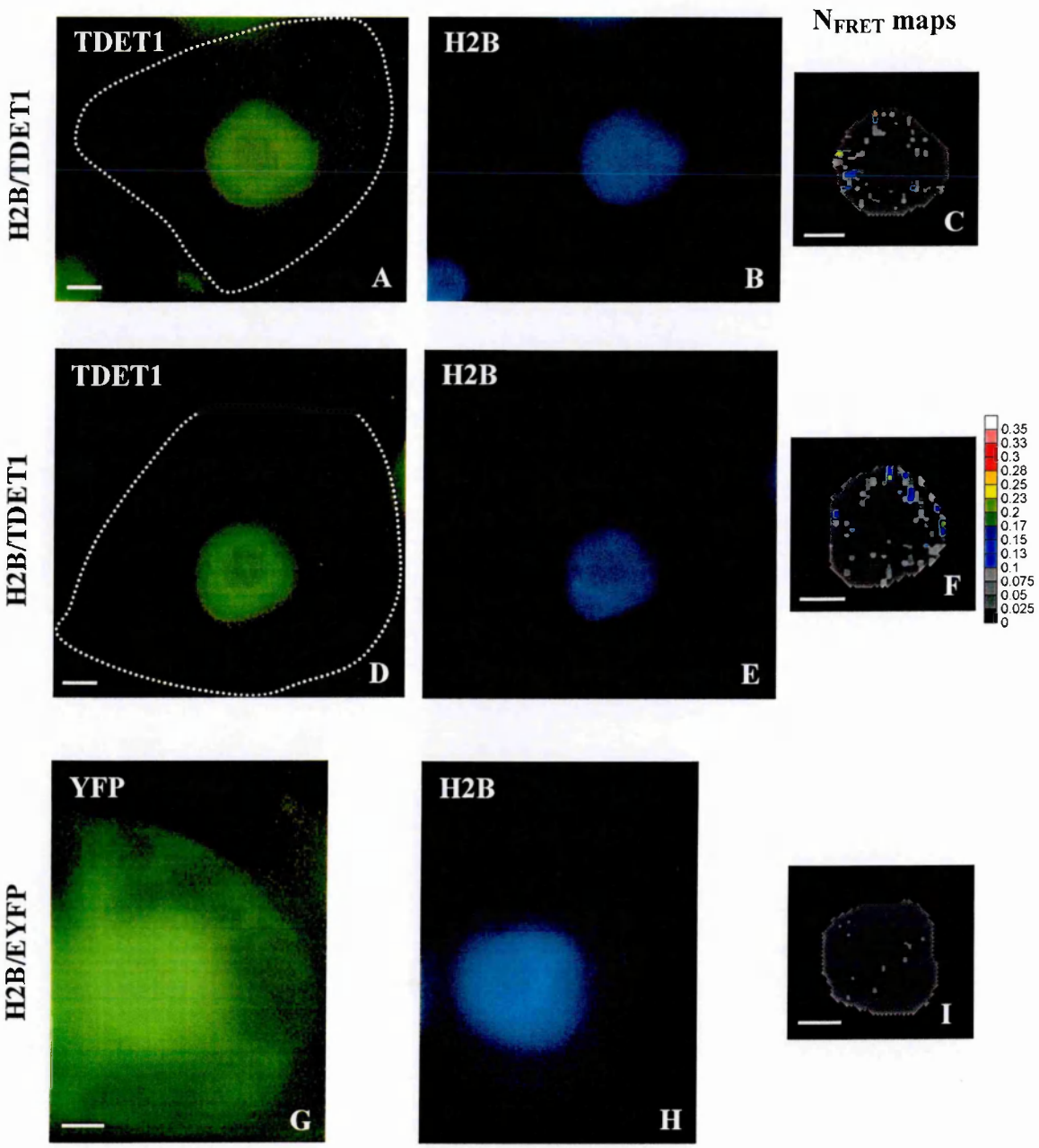

Fig. 20. TDET1 is exclusively nuclear localized and interacts with histone H2B in small peripheral nuclear regions, in cells stably expressing H2B-ECFP and EYFP-TDET1. BY-2 cells stably expressing H2B-ECFP and EYFP-TDET1 or EYFP were imaged and assayed by three-channel FRET. Three representative cells are shown. A-C) and D-F) show two different cells expressing H2B-ECFP/EYFP-TDET1. A, D) TDET1 is exclusively nuclear localized; cell shape is highlighted by a white-dotted line. B, E) histone H2B is nuclear localized. C, F) magnified N_{FRET} maps of the nuclei in pseudocolor: TDET1 interacts with H2B in delimited regions within the nuclear periphery. G-I) refer to a cell expressing H2B-ECFP/EYFP (negative control). G) EYFP is localized in the nucleus and in the cytoplasm. H) H2B is nuclear localized. I) magnified N_{FRET} map of the nucleus in pseudocolor: EYFP does not interact with H2B-ECFP. Colour scale key: grey tones indicate low values characterizing the negative control. The scale bars are 5 μm.

3.3 CHROMATIN IMAGING

3.3.1 H2B-ECFP/H2A-EYFP bimolecular approach

In an attempt to study chromatin dynamics in living cells, a set of constructs was made in which the two GFP variants, ECFP and EYFP, were fused to the tomato histones H2B and H2A. These two histones form dimers within the nucleosome, the basic components of nuclear chromatin. A detectable interaction between their two fluorescent tags was expected on the basis of the crystallographic structure of the nucleosome, in which the two H2B monomers are close enough to the H2A monomers to produce a detectable interaction by FRET (Fig. 21). In fact, a distance of around 7 nm was estimated between the C-termini of the histones of each dimer, by using a suitable software and the nucleosome crystallographic data (see *2.9.2*). Assuming that this is the distance between the two histone fluorescent tags after incorporation into the nucleosome and given the critical Förster distance Ro for ECFP and EYFP ($\kappa = 2/3$) of approximately 5 nm (see *3.1.1*), the expected efficiency of FRET calculated by the Förster equation would be ~20%. These GFP-histone fusions were therefore expected to generate a reasonable FRET signal. Furthermore, they might also be used to report chromatin structure data, such as its grade of condensation, because the efficiency of FRET between the fluorescently tagged histones incorporated into the chromatin structure in a nucleosome context was expected to be dependent to some extent on this geometrical parameter.

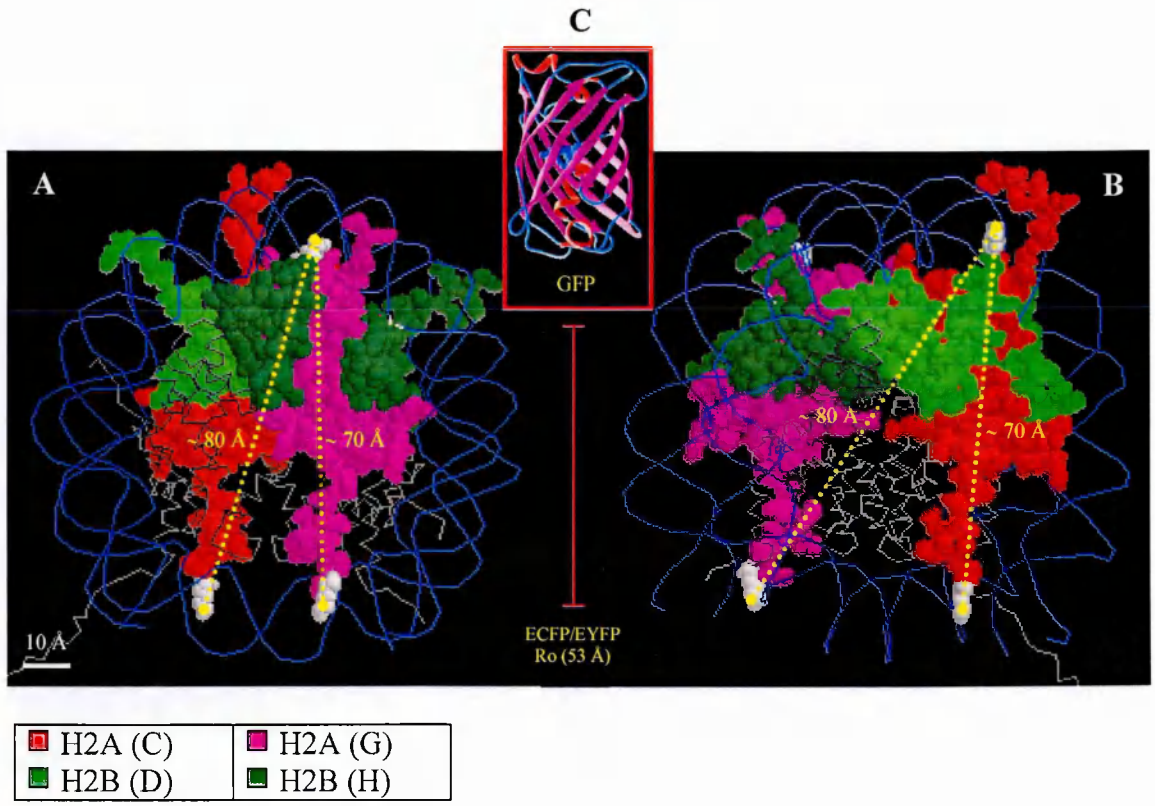

Fig. 21 The distance between the C-termini of histone H2B and H2A is comparable to the Ro critical Förster radius of ECFP and EYFP. A, B) Two views of a nucleosome, in which only histone H2A and H2B are in evidence, are shown. C) Inset represents a GFP molecule of the same scale of A and B to show proportions. The yellow-dots are the distances between the C-termini of H2A and H2B, as estimated by SwissPdbViewer software. Below the GFP inset, for comparison, the Förster distance between ECFP and EYFP is shown as a red line with the same scale of the nucleosome.

A first set of histone fusions tested were H2B-ECFP and H2A-EYFP. These were co-transfected in BY-2 cells. As a negative control we used cells co-transfected with H2B-ECFP and EYFP. Eighteen hours after transfection, histone fusions were found localized exclusively in the nucleus (Fig. 23A, B, D, E and 24B). Furthermore, in cells co-transfected with the two histone fusions, the ECFP- and EYFP- derived fluorescence colocalized extensively, as indicated by a calculated correlation coefficient higher than 0.95 between the images in the acceptor and donor channels (data not shown).

Fluorescent cells were assayed by three-channel FRET following the procedures described in detail in Materials and Methods. N_{FRET} was calculated to quantify FRET in ROIs that corresponded to the nuclei of the cells.

A comparison of mean N_{FRET} values derived from the H2B-ECFP/H2A-EYFP co-transfected cells revealed a statistically significant increase in the N_{FRET} mean values of histone co-transfected cells of 10-fold compared to the negative control (Table 3).

From the analysis of $N_{FRET\,(x,y)}$ pixel frequency histograms (Fig. 22) on the global pixel population, some frequency distribution peaks were recognizable in the H2B-ECFP/H2A-EYFP co-transfected cells, indicating the presence of some pixel populations that were clearly distinguishable from the mean $N_{FRET\,(x,y)}$ values. The significance of these pixel populations was further reinforced by the fact that pixel populations in negative control cells localized into a single peak with low $N_{FRET\,(x,y)}$ values. This result suggested that the "two-histone" system could reveal pixel populations with different FRET values within the nuclei of BY-2 cells.

3.3.1.1 H2B-ECFP/H2A-EYFP Fluorescence Patterns

The nuclei of cells transfected with the H2B-ECFP/H2A-EYFP fusions revealed different fluorescence patterns that were characterized by a uniform background in which the following objects could be distinguished (Fig. 23A, B, D, E):

1. One or a few "holes" (i.e., regions with fluorescence lower than background levels). These structures were likely to represent nucleoli of cells in interphase, in which the chromatin density is expected to be lower or perhaps (at least in some regions) devoid of nucleosomes (Conconi et al., 1992; González-Melendi et al., 1998).
2. One large ring structure (that in three dimensions could correspond to a cage) likely within or around a nucleolus that could correspond to the intranucleolar condensed chromatin regions formed by arrays of inactive rDNA genes containing nucleosomes, whose existence was suggested by Jasencakova et al. (Jasencakova et al., 2000), or to paranucleolar heterochromatic regions (Kanda et al.,1998).
3. Some round small bright objects that might correspond to heterochromatic regions.

To exclude the possibility that these results were due to artefacts such as the formation of inactive aggregates of the GFP fusions, the fluorescence in cells containing histone fusions was compared to that obtained with the DNA-labelling dye, Hoechst 33342. Indeed, it was found that the patterns colocalized perfectly (data not shown), so it was concluded that H2B-ECFP and H2A-EYFP were reliable reporters for chromatin labelling in BY-2 cells in vivo.

3.3.1.2 H2B-ECFP/H2A-EYFP FRET imaging

From analysis of $N_{FRET\,(x,y)}$ images (Fig. 23C, F) it was evident that the first two peaks of the histogram, corresponding to the lowest mean $N_{FRET\,(x,y)}$ values, corresponded to nucleoli at lower fluorescence and to regions mostly at the periphery of the nucleus of cells containing the nucleolus ring structure, whereas pixels of higher mean $N_{FRET\,(x,y)}$

values were localized within the ring structure, in the small rounded objects possibly corresponding to heterochromatin, or at the periphery of cells displaying nucleoli with lower fluorescence.

Although these results were encouraging, because the N_{FRET} values correlated with the apparent chromatin density that had been revealed by the relative fluorescence intensity in the different regions of the nuclei of each cell, two open questions remained:

1. Is the relative fluorescence intensity of the GFP histone fusion a reliable marker of the compaction state of chromatin or, less demanding, of chromatin density (i.e., of chromatin concentration)?
2. What is the resolution of chromatin state determination by FRET analysis?

Regarding the first question, one could argue that GFP histone fusion-derived fluorescence indicates only how crowded the observed region is. This may or may not correspond to a higher chromatin density because the relative intensity of the different regions of a fluorescence image is affected by the thickness of the regions themselves (see *1.3.1.2*). For example, a two-fold difference in the thickness of two regions would produce a two-fold difference in the fluorescence, even though the GFP concentration is the same in both regions. An internal control of known chromatin compaction state would therefore be required to infer that a certain relative fluorescence intensity is diagnostic of a certain chromatin state.

These considerations negatively affect the reliability of using relative fluorescence intensity to measure chromatin compaction state. In contrast, measurements of FRET should be more reliable because FRET efficiency is linked to the geometry of the fluorescent histone tags incorporated in the chromatin in a nucleosome context and at a molecular scale. Therefore N_{FRET} values should reveal information about the molecular structure of chromatin, and not simply about chromatin concentration. As such, the second open question comes into play. How can one

estimate the resolution of the FRET-based method in distinguishing different chromatin compaction states, in vivo?

One possibility would be to measure FRET after cell fixation, by immunodetection of chromatin structures. This approach, however, suffers two main drawbacks, that it can introduce artifacts due to cell fixation, and that it requires a third fluorescent label that would complicate FRET quantification. Consequently, the accuracy of these in vitro measurements would not be expected to be representative of the in vivo measurements.

A different approach would be to use in vivo reporters of chromatin state such as fusions of GFP with, for example, heterochromatin targeting proteins such as heterochromatin protein 1 (HP1; Singh and Georgatos, 2002). However, complications arising from triple labelling of the sample would remain.

It was consequently decided to avoid use of these exogenous reporters of chromatin state. Nonetheless, because results obtained by correlating FRET values with prior information about the expected location of heterochromatin in the nucleus were sometimes unexpected (for example, heterochromatin should be predominantly peripheral in the nucleus, but only in a few cases N_{FRET} values were higher at the nuclear periphery), it was considered necessary to confirm them by an additional approach. To do this, mitotic chromosomes were used as reliable "endogenous" reporters of the known highest chromatin compaction state to examine whether it was possible to correlate N_{FRET} values detected in mitotic chromosomes with their increased chromatin compaction state.

For these experiments I first attempted to generate stable BY-2 cell lines expressing H2B-ECFP and H2A-EYFP in order subsequently to synchronize them with the DNA polymerase inhibitor aphidicolin, to obtain cells arrested at the same cell-cycle stage. Unfortunately, after repeated trials I was not able to select a viable, stable cell

line, most probably because the incorporation of up to 4 tagged histones in each nucleosome was toxic for the cells.

Table 3 Statistical analysis of results shown in Figs. 22-24.		
	H2B-ECFP+H2A-EYFP	***H2B-ECFP+EYFP***
Mean N_{FRET}	**0.294**	**0.026**
σ (standard dev.)	0.147	0.013
No. of Observed Cells	25	20
t-test P value	**<1%**	

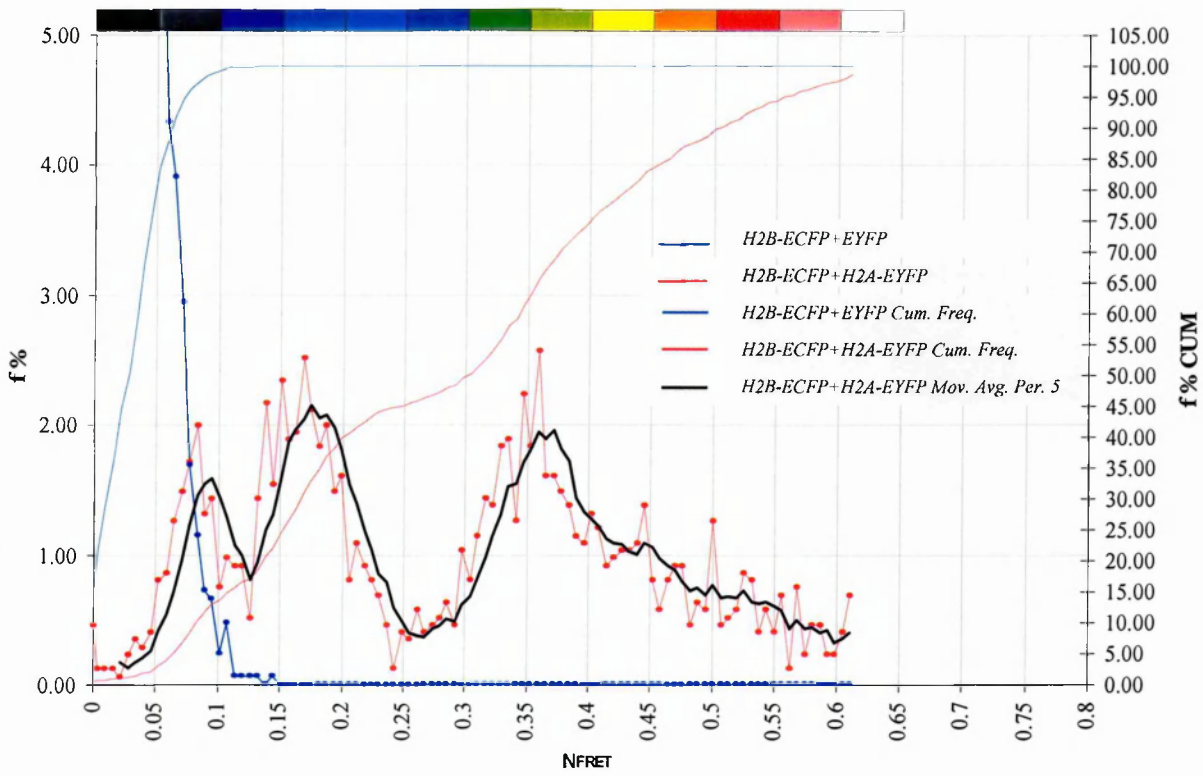

Fig. 22. Cells transfected with H2B-ECFP and H2A-EYFP display frequency distributions of N_{FRET} values characterized by three peaks, which identify three pixel populations that correspond to different nuclear structures/regions. Pixel frequency distributions of N_{FRET} values from all the cells of the experiment from which the images of Figs. 23, 24 were selected are shown. The ring structure, the brighter objects (indicated by arrows in Fig. 23) and often the nuclear peripheries shown in Fig. 23 have N_{FRET} values falling within the third peak containing the highest values. Nucleoli correspond mainly to the middle and first peaks. For definitions of f%, f% CUM and Mov. Avg. Per. 5, see remarks in legend of Fig. 17.

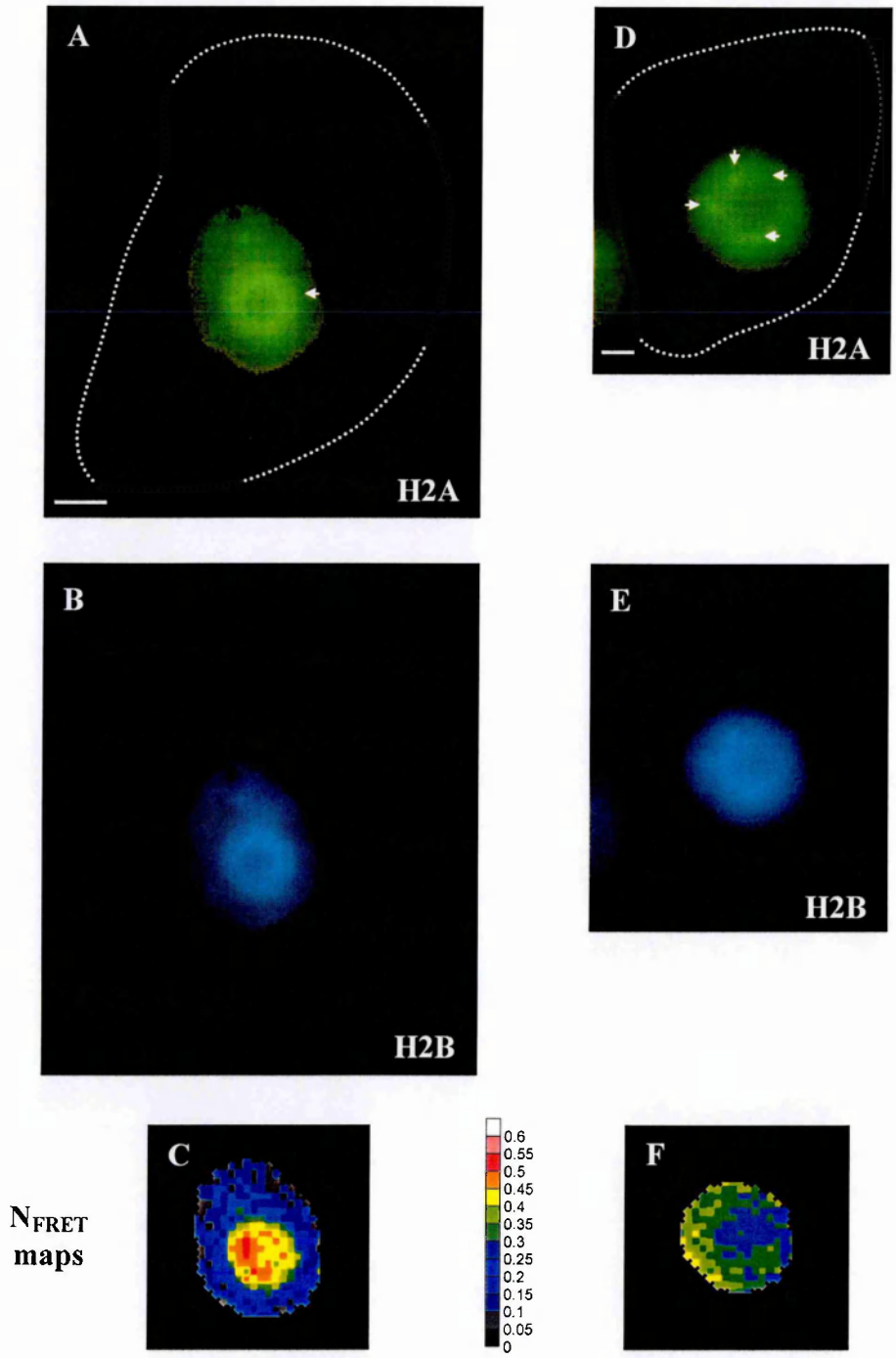

Fig. 23. In cells transiently expressing H2B-ECFP and H2A-EYFP, different structures are recognizable and different nuclear regions are characterized by different N_{FRET} values, suggesting that the reciprocal position of ECFP and EYFP, which is driven by histone-interaction, could change on the basis of chromatin structure. BY-2 cells co-transfected with H2B-ECFP and H2A-EYFP were imaged and assayed by three-channel FRET 18 hours after transfection. A-C) and D-F) refer to two different representative cells transfected with H2B-ECFP and H2A-EYFP. A, B) histone H2A and H2B are exclusively nuclear localized and co-localize. Cell is shown by a white-dotted line. A ring structure, indicated by an arrow, is present around the nucleolus. C) N_{FRET} map of the nucleus in pseudocolor: the ring structure has higher N_{FRET} values and is clearly distinguishable from the peripheral regions. D, E) second example of a cell co-transfected with H2B-ECFP and H2A-EYFP. Cell is shown by a white dotted line. A few peripheral brighter objects, indicated by arrows, are present. F) N_{FRET} map of nucleus in pseudocolor: higher N_{FRET} values are localized to the nuclear periphery. The nucleolus displays lower values. The scale bars are 5 μm.

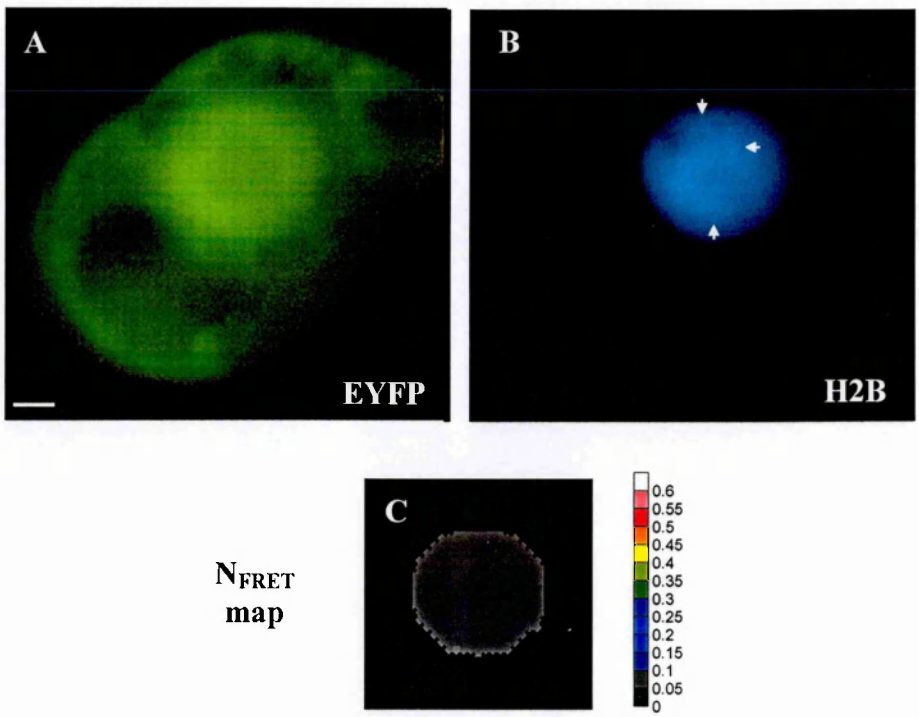

Fig. 24 In cells transiently expressing H2B-ECFP and EYFP, ECFP does not interact with EYFP. One representative negative control cell for the experiment in fig. 23 is reported. A) EYFP is both localized in the nucleus and cytoplasm. B) histone H2B is nuclear localized. Small structures, indicated by arrows, are present. C) N_{FRET} map of the nucleus in pseudocolor. H2B-ECFP does not interact with EYFP. The scale bar is 5 μm.

3.3.2 ECFP-EYFP-H2B Unimolecular Approach

In order to reduce problems arising from the incorporation of an excessive number of tagged histone monomers into nucleosomes, an additional fusion protein (Fig. 4C) was designed in which both GFP variants were fused to a single histone H2B (denoted ECFP-EYFP-H2B). With such a construct, a maximum of two monomers of GFP-tagged histones could be incorporated into each nucleosome. A first fusion, denoted ECFP-EYFP, was generated by fusing each of the two GFP variants together, separated by a flexible linker containing a Gly-Gly dipeptide. This fusion was then fused to the N-terminus of tomato histone H2B with an analogous flexible linker to obtain ECFP-EYFP-H2B. Fusion to the N-terminus was preferred to the C-terminus because the N-terminus is longer and more flexible, two characteristics that were expected to increase the probability of obtaining viable cell lines and of probing differences in nuclear chromatin with higher accuracy.

Because the ECFP-EYFP-H2B fusion contains both GFP variants localized close together (covalently bound), a high basal FRET efficiency was expected independently of incorporation into chromatin. Nonetheless, fluctuations around basal values were also expected after integration of the fusion into the chromatin structure, on the basis of the following considerations. The rationale behind the application of the ECFP-EYFP-H2B construct was to exploit the double dependence of FRET efficiency on the orientation factor κ and the distance R between the donor and acceptor (see *1.3.2*). The two GFP moieties of a ECFP-EYFP-H2B molecule should have a free rotational movement when not incorporated into any structure, corresponding to a κ value of 2/3. On the contrary, when fixed within a structure such as chromatin, the deriving steric hindrance should reduce free movement, thus reducing (or increasing) the κ value. Furthermore, a change in the distance between the two ECFP and EYFP

moieties should occur due to the "pressure" being exerted on them from the surrounding chromatin environment, thanks to the connecting flexible linker. It was therefore hypothesized that when chromatin decorated with ECFP-EYFP-H2B changed its density, e.g., during changes from an open structure to a closed structure in heterochromatin or in mitotic chromosomes, the fusion would have been able to report this change because of a modified efficiency of energy transfer between the donor and acceptor GFPs.

3.3.2.1 Transient Assays

To test whether the intramolecular ECFP-EYFP histone fusion could be useful for chromatin imaging, it was compared with the ECFP-EYFP fusion as a control. This was not expected to be incorporated into any structures within the nucleus but to remain only in the nucleoplasm, like the wild-type GFP protein. ECFP-EYFP-H2B and ECFP-EYFP fusions were therefore transfected into BY-2 cells. Eighteen hours after transfection, ECFP-EYFP fluorescence was found in the cytosol and in the nucleus, similarly to GFP (Fig. 26D, E). ECFP-EYFP-H2B, on the contrary, was found exclusively in the nucleus (Fig. 26A, B) and its fluorescence colocalized with the DNA stain Hoechst 33342 (data not shown). The ECFP-EYFP-H2B fusion was therefore likely to be incorporated into nuclear chromatin in BY-2 cells.

Fluorescent cells were assayed by three-channel FRET following the procedures described in Materials and Methods. The $netF'_A$ was calculated to quantify FRET in ROIs corresponding to the nuclei of the cells. This quantity was preferred to N_{FRET} because, being calculated from fewer fluorescence measurements, it is less affected by measurement errors and so gives higher accuracy. Indeed, since the molar ratio of ECFP and EYFP tags is 1 in the ECFP-EYFP and ECFP-EYFP-H2B unimolecular constructs, normalization for both tags (i.e., donor and acceptor) in order to take into account the

actual donor and acceptor concentrations, as realized with N_{FRET}, is unnecessary because normalization by acceptor or donor fluorescence already provides the desired correction (see Materials and Methods). A comparison of mean $netF'_A$ values derived from ECFP-EYFP-H2B with those from ECFP-EYFP transfected cells (Table 4) showed a statistically significant increase of the ECFP-EYFP-H2B values of about 17%, inferring that ECFP-EYFP-H2B may be able to distinguish an "open" environment from a "closed" environment, such as within chromatin. Analysis of the histograms (Fig. 25) showed the expected shift, although a "bipartite" peak, probably due to transient expression of the constructs, was found for the control cells (see below). Moreover, the histogram from ECFP-EYFP-H2B transfected cells showed three peaks, i.e., pixel populations.

ECFP-EYFP-H2B fluorescence images were comparable to those obtained from cells co-transfected with H2B-ECFP and H2A-EYFP except for the absence of the ring structure associated with nucleoli (Fig. 26A, B). Also $netF'_{A(x,y)}$ images of ECFP-EYFP-H2B transfected cells revealed distributions similar to those obtained from H2B-ECFP/H2A-EYFP expressing cells (Fig. 26C). The $netF'_A$ values corresponding to the three peaks of the histogram were found at the level of single cells, indicating that ECFP-EYFP-H2B was able to distinguish three pixel populations of different $netF'_A$ values coexisting within single cells, i.e., one population with the lowest values which corresponded most likely to the H2B fusion not incorporated into chromatin (an effect of transient expression), and two populations of higher values that corresponded to two classes of chromatin states, possibly euchromatin and heterochromatin.

ECFP-EYFP transfected cells showed uniformly distributed $netF'_{A(x,y)}$ values (Fig. 26F). It was found, however, that some nuclei had $netF'_{A(x,y)}$ values that corresponded to the first peak of the histogram of lower values, whereas others had values corresponding to the second peak. These results showed therefore that the

bipartite peaks shown in the histogram reflected a netF'$_{A(x,y)}$ inter-cellular variability rather than an intracellular variability. In spite of such unexpected variability due to the presence of aberrant cells, these preliminary results from transiently transfected cells were encouraging and led me to perform subsequent experiments with cells stably expressing the intramolecular FRET-based ECFP-EYFP constructs.

Table 4
Statistical analysis of results shown in Figs. 25 and 26.

	ECFP-EYFP-H2B	***ECFP-EYFP***
Mean N_{FRET}	**0.841**	**0.725**
σ (standard dev.)	0.096	0.057
No. Of Observed Cells	10	10
t-test P value	**2.3 %**	

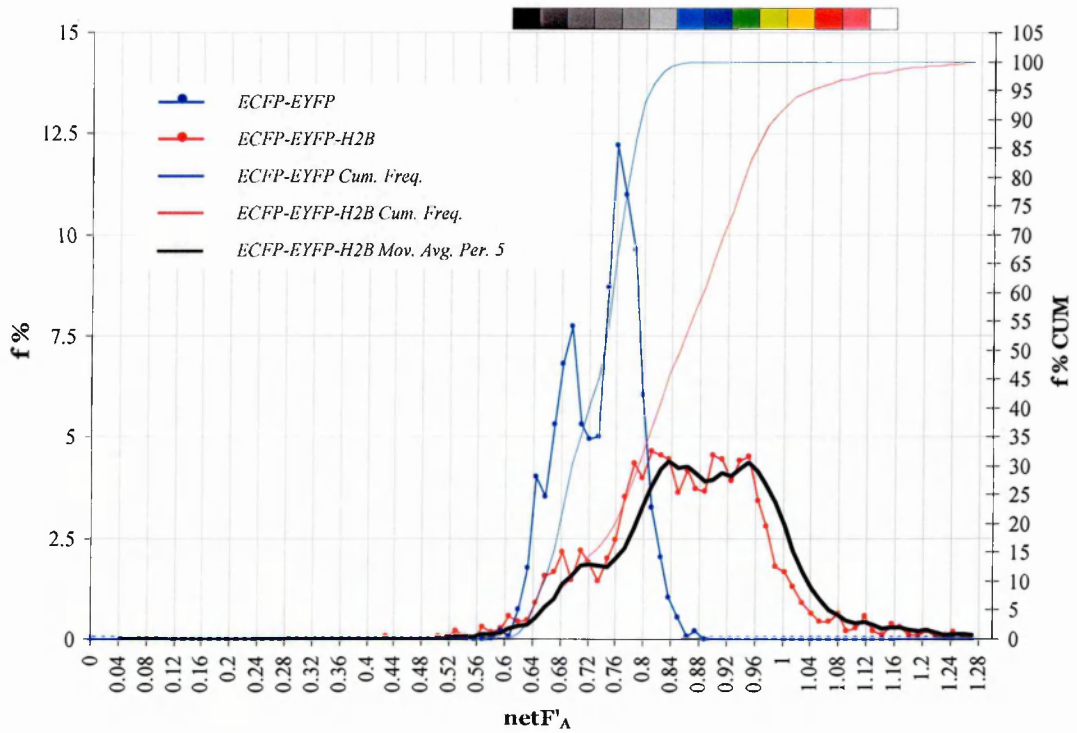

Fig. 25. Cells transfected with ECFP-EYFP-H2B display a frequency distribution of netF'$_A$ values characterized by a composite peak/peaks. Those transfected with ECFP-EYFP show a "bipartite" peak. Pixel frequency distributions of netF'$_A$ values from all the cells of the experiment from which the images of Fig. 26 were selected are shown. ECFP-EYFP-H2B expressing cells show at least three partially overlapping peaks whose values were all found in individual cells (see Fig. 26C). On the contrary, ECFP-EYFP expressing cells show two peaks that were found to represent two cell populations of different average netF'$_A$ values and therefore reflect an intercellular variability. These results, which were different from those obtained from stable lines (see Figs. 27, 28), were probably a consequence of transient expression of the constructs. For definitions of f%, f% CUM and Mov. Avg. Per. 5, see remarks in legend of Fig. 17.

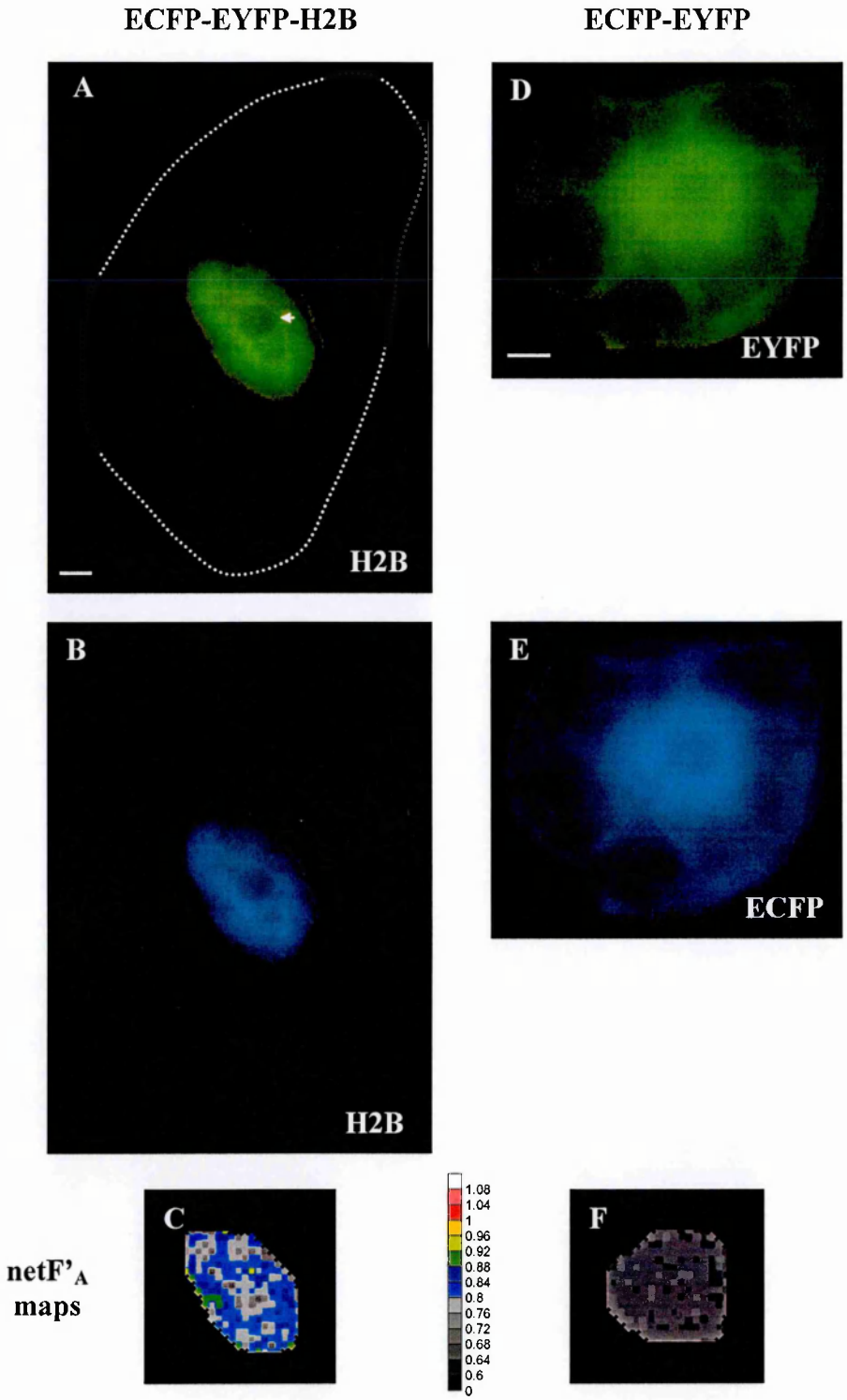

Fig. 26. In cells transiently expressing ECFP-EYFP-H2B, the histone H2B fusion is nuclear localized and netF'$_A$ values are higher than in ECFP-EYFP expressing cells. Moreover, higher values are localized in the nuclear periphery and those lower are in the nucleolus. BY-2 cells co-transfected with ECFP-EYFP-H2B or ECFP-EYFP were imaged and assayed by three-channel FRET 18 hours after transfection. Two representative cells are reported. A-C) refer to a cell transfected with ECFP-EYFP-H2B. A, B) ECFP-EYFP-H2B is exclusively nuclear localized. The cell periphery is shown by a white dotted line. C) netF'$_A$ map of the nucleus in pseudocolor: higher netF'$_A$ values localize to the nuclear periphery, lower values are found in the nucleolus (arrow). D-F) refer to a cell transfected with ECFP-EYFP (negative control). D, E) ECFP-EYFP is localized in the nucleus and the cytoplasm. F) netF'$_A$ map of the nucleus in pseudocolor: netF'$_A$ values in nuclei of control cells are lower than those in ECFP-EYFP-H2B cells. The scale bars are 5 μm.

3.3.2.2 Assays in stable cell lines

ECFP-EYFP-H2B and ECFP-EYFP transfected cells were plated on selective media to isolate stable cell lines. For both constructs, several viable lines were obtained. Among them, one was chosen for each construct for subsequent experiments, on the basis mainly of fluorescence intensity.

To test whether the ECFP-EYFP-H2B fusion could be used to reveal variations between different chromatin structures, the BY-2 cell lines stably expressing ECFP-EYFP-H2B and ECFP-EYFP were synchronized with the DNA polymerase inhibitor aphidicolin (see *2.7.2*). After release from cell cycle arrest these cells constituted a very homogeneous material in that almost all the cells were blocked in interphase, as expected. The chromatin within the nucleus of these cells was not (homogeneously) compacted, but once the cells had entered mitosis, the chromatin would have become highly condensed as the chromosomes had reorganized.

After release from inhibition, the two cell lines were assayed by three-channel FRET at intervals of around 45 min until entry into mitosis. The collected images were divided in three sets, 1) from ECFP-EYFP control cells, 2) from ECFP-EYFP-H2B expressing cells in interphase, and 3) from ECFP-EYFP-H2B expressing cells in mitosis. The interphase and mitotic cells were identified by histone-GFP derived fluorescence, on the basis of their well known chromatin patterns. ECFP-EYFP control cells, lacking a chromosome tag, were selected irrespective of cell stage but at the same time as the chromosome tagged cells. The selected ROIs corresponded to the whole nucleus for the ECFP-EYFP control and for the ECFP-EYFP-H2B interphase cells, whereas for the cells in mitosis the analysed regions corresponded to the chromosome ensemble in prophase, metaphase or anaphase (see below for the criteria applied in selecting ROIs).

A comparison of mean netF'$_A$ values in control and ECFP-EYFP-H2B interphase cells showed only minor differences with respect to what was obtained in the transient assay, thus confirming these previous results (Table 5). The differences mainly concerned the absolute values of netF'$_A$ of control and interphase cells, which were higher, very likely due to the optical filter upgrade of our system that was made at this time to increase sensitivity in FRET detection. Moreover, a statistically significant difference of around 7.5% was found in the mean netF'$_A$ value between mitotic and interphase cells (Table 5). From analysis of the netF'$_{A(x,y)}$ pixel frequency histograms (Fig. 27) on the global pixel populations, each group of images showed a single frequency distribution peak except for that derived from interphase cells which displayed two peaks, in analogy with what was obtained from cells transiently expressing ECFP-EYFP-H2B (see above). From the histograms and from the cumulative frequency curves, the shift in mean value was evident. Although a consistent overlap was found between the peak relative to the interphase cells and that of mitotic cells, a consistent percentage of pixels in mitotic cells had netF'$_{A(x,y)}$ values greater than 1.6. This value constituted a "mitosis threshold" in the netF'$_{A(x,y)}$ value, because only a small percentage of pixels from the interphase cells (less than 5%) had a value equal or higher than this, whereas no pixels derived from the control set reached this value.

The three peaks of the three sets of cells displayed a variable width which derived from the combination of:

1) intercellular variability expressed by the standard deviation (σ), shown in Table 5;

2) intracellular variability expressed by the standard deviation calculated for each cell.

The intercellular variability was found to be higher for cells in mitosis and interphase than for control cells. Moreover, the intracellular standard deviation of netF'$_{A(x,y)}$, calculated for the three groups of cells paralleled this result with an average value of approximately 0.025 for control cells (i.e., values of single cells ranged in the interval

[mean value ± 2 x 0.025]) and 0.05 for interphase cells and mitotic cells (i.e., values of single cells ranged in the interval [mean value ± 2 x 0.05]). These results showed the expected lower heterogeneity of $netF'_{A(x,y)}$ values in control cells where the unavoidable variability was very likely due at least in part to the system-linked noise. Conversely, the higher heterogeneity of the values of interphase and mitotic cells was in agreement with the idea that if ECFP-EYFP-H2B had been integrated into the chromatin it would have been able to sense different chromatin structures and therefore would have displayed a certain degree of intercellular heterogeneity as a consequence of different cellular states. Variability would have also been expected at the intracellular level, i.e., within each cell, as a consequence of the coexistence of different structures, such as heterochromatin, euchromatin, etc.

Fluorescence from ECFP-EYFP control cells had localization patterns analogous to that of GFP, and ECFP-EYFP-H2B fluorescence images in interphase cells were comparable to those obtained previously from cells co-transfected with H2B-ECFP and H2A-EYFP (Fig. 28A, K). Fluorescence from ECFP-EYFP-H2B mitotic cells exhibited the known patterns of the different mitotic stages such as a unique indented fluorescent body, corresponding to metaphase, or two facing fluorescent bodies, corresponding to anaphase (Fig. 28B-F). These patterns, which showed that ECFP-EYFP-H2B fluorescence followed chromosome reorganization and movements, constituted clear evidence that this histone fusion was indeed integrated into chromatin.

In images generated from $netF'_{A(x,y)}$ values, the ECFP-EYFP control nuclei displayed uniform $netF'_{A(x,y)}$ values within the limits of the above mentioned intracellular variability (Fig. 28L). A more complex pattern was found in ECFP-EYFP-H2B-labelled interphase cells, where regions with higher $netF'_{A(x,y)}$ values tended to localize to the nuclear periphery (Fig. 28F). Unfortunately, although mitotic cells had higher $netF'_{A(x,y)}$ values than interphase cells, single chromosomes could not be easily

resolved because of the use of the macro-pixel (see Material and Methods) in processing the images (Fig. 28G-J). Although the use of a single-pixel analysis could, in principle, have overcome this limitation, it was decided not to apply it, in order to avoid increase in background noise. Consequently, it was impossible to push the FRET analysis to sub-chromosome resolution. Moreover, a relevant out of focus blur was found to be mainly localized at the periphery of each chromosome ensemble. This degraded the quality of images contributing to a further decrease in resolution. This limitation could be overcome by the treatment of images with suitable advanced deconvolution algorithms to reduce out of focus blur (see *1.3.1.3*). Unfortunately, such software was not available during the present thesis work. It was therefore decided to cut out the most disturbed regions of the images of mitotic cells by appropriately selecting ROIs. Moreover, $netF'_{A(x,y)}$ values were calculated in the discarded regions and were found to be higher than in the selected regions. Consequently, exclusion of these regions from FRET analysis in mitotic cells likely led to an underestimation of $netF'_{A}$.

Although these results question the ability of the ECFP-EYFP-H2B fusion to visualize different chromatin states, we believe that the limited success of these experiments is more a problem of accuracy in measuring FRET efficiencies with the system that was used, rather than a failure in the hypothesized approach.

Table 5 Statistical analysis of results shown in Figs. 27 and 28.		
A)	***ECFP-EYFP-H2B stable Mitotic***	***ECFP-EYFP-H2B stable Interphase***
Mean netF'$_A$	**1.478**	**1.345**
σ (standard dev.)	0.075	0.073
No. of Observed Cells	20	17
t-test P value	**<1%**	

B)	***ECFP-EYFP-H2B stable Mitotic***	***ECFP-EYFP stable***
Mean netF'$_A$	**1.478**	**1.262**
σ (standard dev.)	0.075	0.033
No. of Observed Cells	20	16
t-test P value	**<1%**	

C)	***ECFP-EYFP-H2B stable Interphase***	***ECFP-EYFP stable***
Mean netF'$_A$	**1.345**	**1.262**
σ (standard dev.)	0.073	0.033
No. of Observed Cells	17	16
t-test P value	**<1%**	

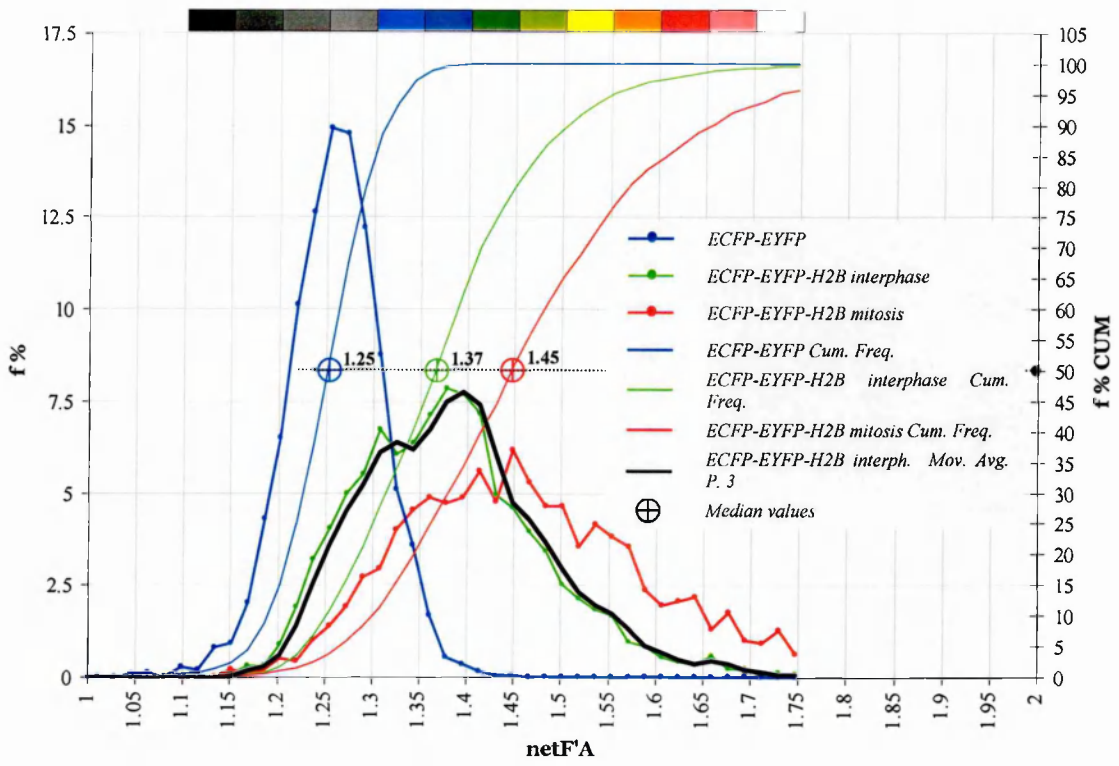

Fig. 27. Cells that stably express ECFP-EYFP-H2B display frequency distributions of netF'$_A$ values which are shifted towards higher values with respect to that of cells expressing ECFP-EYFP. Pixel frequency distributions of netF'$_A$ values from all the cells of the experiment from which images in Fig. 28 were selected are shown. Median values (approximating very well the mean values) are shown on the cumulative frequency curves to highlight the shift in netF'$_A$ values. Note that beside this characteristic, which is corroborated by the statistical data in Table 5A-C, the width of the peaks derived from ECFP-EYFP-H2B expressing cells also shows an analogous shift. This reflects an increase in the inter- and intra-cellular netF'$_A$ variability in passing from control cells to interphase and mitotic cells (see text). For definitions of f%, f% CUM and Mov. Avg. Per. 5, see remarks in legend of Fig. 17.

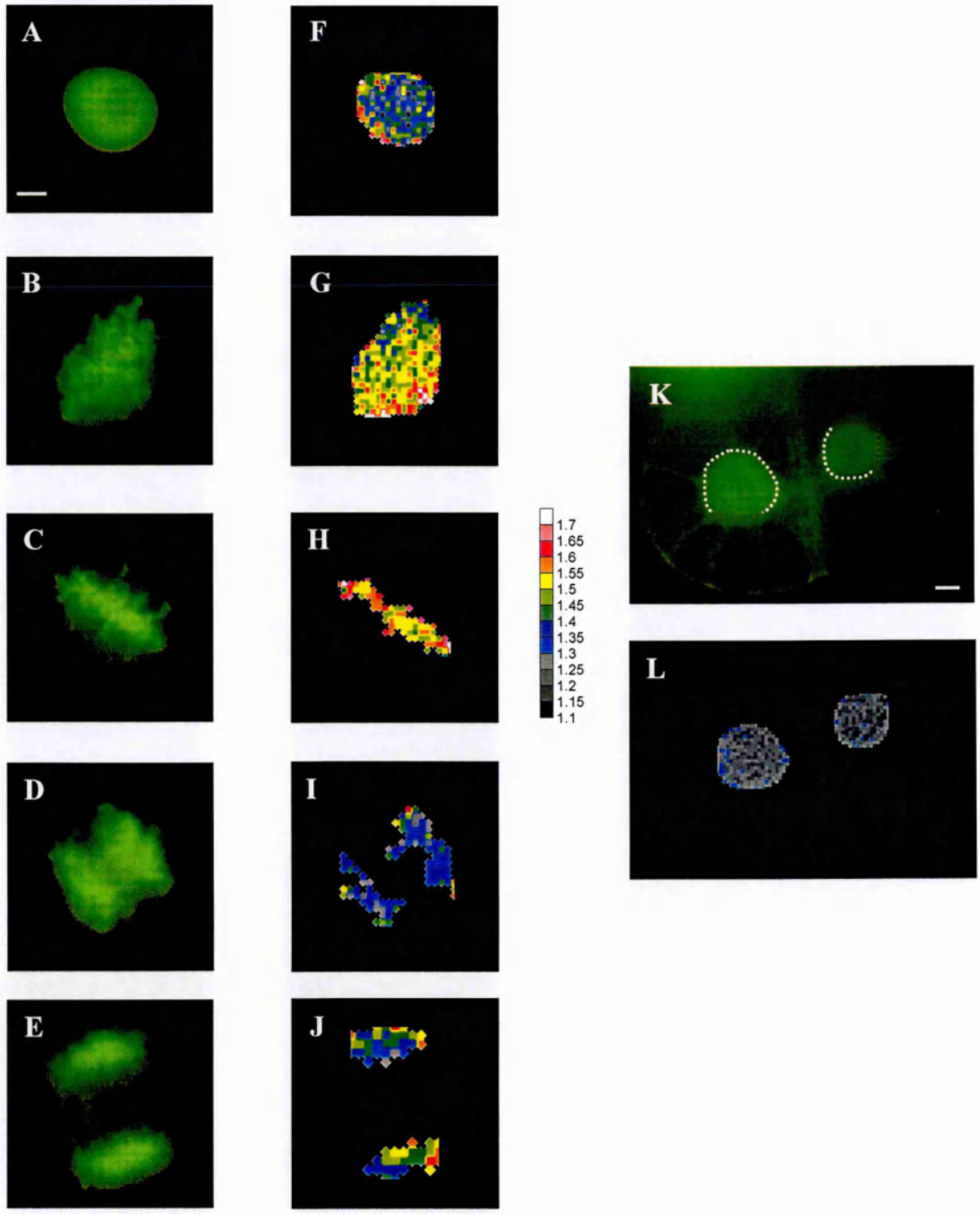

Fig. 28. ECFP-EYFP-H2B stably expressed in BY-2 cells is incorporated into chromatin and allows visualization of chromatin dynamics during the cell cycle. BY-2 cells stably expressing ECFP-EYFP-H2B or ECFP-EYFP were synchronized by aphidicolin, which blocks cells in S phase. After release of the block, cells in different cell stages were imaged and assayed by three channel FRET to determine the E- (efficiency of FRET) related amount netF'$_A$ in each pixel of the regions occupied by chromatin. A-E) are fluorescence images of 5 different cells expressing ECFP-EYFP-H2B, in which only the cellular portion containing the chromosomes is shown; F-J) are the netF'$_A$ maps in the pseudocolor scale shown, corresponding to the fluorescence images on the left. Images are ordered in a cell cycle sequence and represent: A) Interphase; B) Prophase; C) Metaphase; D) Anaphase; E) Telophase. K, L) refer to two adjacent control cells expressing ECFP-EYFP. K) is the fluorescence image, L) is the netF'$_A$ map of the regions shown by white dotted circles. Note that the increase of netF'$_A$ in passing from control cells to interphase and mitotic cells is very evident. The main difference between interphase and mitotic cells is the fraction of pixels with higher netF'$_A$. In interphase cells these are fewer and are mainly localized to the nuclear periphery, very likely confined within heterochromatic regions, whereas in mitotic cells they are spread over the entire chromosome ensemble. However, mitotic cells with pixels with lower values were also found. This can explain the overlap between the histograms shown in Fig. 27. The scale bars are 5 μm.

3.4 IMAGING OF LIGHT SIGNALLING COMPONENTS IN BY-2 CELLS

3.4.1 PIF3 studies

Phytochrome Interacting Factor 3 (PIF3) was discovered by Ni and colleagues (Ni et al., 1999) using a yeast two-hybrid screen for proteins binding to the C-terminal domain of phyA and phyB. It was subsequently shown that PIF3 is a constitutively nuclear localized sequence-specific DNA binding protein that targets G-box motifs (Martinez-Garcia et al., 2000). Moreover, by in vitro experiments, the Pfr form of phyB was found to bind PIF3 not only in the free form but also when it is bound to DNA, suggesting that phytochrome could be targeted by PIF3 to light-responsive promoters to regulate specific gene activities (Martinez-Garcia et al., 2000).

3.4.1.1 Phytochrome interaction

The FRET-based microscopy system developed during this thesis appeared usable to test the interaction between phytochrome and PIF3 in living cells and to localize the DNA binding sites of PIF3 in the nucleus. Moreover, it was of interest to study PIF3 subnuclear localization.

In order to study the interaction of PIF3 with phytochrome in vivo, an ECFP-PIF3 fusion was generated and co-transfected with a tomato phyB2-EYFP fusion in BY-2 cells. As a negative control we co-transfected ECFP-PIF3 and EYFP. After eighteen hours in light, fluorescent cells were assayed by three channel FRET. FRET was quantified by calculating N_{FRET} in ROIs corresponding to the nuclear regions of the cells.

The mean N_{FRET} value from ECFP-PIF3/phyB2-EYFP co-transfected cells was found to be around 30-fold higher than that from the negative control cells. This data, which was corroborated by the t-test statistical analysis, showing that this difference

was highly significant (Table 6), indicated a specific interaction between PIF3 and phyB2.

Further analysis of $N_{FRET(x,y)}$ pixel frequency histograms identified a single peak, centred around an $N_{FRET(x,y)}$ value of approximately 0.08 (Fig. 29). However, a tail of higher values was also found, indicating the existence of a single main pixel population together with some pixel subpopulations.

Table 6 Statistical analysis of results shown in Figs. 29-31.

A)	***ECFP-PIF3+EYFP-phyB2***	***ECFP-PIF3+EYFP***
Mean N_{FRET}	**0.060**	**0.002**
σ (standard dev.)	0.051	0.002
No. of Observed Cells	10	10
t-test P value	**<1%**	

B)	***ECFP-PIF3+H2A-EYFP***	***ECFP-PIF3+EYFP***
Mean N_{FRET}	**0.001**	**0.002**
σ (standard dev.)	0.003	0.002
No. of Observed Cells	10	10
t-test P value	**>>5%**	

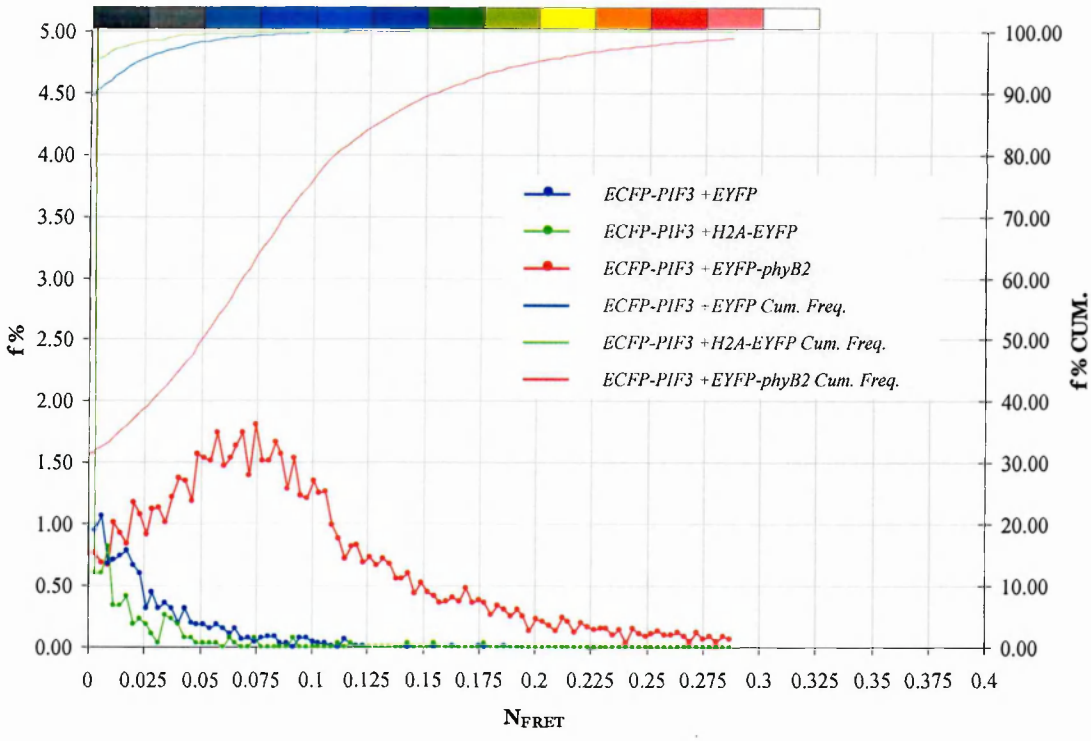

Fig. 29. Cells transfected with ECFP-PIF3 and EYFP-phyB2 display frequency distributions of N_{FRET} characterized by a single peak and a long tail. Pixel frequency distributions of N_{FRET} values are shown from all the cells of the experiment from which images in Figs. 30, 31 were selected. As shown in Fig. 30F, many speckles and ample nuclear regions had values corresponding to the peak value; a few speckles, indicated in Fig. 30C by arrows, and regions around the nuclear periphery had higher values falling within the tail. The distribution from ECFP-PIF3 and H2A-EYFP co-transfected cells is very similar to that derived from negative control cells (ECFP-PIF3+EYFP). T-test and image analysis confirmed that PIF3 and H2A did not interact. For definitions of f% and f% CUM, see remarks in legend of fig. 17.

Analysis of fluorescence images of the cells showed that both ECFP-PIF3 and EYFP-phyB2 localized exclusively to the nucleus of BY-2 cells (Fig. 30D, E). Moreover, both proteins were found to form small, round speckles in these nuclei, as described previously for phytochromes (see *1.1.1.3*), and very interestingly were found to perfectly colocalize in these speckles (Fig. 30A-C). On the contrary, in control cells, only ECFP-PIF3 displayed speckles, implying that at least the exogenous phytochrome is not required for PIF3 speckle formation, whereas EYFP showed its typical diffuse fluorescence pattern (Fig. 31A, B).

Analysis of $N_{FRET(x,y)}$ images revealed interaction between PIF3 and phyB2 within the speckles with a mean value of around 0.08, although a similar mean value was found in other regions of the nucleus as well, suggesting that PIF3 and phyB2 interacted not only within the speckles but also in other nuclear regions (Fig. 30F). Conversely, in cells co-transfected with ECFP-PIF3 and EYFP, although ECFP-PIF3 formed speckles, these did not show any FRET, suggesting indeed that the PIF3/phyB2 colocalization was due to a specific interaction rather than, for example, to a simple cosegregation into aggregates generated as a consequence of protein overexpression (Fig. 31C). Moreover, in some speckles, as well as in other peripheral nuclear regions, higher $N_{FRET(x,y)}$ values were found. This could mean that in these regions the two proteins interacted with a different geometry and consequently displayed a higher FRET efficiency or, more likely, that these regions were characterized by a higher concentration of PIF3/phyB2 complexes considering the N_{FRET}-dependence on the molar fraction of FRET-complex vs free donor and acceptor (fusion) molecules (see *2.7.1.1*).

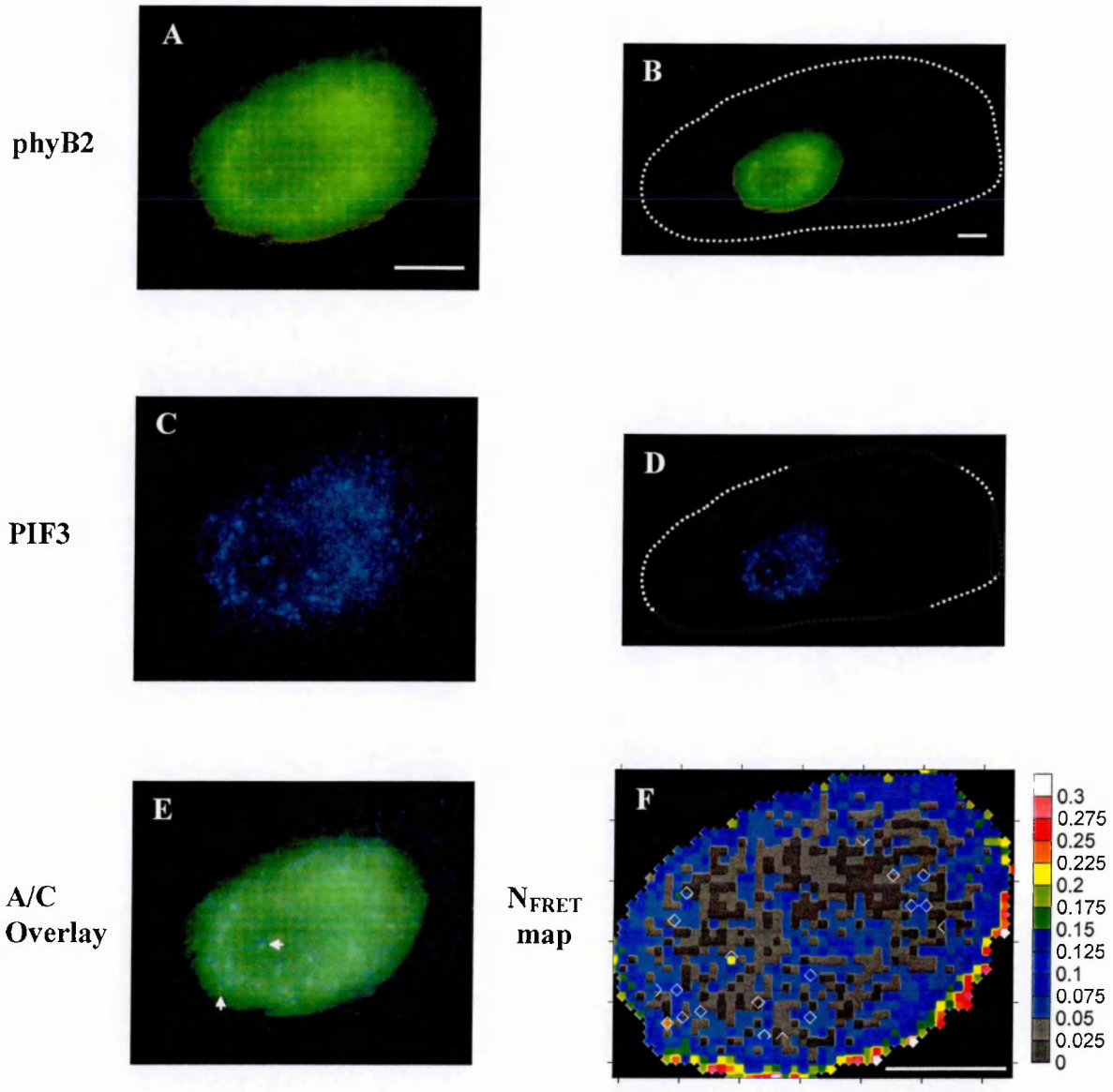

Fig. 30. ECFP-PIF3 and phyB2-EYFP co-localize to nuclear speckles within which they interact. BY-2 cells co-transfected with ECFP-PIF3 and EYFP-phyB2 were imaged and assayed by three-channel FRET 18 hours after transfection, in light conditions. One representative cell is shown. In B and D the whole cell is shown with the cell periphery indicated by white dots: PIF3 and phyB2 localize exclusively to the nucleus. A, C) magnified images of the nucleus. E) is the A/C overlay: PIF3 and phyB2 co-localize to numerous nuclear speckles. Moreover, a diffuse signal is present within the nucleus. F) N_{FRET} map of the nucleus in pseudocolor: PIF3 and phyB2 interact in many speckles (evidenced as empty white boxes). An interaction is also found elsewhere in the nucleus. Colour scale key: grey tones indicate low values characteristic of the negative control. The scale bars are 5 μm.

3.4.1.2 Histone H2A interaction

Moreover, an attempt was made to localize PIF3/DNA interaction sites in living cells. In the above experiment, beside the ECFP-PIF3/phyB2-EYFP and ECFP-PIF3/EYFP transfections, a histone H2A-EYFP fusion was co-transfected with ECFP-PIF3 in BY-2 cells, as a chromatin (and nuclear) marker. After eighteen hours in dim light, cells were imaged and assayed for FRET.

The histone fusion showed the expected nuclear localization whereas ECFP-PIF3 was found to be localized in nuclear speckles, as was found in the previous transfection (Fig. 31D, E). However, histogram and FRET image analyses showed no difference with respect to the negative control cells, indicating no interaction between PIF3 and histone H2A (Table 6B, Figs. 29 and 31C, F). This result could be interpreted in different ways. One possibility is that the PIF3 fusion cannot bind DNA or, more likely, that the PIF3/DNA interaction exceeds the maximum resolution allowed by the system used and thus escaped microscopy detection. This could indeed be the case because PIF3 has been shown to interact with only a few G-box containing light responsive promoters (Martinez-Garcia et al., 2000). Finally, an additional possibility is that the histone fusion is not appropriate to label PIF3 controlled promoters because nucleosomes (and therefore histones) were simply not present in these regions, as has been shown may be the case for regions being actively transcribed (Workman et al.,1991; van Holde et al., 1992; Svaren and Horz, 1993; Croston and Kadonaga,1993; Alberts et al., 2002).

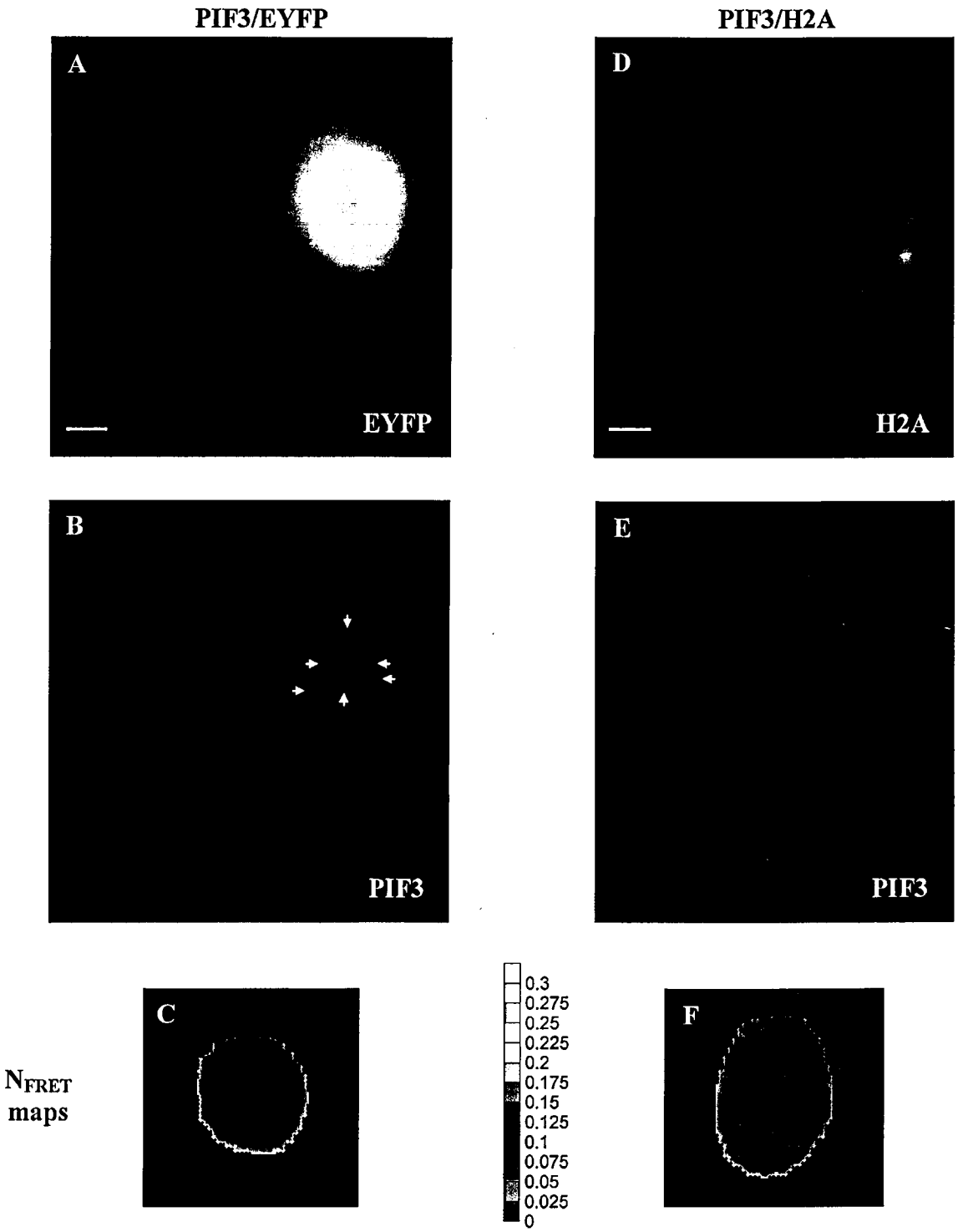

Fig. 31 PIF3 does not interact with histone H2A. One representative negative control cell for the experiment in Fig.30 is shown together with a representative cell transfected with ECFP-PIF3 and H2A-EYFP. A-C) show a cell co-expressing ECFP-PIF3/EYFP. D-F) show a cell co-expressing ECFP-PIF3/H2A-EYFP. A) EYFP is nuclear and cytoplasmically localized. B) PIF3 is localized exclusively to the nucleus and forms speckles (some of them indicated by arrows). C) N_{FRET} map of the nucleus in pseudocolor: PIF3 does not interact with EYFP either in the speckles or in other nuclear regions. D-E) histone H2A and PIF3 colocalize but they do not interact (F). The scale bars are 5 μm.

3.4.2 Localization studies of COP1 and HY5

The *CONSTITUTIVE PHOTOMORPHOGENIC 1* (*COP1*) locus, which has been identi-fied by genetic screens for mutants that display characteristics of light-grown seedlings in complete darkness, encodes a repressor of light-dependent gene transcription which has recently been demonstrated to be involved in the down-regulation of around 20% of Arabidopsis genes in the dark (Ma et al., 2002), most likely through the targeting of light regulated transcription factors (e.g. HY5, HYH and SPA1) to the proteasome for degradation (Osterlund et al., 2000a).

Considering the important role of COP1 in the control of photomorphogenesis, we decided to perform a localization study of this protein with HY5, one of its targets, which has been found to interact directly (Ang et al., 1998). We examined the localization of these two proteins in BY-2 cells, in dark and light conditions. The activity of both proteins has been previously demonstrated to be regulated by illumination conditions. COP1 accumulates in the nucleus in darkness whereas it diminishes strongly in the light and eventually relocalizes to the cytoplasm (von Arnim and Deng, 1994). HY5 is a constitutively nuclear localized protein (Ang et al., 1998) which has been demonstrated to reversibly accumulate to about 20-fold within 15 hours after shifting Arabidopsis seedlings from darkness into light (Osterlund et al., 2000a, 2000b).

In order to study localization of COP1 and HY5, tomato COP1 (TCOP1) and tomato HY5 (THY5) were fused to ECFP to generate the ECFP-TCOP1 and ECFP-THY5 fusions that were then co-transfected together with H2A-EYFP, as a nuclear marker, in BY-2 cells. Following transfection, cells were maintained in either light or complete darkness for 18 hours and were observed in the fluorescence microscope.

Tomato COP1 was found to be nuclear localized in the dark mainly within speckles, as previously reported (Fig. 32; von Arnim and Deng, 1994; von Arnim et al., 1998; Ang et al., 1998; Stacey and von Arnim, 1999). However, contrary to previous observations, cells incubated in light conditions displayed an analogous localization and no ECFP-TCOP1 fluorescence was ever found in the cytoplasm, either in light or in darkness (Fig. 32A, B, F, G). Moreover, a fraction of ECFP-TCOP1 was found to be localized to the nuclear periphery and, because it did not co-localize with the histone fusion, this could be indicative of a nuclear membrane localization (Fig. 32E, J).

Tomato HY5 was found to be completely nuclear localized both in the light and in the dark (as previously reported) without any apparent subnuclear localization (Fig. 33B, D). Moreover, the levels of protein, as estimated by fluorescence intensity, were found to be very similar (data not shown) regardless of the light conditions, in apparent contrast with what has been reported in the literature (Osterlund et al., 2000a, 2000b). The lack of dark-dependent degradation of HY5 could be due to different causes, such as deregulation of the fusion protein most likely caused by HY5 overexpression. An additional possibility could be that BY-2 cells are not suitable for studying light responses (see Discussion).

Finally, an indirect interaction of the transcription factor HY5 with histone H2A was examined, because HY5 has been demonstrated to bind DNA to the G-box motif in the promoter of light-inducible genes (Chattopadhyay et al., 1998). Cells co-transfected with ECFP-THY5 and H2A-EYFP were assayed by three-channel FRET. However, neither N_{FRET} global analyses (histograms and statistical t-tests) nor image analysis revealed any direct interaction between HY5 and H2A (data not shown), very likely for reasons analogous to those discussed for PIF3/H2A interaction (see *3.4.2*).

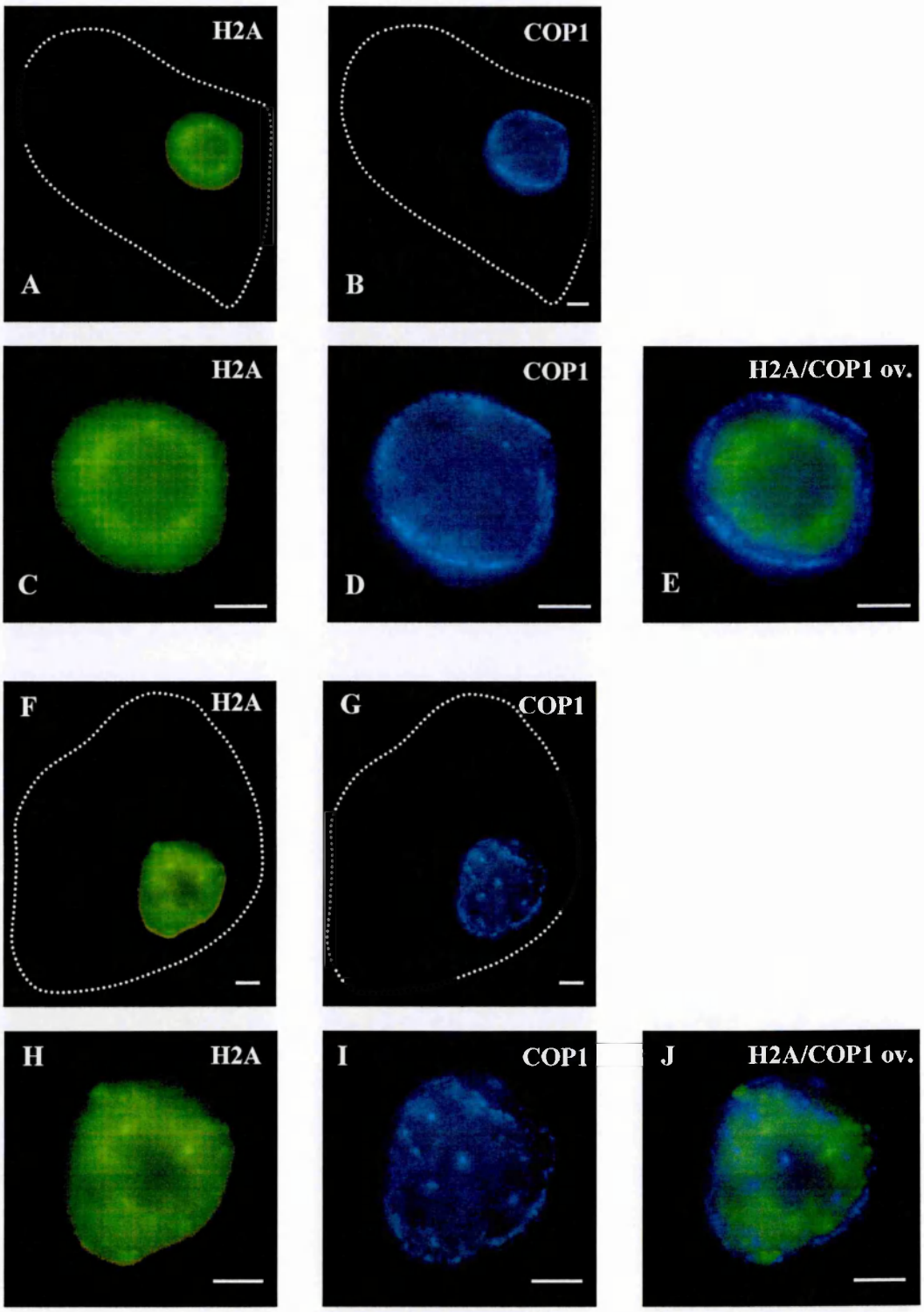

Fig. 32. COP1 is nuclear localized both in the dark and in the light and forms numerous speckles, but does not colocalize with histone H2A. BY-2 cells were co-transfected with ECFP-TCOP1 and H2A-EYFP and imaged after 18 hours of incubation in the dark or in the light. No difference was found between light and dark incubated cells. A-E) and F-J) refer to two representative cells. C, D) and H, I) show the magnified nuclei deriving, respectively, from A, B) and F, G). E and J show, respectively, the C/D and H/I overlays: COP1 forms nuclear speckles and appears to be localized also to the nuclear periphery. Moreover, it does not colocalize with histone H2A. Cell peripheries are indicated by white dots. The scale bars are 5 μm.

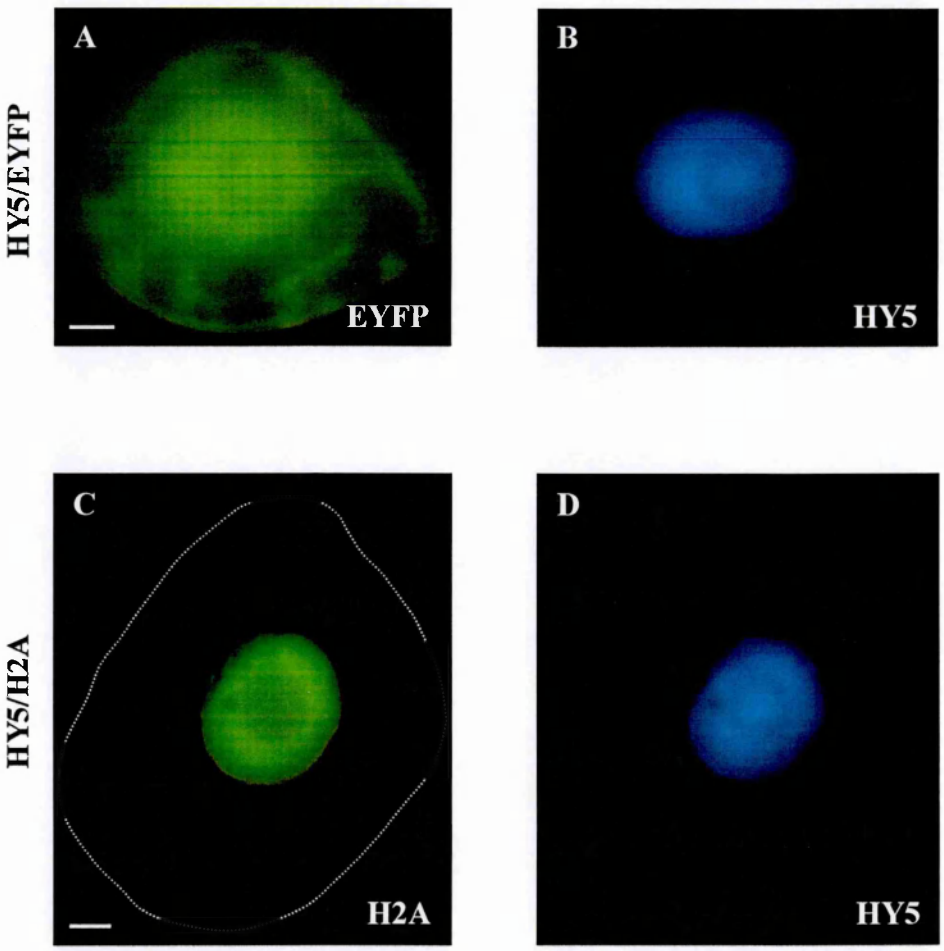

Fig. 33. HY5 is constitutively nuclear localized. BY-2 cells were co-transfected with ECFP-THY5 and H2A-EYFP or EYFP and imaged after 18 hours of incubation in the dark or in the light. No difference was found between light and dark incubated cells. One representative cell for each transfection is reported. A and B) refer to a cell co-transfected with ECFP-THY5 and EYFP. C and D) refer to a cell co-transfected with ECFP-THY5 and H2A-EYFP. A) EYFP is cytoplasmically and nuclear localized. B) HY5 is exclusively nuclear localized. C and D) HY5 and histone H2A colocalize into the nucleus (but do not interact –data not shown). Scale bars are 5 μm.

DISCUSSION

The results presented in this thesis provide suggestive evidence that DET1 binds to non-acetylated H2B tails within the context of the nucleosome. Also of significance is the utilization of FRET imaging using GFP variants to demonstrate this interaction within the nucleus of living plant cells. This is one of the first reports in plants of intermolecular FRET measurements using GFP variants (Immink et al., 2002; Mas et al., 2000). This technique should permit the subcellular imaging in real time of other protein:protein interactions in plant cells (Formiggini and Bowler, Manuscript in preparation). For example, preliminary results are included in this thesis for the interaction and localization of PIF3 and phyB2.

What is also very promising is the system established in this thesis aiming to visualize chromatin dynamics in single living cells. This system was used to follow chromatin reorganization which accompanies mitosis and showed its capability to distinguish chromatin of cells in interphase from chromatin in mitotic chromosomes on the basis of FRET determinations.

4.1 DET1 AND CHROMATIN REMODELLING

Arabidopsis *det1* mutants display a dramatic phenotype of constitutive photomorphogenesis in the absence of light that is very similar to the phenotype of *cop1* mutants (Chory et al., 1989; Deng et al., 1991). It has been found that hundreds of genes are deregulated in the dark in such mutants (Wang et al., 2001; Schroeder et al., 2002). This information infers the importance of DET1 as a repressor of photomorphogenesis. Our results therefore imply that chromatin remodelling is an important event regulating the alterations of gene expression occurring during photomorphogenesis. Most simply, one could speculate that the chromatin context of photoregulated genes is characterized

by non-acetylated histone tails, and that the role of DET1 in the absence of photomorphogenic signals is to maintain this repressive chromatin state by interacting with unmodified H2B tails (Fig. 34). Such a hypothesis is consistent with our knowledge of histone tail modifications in other eukaryotes, in which it has been shown that repressed regions of chromatin are characterized largely by the presence of unmodified histone tails (Strahl and Allis, 2000; Jenuwein and Allis, 2001). In such a scenario, the subsequent modification of H2B tails would relax the chromatin structure around photoregulated genes and permit their expression (Fig. 34). The results presented infer that acetylation of H2B tails may be an important step following light stimulation of dark grown seedlings, although we cannot exclude that other modifications, most likely methylation or phosphorylation, are involved.

An enormous amount of research has demonstrated the importance of histone H3 and H4 tail modifications in the epigenetic control of gene expression in non-plant eukaryotic cells (Strahl and Allis, 2000; Jenuwein and Allis, 2001; Eberharter and Becker, 2002). To our knowledge DET1 in fact represents the first protein that specifically binds H2B tails. The presence of an expressed *DET1* homolog in the mouse and human genomes (Berloco et al., 2001) implies that it has a similar activity in other eukaryotes. But if H3 and H4 tails are the major targets for post-translational modifications that influence gene expression in these organisms, why should H2B tail modifications play an analogous role in plants? One possibility is that in plants H2A- and H2B-tail targeted modifications play the role of H3 and H4 modifications of other eukaryotes. In support for such a reversal of roles is a recent finding that acetylation of H3 and H4 tails correlates with DNA replication during mitosis in plant cells whereas H2A and H2B are the major targets for modification during mitosis in other eukaryotes (Jasencakova et al., 2000).

Studies of histone modifications in yeast and animal cells have led to the 'Histone Code Hypothesis,' whereby specific combinatorial modifications provide a 'code' for docking of different chromatin remodelling proteins (Strahl and Allis, 2000; Jenuwein and Allis, 2001). In line with such a hypothesis, one could predict the existence of a specific histone code that would signal chromatin remodelling around photoregulated genes. Currently the only evidence that supports the existence of such a code is that DET1 binds preferentially to non-acetylated H2B tails. In vivo analysis of DET1/H2B interactions presented in this thesis shows that interactions occur only in small regions of the nucleus. According to the very low level of expression of endogenous DET1 in plants (unpublished observation), these regions could correspond to chromatin areas containing a few key genes directly regulated by DET1, which could control other light-activated genes. However, in cells transiently expressing histone H2B and DET1 fusions, interaction sites were found in much more extended nuclear regions. This was probably due to low histone-fusion chromatin "assimilation" in transiently expressing cells. Namely, in transiently expressing cells histone fusion molecules may be incorporated into the chromatin but may not contain any tail modifications. These results question the nature of the physiological histone code which signals DET1 binding. It appears, in fact, that DET1 can bind unmodified H2B tails not only *in vitro* but also *in vivo*. However, in cells stably expressing the H2B fusion, which can presumably be perfectly integrated in the chromatin context, DET1 interaction appeared much more selective than in transiently expressing cells, either because only a fraction of the tails of GFP tagged-histone remained unmodified in cell lines or more probably because a more complex histone code (or perhaps even nucleosome code), which could not develop in cells transiently expressing the fusions, provides the necessary specificity to the DET1/H2B interaction. If this was the case DET1 would be

unlikely to act alone. Indeed, an independent study provides evidence that DET1 is part of a multisubunit protein complex (see below; Schroeder et al., 2002).

Mutation of the *DET1* homolog in Drosophila, known as *abo*, results in a maternal-effect lethality during early embryogenesis (Berloco 2001). In corroboration with our results, Abo has been shown to bind to Drosophila chromosomes. Curiously, the protein localizes specifically to the histone gene cluster and negatively regulates their expression. Although these studies did not explore how Abo targets this chromosomal region, results presented here would predict that it does so via recognition of a specific histone code. It is unlikely, however, that DET1 targets histone genes in plants, (i) because they are not clustered, and (ii) because no evidence was found that histone gene expression is deregulated in tomato *hp-2* mutants (Unpublished observations).

Furthermore, results presented infer that HATs and HDACs are likely to play an important role in regulating changes in gene expression during photomorphogenesis. Reverse genetics approaches in which the expression of individual genes have been modulated have so far revealed only pleiotropic effects (Verbsky and Richards, 2001) although the fact that the Arabidopsis genome contains 12 *HAT* genes and 15 *HDAC* genes (www.chromdb.org) reveals that individual enzymes are likely to be found that target histones within specific nucleosome contexts. Notwithstanding, forward genetics screens for photomorphogenic mutants have so far failed to implicate a role for histone acetylation in light-mediated responses.

An independent study (Schroeder et al., 2002) has provided evidence that Arabidopsis DET1 is part of a nuclear-localized complex of approximately 350 kDa. One of the proteins within this complex has been identified as an Arabidopsis homolog of vertebrate DDB1 (UV-Damaged DNA Binding Protein 1), a subunit of the nucleotide excision repair enzyme which is defective in xeroderma pigmentosa-E patients (Chu

and Chang, 1988). Interestingly, in human cells DDB1 has been found to be a component of the STAGA complex, a chromatin-acetylating transcripional coactivator that also contains GCN5, a histone acetyltransferase (Martinez et al., 2001), and also with the TFTC HAT complex (Brand et al., 2001). Although human DET1 has not yet been identified as part of these complexes, these results nonetheless provide further suggestive evidence for the association of DET1 with chromatin.

In summary, results from this thesis showing that DET1 binds unmodified H2B tails within a nucleosome context in vitro and in vivo, coupled with the dramatic phenotypes of *det1* mutants, infers that chromatin remodelling is likely to play an important role in the regulation of gene expression during photomorphogenesis. Most likely, DET1 may limit access of positive regulatory factors to the promoters of photoregulated genes (Fig. 34). Further evidence for such a mechanism must derive from experiments aimed at identifying histone tail modifications within the nucleosomes associated with light-regulated genes. The availability of genome-wide analyses of photoregulated gene expression in Arabidopsis may permit the identification of 'hot spots' for chromatin remodelling within the genome. In parallel, identification of the genes to which DET1 is targeted via its association with H2B tails will reveal more information about the functional significance of this interaction. Utilization of the chromatin immunoprecipitation technique (e.g., Cosma et al., 1999; Breiling et al., 2001) in Arabidopsis should allow these important questions to be addressed.

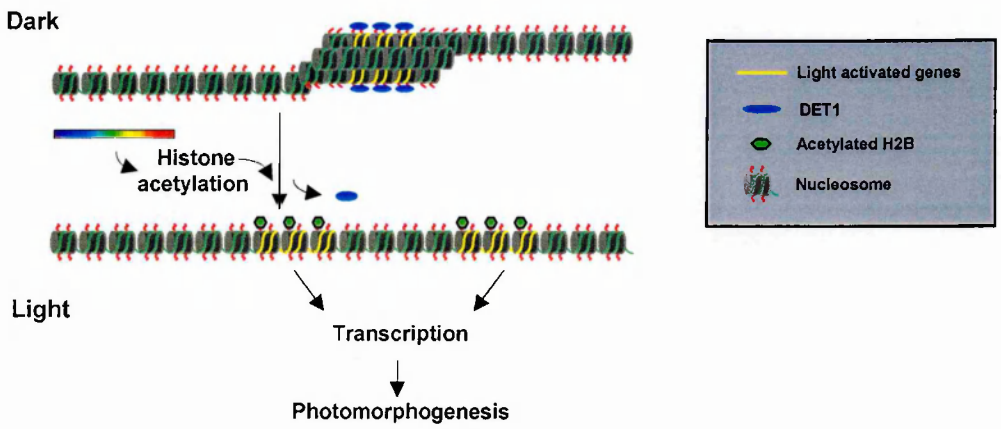

Fig. 34. Model for Function of DET1. Based on the results presented and on the phenotype of *det1* mutants we propose a model for DET1 function. In dark (etiolated) conditions light regulated genes are not expressed and may therefore be localized within densely packed chromatin domains. DET1 binds to the non-acetylated H2B tails of the nucleosomes surrounding the promoters of these genes, maintaining them in a repressed state. Light stimulation then leads to histone H2B acetylation (due to activation of an acetylase and/or deactivation of a deacetylase) followed by release of DET1, thus permitting transcriptional activation of genes involved in the de-etiolation response.

4.2 VISUALIZATION OF CHROMATIN CHANGES IN VIVO

The ability to visualize chromosomes in the microscope has allowed observation of mitotic chromosome segregation in living cells for almost one hundred years. This has been crucial for dissecting the molecular mechanisms underlying chromosome segregation. On the contrary, visualization of decondensed interphase chromosomes has been technically challenging up until very recently. Interesting questions such as the relationship between interphase chromosome structure/dynamics and regulation of transcription or DNA replication have been difficult to approach and the only data available, derived from immunostaining and *in situ* hybridization, relies mostly on static images from fixed cells. Consequently, although some results have been obtained they were not devoid of concerns over preparation artifacts caused by fixation.

A great advancement has been due to the development of fluorescent dyes or fluorescently-labelled nucleotides and proteins which could be introduced into cells to directly observe mitotic and interphase chromosome dynamics in vivo (Belmont et al., 1989; Zink and Cremer, 1998). The recent application of green fluorescent proteins (GFP; see Introduction *1.4*) has allowed a further improvement. GFP can be used to label specific nuclear proteins which are known to interact with chromatin, thus allowing *in vivo* chromatin staining. The advantages of such an approach are wide ranging. For example, although fluorescent dyes specific for DNA such as Hoechst 33342 allow in vivo observations, their applications are limited by a series of drawbacks, e.g., the necessity of using UV irradiation for their visualization, which can damage cells and can result in cell cycle arrest. Moreover, Hoechst 33342 has been demonstrated to affect cell cycle progression, arresting cells in G2 phase (Tobey et al., 1990). Other DNA dyes can, in addition, cause mutations in DNA because they are intercalating substances. Furthermore, the use of these dyes requires that each cell line

to be analysed must be examined individually to optimize time of incubation and concentration of the dye, thus necessitating a significant investment of time.

Finally, one of the main disadvantages of these older approaches when compared to the GFP-based approaches is that they allow neither long-term analyses nor studies in whole living organisms. GFP fusions, on the other hand, can be expressed constitutively (or if necessary in a regulated manner) in transgenic organisms (not only single cells). Therefore, because GFP is usually non toxic and can be detected by non-damaging blue-green wavelengths, the structure and dynamics of GFP-labelled chromatin in transgenic organisms could be studied over a short (i.e., minutes to hours) or a long (i.e., days to weeks) time scale. Such a possibility should allow important questions to be answered such as the relationship between chromatin structure and cell type and developmental stages.

To date, the application of GFP to chromatin studies has been successful with the use of fusions between histone H2B and GFP as chromatin stains (Kanda et al., 1998), and systems in which specific chromosome sites are tagged, for example, by repeats of bacterial operator sequences, and then visualized using GFP fusions to the specific repressor proteins (Belmont et al., 1998a; Belmont and Straight, 1998b; Belmont, 2001; Muller et al., 2001). Using these systems researchers have been able to infer chromatin condensation/decondensation or also its compaction in living cells on the basis of relative fluorescence values of the different chromatin regions or from in vivo measurement of the extension of GFP-labelled chromatin-tagged regions and by relating them to the known basepair sizes of these regions.

In this thesis, a different approach has been attempted. The idea was to use FRET in a GFP-based system to reveal chromatin structures. Differently from the cited methods, this GFP- and FRET-based system could directly provide precise information not only on the chromatin compaction state but also about its structures and, further-

more, with higher resolution. FRET is in fact linked to the geometrical characteristics of the reciprocal positioning of the acceptor/donor fluorescent tags (see *1.3.2* in Introduction) which in turn depends on the positioning of the molecules which are tagged with acceptor and donor. Consequently, if these molecules intimately integrate into the structure being studied, FRET could in principle provide information about its geometry.

Histones H2B and H2A were chosen to satisfy this pre-requisite and were used to generate the two GFP variant-fusions H2B-ECFP and H2A-EYFP, that were co-expressed in plant cells, or the single ECFP-EYFP-H2B fusion. These fusions have been demonstrated in this thesis to be able to stain chromatin after their incorporation into it. Moreover, as expected, it appeared that chromatin can accommodate only a limited number of histone fusions in its structure. In fact, attempts to generate cell lines expressing two histone fusions, whose chromatin would have contained up to four fusion molecules per nucleosome, failed. On the contrary, it was relatively easy to obtain cell lines expressing only one histone fusion (as previously reported by Kanda et al., 1998), which could only be incorporated in a maximum of two copies.

Both co-expression of the two GFP-histone fusions and expression of ECFP-EYFP-H2B in plant cells were able to generate different FRET values (i.e., N_{FRET} or $netF'_A$ values, see *1.3.3, 1.3.4* and *2.7.1*) for different chromatin structures and a positive correlation was found between FRET values and chromatin compaction. Unfortunately, only for ECFP-EYFP-H2B could this correlation be tested against a control of chromatin structure, whereas co-expression of histone fusions will require a further characterization to validate its use, although it could be worthwhile to test a different pair such as H2B-ECFP and H2B-EYFP to try to overcome the histone-fusion chromatin tolerance issue, that otherwise would limit application of histone pairs to transient studies in single cells only. Nonetheless, these results infer that both systems

(or at least ECFP-EYFP-H2B) could indeed be used to identify nuclear regions of determined chromatin structure in living cells by monitoring their FRET signals. Chromatin probe calibration, however, should be completed in order to obtain full exploitation of the tool, for example, by using antibodies against different chromatin states or different histone tail modifications, which are strongly suspected to modify local chromatin structure (see *1.2.2*), and by correlating FRET values detected in the immunostained regions with their known (or hypothesized) chromatin state. After this calibration stage, it should in principle be possible to follow a single living cell throughout its life-cycle observing its chromatin signature and identifying regions, for example, of active gene-transcription or regions where gene expression is repressed, with the possibility to observe changes in real time in the distribution of these regions, as a consequence of proper stimulation, for example, by light. In addition, this would create an impressively powerful observable "chromatin phenotype" that could be exploited to screen the impact of endogenous or exogenous factors on the physiological chromatin signature in order to study this complex system. Furthermore, similar studies could be possible in whole transgenic plants where, for example, it would be possible to study chromatin remodelling in different cell types, e.g,. in meristems during development.

The above mentioned applications will, however require an improvement of the system developed in this thesis. First of all, it is important to be able to classify the observed patterns of chromatin structures to test their reproducibility in certain conditions and, consequently, to be able to define cause/effect relationships. This could be done on a global level by employing image texture analysis (Markey et al., 1999) which can identify conservative patterns in groups of images. At a finer level, systems to mark specific chromatin regions are necessary to correlate a chromatin structure to a defined region containing genes of interest. For example, methods such as that reported

above exploiting sequence-specific DNA binding proteins fused to GFP (a third spectral variant) coupled with insertion of several repeats of the DNA sequence in specific positions of the genome could, in principle, be successfully used.

Another important improvement concerns the accuracy of the FRET measurements. Although the three-channel FRET method used to quantify FRET was successful, it is nonetheless based on steady-state measurements of fluorescence, which are known to be potentially affected by several sources of noise and to require many corrections to be applied (see *1.3.1*, *1.3.4* and *2.7.1*). In order to overcome the consequent potential inaccuracies of these kinds of measurements, an attempt was made to use a kinetic assay, namely donor photobleaching FRET. However, ECFP and EYFP were found to be inappropriate for this kind of assay. Consequently, three-channel FRET was found to be the best system using the equipment available during this thesis, although the results were less accurate than hoped. This is evident from histograms of FRET-value frequency distributions (Figs. 22 and 27) in which peaks corresponding to pixel populations of homogeneous FRET values displayed widths of approximately ±30% of the peak value for the two-histone system and ±15% for the single histone system. Without doubt, this is a major limit of the approach for single cell studies because this variability decreases dramatically the resolution of the FRET measurements, thus preventing a reliable detection of small differences (compared to the variability) for which instead there could be considerable interest. It seems, however, reasonable to think that the system could be improved in this regard by employing a more accurate and sensitive detection system (i.e., CCD camera) and/or other methods to quantify FRET such as FLIM (Fluorescence Lifetime Imaging) which is based on life-time measurements.

Finally, further improvements could be possible by modifying the molecular structure of the ECFP-EYFP-H2B fusion, e.g. by altering the linker structure (Zhang et al., 2002).

4.3 IMAGING OF PIF3, PHYB2, COP1 AND HY5

Data presented in this thesis show that PIF3 interacts with phytochrome in living BY-2 cells. This confirms the in vitro data obtained previously (Ni et al., 1999). Moreover, it has been shown that PIF3 forms numerous nuclear speckles that colocalize with the phytochrome speckles. There is emerging evidence that phytochrome speckles are not artifactual (e.g., inactive aggregates of GFP fusions; see *1.1.1.3* and Nagy and Schäfer, 2002). Colocalization and in vivo interaction with PIF3 strongly support this idea. One possibility for the physiological meaning of these speckles is that they form and localize onto chromatin sites where the genes controlled by PIF3 and phytochrome are located. To test this hypothesis I tried to visualize an interaction between PIF3 and H2A as a chromatin marker but unfortunately no interaction could be detected. This result, as already discussed (see *3.4.1.2*), cannot be used to reject the hypothesis and to conclude that PIF3 speckles are not sites of PIF3/DNA interaction because the used approach could be simply inappropriate to reveal the interaction. This question therefore remains open.

An additional observation was that PIF3 forms speckles in BY-2 cells either when co-expressed with phytochrome or when expressed alone. This can be interpreted in two distinct ways, depending on the capability of BY-2 cells to express endogenous light signal transduction components, in this case phytochrome. If BY-2 cells contain phytochrome, this could interact with PIF3 to mediate speckle formation. If BY-2 cells do not contain phytochrome, PIF3 speckle formation should be considered phytochrome-independent. The fact that BY-2 cells normally grow in darkness and are

devoid of chlorophyll could support the second hypothesis, suggesting that this cell line does not need light signal transduction and therefore could have lost its capacity for light signalling. However, to the best of my knowledge, there are no experimental evidence that support this idea.

Another observation was that some speckles displayed higher N_{FRET} values. As already mentioned (see *2.7.1.1*), N_{FRET} depends on the fraction (P) of the concentration of the complex exhibiting FRET to total donor and acceptor concentrations. Consequently, a difference among N_{FRET} values in different speckles could reflect a difference in the P fraction due to a difference in both PIF3 and phytochrome concentrations and/or affinity. This would imply that PIF3/phytochrome speckles are formed by other components, which could modulate their interaction.

COP1 and HY5 displayed the expected nuclear localization in BY-2 cells. Incubation in the dark or in the light, however, did not generate any detectable difference in their localization. This result for COP1 is very similar to what has been found in Arabidopsis root cells where the localization was exclusively nuclear, irrespective of illumination conditions (von Arnim and Deng, 1994). For HY5, no difference in the level of nuclear protein was detected in cells incubated in the dark or in the light, maybe because of overexpression of the HY5 fusion that could have masked HY5 degradation in the dark.

These results would indicate that, indeed, the BY-2 cell line has a limited suitability for studying components of light signal transduction, in that a deregulation of light signalling components appears to be present. These limits, however, do not contradict the results obtained in this thesis because a growing number of studies in fields such as cytokinesis, auxin responses, cell cycle, protein transport and many others demonstrate that BY-2 cells are intact in many basic plant cellular processes.

FUTURE DIRECTIONS

A lot of work is still required to elucidate the mechanisms of DET1 activity. We demonstrated its putative role in chromatin modifications, but its direct role has still to be revealed. One possibility to elucidate DET1 activity could rely on using the histone-based chromatin probe in combination with a GFP-tagged DET1 in a "multi-FRET" approach, to try to correlate regions of interaction between histone H2B and DET1 with an increased chromatin-probe FRET signal (e.g., using a probe that is positively correlated with the degree of chromatin density). An expected result would be that in regions where DET1 interacts with histone H2B, chromatin is more compacted and thus gene expression is inhibited.

Moreover, in order to clarify the putative mechanisms that could control DET1 activity, it will be important to test light/dark dependence of DET1/histone interaction (dark could trigger DET1/histone interaction whereas light would abort it). For these experiments, in order to ensure that the light signal transduction pathways are intact in the cells under study, BY-2 cells should be substituted by a different plant model, such as Arabidopsis. In addition, fundamental findings on DET1 function and its regulation will derive from studies of the proteins that make up the DET1 complex.

Concerning the physiological role of PIF3/phy interaction, one important experiment which should provide important clues could derive from studying the effect of regulated red/far-red light irradiation on the PIF3/phy interaction by measuring FRET in living cells. Phytochrome activation is in fact strongly dependent on red light whereas far-red reverses the process (see Introduction). Consequently, if the detected interaction was relevant, one would expect to observe a PIF3/phytochrome interaction in red light, whereas exposure to far-red light would be expected to release this

interaction. Also in this case, experiments should be performed preferentially in Arabidopsis.

The histone-based probe for chromatin structure can theoretically be improved to increase its capacity to resolve different chromatin structures (as has been proposed above in Discussion). In this regard, a very good test (and feed-back) could derive from studies *in planta*, e.g., in Arabidopsis, by observing chromatin dynamics in meristems during development. A further step would include similar studies in developmental mutants to identify controlling mechanisms.

REFERENCES

Ahmad, M. & Cashmore, A. R. HY4 gene of A. thaliana encodes a protein with characteristics of a blue-light photoreceptor. *Nature* **366**, 162-6. (1993).

Ahmad, M., Jarillo, J. A., Smirnova, O. & Cashmore, A. R. The CRY1 blue light photoreceptor of Arabidopsis interacts with phytochrome A in vitro. *Mol Cell* **1**, 939-48. (1998).

Ahmad, M., Jarillo, J. A. & Cashmore, A. R. Chimeric proteins between cry1 and cry2 Arabidopsis blue light photoreceptors indicate overlapping functions and varying protein stability. *Plant Cell* **10**, 197-207. (1998).

Alberts, B., Bray, D., Lewis, J., Raff, M., Roberts, K. & Watson, J. D. in *Molecular Biology of the Cell* (Garland Publishing, New York, 1994).

Alberts, B., Johnson, A., Lewis, J., Raff, M., Roberts, K. & Walter, P. in *Molecular biology of the cell* 191-234 (Garland Science, New York, 2002).

Allen, G. C., Spiker, S. & Thompson, W. F. Use of matrix attachment regions (MARs) to minimize transgene silencing. *Plant Mol Biol* **43**, 361-76. (2000).

Ang, L. H. & Deng, X. W. Regulatory hierarchy of photomorphogenic loci: allele-specific and light-dependent interaction between the HY5 and COP1 loci. *Plant Cell* **6**, 613-28. (1994).

Ang, L. H., Chattopadhyay, S., Wei, N., Oyama, T., Okada, K., Batschauer, A. & Deng, X. W. Molecular interaction between COP1 and HY5 defines a regulatory switch for light control of Arabidopsis development. *Mol Cell* **1**, 213-22. (1998).

Arabidopsis Genome Initiative. Analysis of the genome sequence of the flowering plant *Arabidopsis thaliana*. *Nature* **408**, 796-815 (2000).

Ashburner, M. Puffs, genes, and hormones revisited. *Cell* **61**, 1-3. (1990).

Ausio, J., Dong, F. & van Holde, K. E. Use of selectively trypsinized nucleosome core particles to analyze the role of the histone "tails" in the stabilization of the nucleosome. *J Mol Biol* **206**, 451-63. (1989).

Belmont, A. S., Braunfeld, M. B., Sedat, J. W. & Agard, D. A. Large-scale chromatin structural domains within mitotic and interphase chromosomes in vivo and in vitro. *Chromosoma* **98**, 129-43. (1989).

Belmont, A. S. & al., e. Visualization of large scale chromatin structure and dynamics using the lac operator/lac repressor reporter system. *Methods Cell Biol.* **58**, 99-124 (1998).

Belmont, A. S. & Straight, A. F. In vivo visualization of chromosomes using lac operator-repressor binding. *Trends Cell Biol* **8**, 121-4. (1998).

Belmont, A. S. Visualizing chromosome dynamics with GFP. *Trends Cell Biol* **11**, 250-7. (2001).

Berloco, M., Fanti, L., Breiling, A., Orlando, V. & Pimpinelli, S. The maternal effect gene, abnormal oocyte (abo), of Drosophila melanogaster encodes a specific negative regulator of histones. *Proc Natl Acad Sci U S A* **98**, 12126-31. (2001).

Berman, H. M., Westbrook, J., Feng, Z., Gilliland, G., Bhat, T. N., Weissig, H., Shindyalov, I. N. & Bourne, P. E. The Protein Data Bank. *Nucleic Acids Res* **28**, 235-42. (2000).

Billinton, N. & Knight, A. W. Seeing the wood through the trees: a review of techniques for distinguishing green fluorescent protein from endogenous autofluorescence. *Anal Biochem* **291**, 175-97. (2001).

Blinks, J. R., Prendergast, F. G., and Allen, D. G. Photoproteins as biological calcium indicators. *Pharmacol. Rev.* **28**:1-93 (1976).

Bowler, C., Neuhaus, G., Yamagata, H. & Chua, N. H. Cyclic GMP and calcium mediate phytochrome phototransduction. *Cell* **77**, 73-81. (1994).

Brand, M., Moggs, J. G., Oulad-Abdelghani, M., Lejeune, F., Dilworth, F. J., Stevenin, J., Almouzni, G. & Tora, L. UV-damaged DNA-binding protein in the TFTC complex links DNA damage recognition to nucleosome acetylation. *Embo J* **20**, 3187-96. (2001).

Breiling, A., Turner, B. M., Bianchi, M. E. & Orlando, V. General transcription factors bind promoters repressed by Polycomb group proteins. *Nature* **412**, 651-5. (2001).

Briggs, W. R., Beck, C. F., Cashmore, A. R., Christie, J. M., Hughes, J., Jarillo, J. A., Kagawa, T., Kanegae, H., Liscum, E., Nagatani, A., Okada, K., Salomon, M., Rudiger, W., Sakai, T., Takano, M., Wada, M. & Watson, J. C. The phototropin family of photoreceptors. *Plant Cell* **13**, 993-7. (2001).

Briggs, W. R. & Christie, J. M. Phototropins 1 and 2: versatile plant blue-light receptors. *Trends Plant Sci* **7**, 204-10. (2002).

Butler, W. L., Norris, K. H., Siegelman, H. A. & Hendricks, S. B. Detection, Assay, and Preliminary Purification of the Pigment Controlling Photoresponsive Development of Plants *Proc Natl Acad Sci U S A* **45**, 1703-1708 (1959).

Callan, H. G. Lampbrush chromosomes. *Mol Biol Biochem Biophys* **36**, 1-252. (1986).

Carruthers, L. M. & Hansen, J. C. The core histone N termini function independently of linker histones during chromatin condensation. *J Biol Chem* **275**, 37285-90. (2000).

Cashmore, A. R., Jarillo, J. A., Wu, Y. J. & Liu, D. Cryptochromes: blue light receptors for plants and animals. *Science* **284**, 760-5. (1999).

Cavalli, G. & Paro, R. The Drosophila Fab-7 chromosomal element conveys epigenetic inheritance during mitosis and meiosis. *Cell* **93**, 505-18. (1998).

Cavalli, G. & Paro, R. Epigenetic inheritance of active chromatin after removal of the main transactivator. *Science* **286**, 955-8. (1999).

Chattopadhyay, S., Ang, L. H., Puente, P., Deng, X. W. & Wei, N. Arabidopsis bZIP protein HY5 directly interacts with light-responsive promoters in mediating light control of gene expression. *Plant Cell* **10**, 673-83. (1998).

Choi, G., Yi, H., Lee, J., Kwon, Y. K., Soh, M. S., Shin, B., Luka, Z., Hahn, T. R. & Song, P. S. Phytochrome signalling is mediated through nucleoside diphosphate kinase 2. *Nature* **401**, 610-3. (1999).

Chory, J., Peto, C., Feinbaum, R., Pratt, L. & Ausubel, F. Arabidopsis thaliana mutant that develops as a light-grown plant in the absence of light. *Cell* **58**, 991-9. (1989).

Chu, G. & Chang, E. Xeroderma pigmentosum group E cells lack a nuclear factor that binds to damaged DNA. *Science* **242**, 564-7. (1988).

Chua, Y. L., Brown, A. P. & Gray, J. C. Targeted histone acetylation and altered nuclease accessibility over short regions of the pea plastocyanin gene. *Plant Cell* **13**, 599-612. (2001).

Clack, T., Mathews, S. & Sharrock, R. A. The phytochrome apoprotein family in Arabidopsis is encoded by five genes: the sequences and expression of PHYD and PHYE. *Plant Mol Biol* **25**, 413-27. (1994).

Clegg, R. M. Fluorescence resonance energy transfer and nucleic acids. *Methods Enzymol* **211**, 353-88. (1992).

Clegg, R. M. in *Fluorescence imaging Spectroscopy and Microscopy* (eds. Wang, X. F. & Herman, B.) 179-252 (John Wiley & Sons, Inc., 1996).

Cody, C. W., Prasher, D. C., Westler, W. M., Prendergast, F. G. & Ward, W. W. Chemical structure of the hexapeptide chromophore of the Aequorea green-fluorescent protein. *Biochemistry* **32**, 1212-8. (1993).

Colon-Carmona, A., Chen, D. L., Yeh, K. C. & Abel, S. Aux/IAA proteins are phosphorylated by phytochrome in vitro. *Plant Physiol* **124**, 1728-38. (2000).

Combettes, B., Reichheld, J. P., Chaboute, M. E., Philipps, G., Shen, W. H. & Chaubet-Gigot, N. Study of phase-specific gene expression in synchronized tobacco cells. *Methods Cell Sci* **21**, 109-21. (1999).

Conconi, A., Sogo, J. M. & Ryan, C. A. Ribosomal gene clusters are uniquely proportioned between open and closed chromatin structures in both tomato leaf cells and exponentially growing suspension cultures. *Proc Natl Acad Sci U S A* **89**, 5256-60. (1992).

Cosma, M. P., Tanaka, T. & Nasmyth, K. Ordered recruitment of transcription and chromatin remodeling factors to a cell cycle- and developmentally regulated promoter. *Cell* **97**, 299-311. (1999).

Croston, G. E. & Kadonaga, J. T. Role of chromatin structure in the regulation of transcription by RNA polymerase II. *Curr Opin Cell Biol* **5**, 417-23. (1993).

Cubas, P., Vincent, C. & Coen, E. An epigenetic mutation responsible for natural variation in floral symmetry. *Nature* **401**, 157-61. (1999).

Cubitt, A. B., Heim, R., Adams, S. R., Boyd, A. E., Gross, L. A. & Tsien, R. Y. Understanding, improving and using green fluorescent proteins. *Trends Biochem Sci* **20**, 448-55. (1995).

Cubitt, A. B., Woollenweber, L. A. & Heim, R. Understanding structure-function relationships in the Aequorea victoria green fluorescent protein. *Methods Cell Biol* **58**, 19-30. (1999).

Daban, J. R. Physical constraints in the condensation of eukaryotic chromosomes. Local concentration of DNA versus linear packing ratio in higher order chromatin structures. *Biochemistry* **39**, 3861-6. (2000).

Daneholt, B. Transcription in polytene chromosomes. *Cell* **4**, 1-9. (1975).

Deng, X. W., Caspar, T. & Quail, P. H. cop1: a regulatory locus involved in light-controlled development and gene expression in Arabidopsis. *Genes Dev* **5**, 1172-82. (1991).

Dickson, R. M., Cubitt, A. B., Tsien, R. Y. & Moerner, W. E. On/off blinking and switching behaviour of single molecules of green fluorescent protein. *Nature* **388**, 355-8. (1997).

Eberharter, A. & Becker, P. B. Histone acetylation: a switch between repressive and permissive chromatin. Second in review series on chromatin dynamics. *EMBO Rep* **3**, 224-9. (2002).

Fankhauser, C., Yeh, K. C., Lagarias, J. C., Zhang, H., Elich, T. D. & Chory, J. PKS1, a substrate phosphorylated by phytochrome that modulates light signaling in Arabidopsis. *Science* **284**, 1539-41. (1999).

Finch, J. T. & Klug, A. Solenoidal model for superstructure in chromatin. *Proc Natl Acad Sci U S A* **73**, 1897-901. (1976).

Flaus, A. & Owen-Hughes, T. Mechanisms for ATP-dependent chromatin remodelling. *Curr Opin Genet Dev* **11**, 148-54. (2001).

Förster, T. Intermolecular energy migration and fluorescence. *Ann. Phys. (Leipzig)* **2**, 55-75 (1948).

Foster, R., Gasch, A., Kay, S. & Chua, N. H. in *Methods in Arabidopsis Research* (eds. Koncz, C., Chua, N. H. & Schell, J.) 378-392 (World Scientific, Singapore, 1992).

Gadella, T. W., Jr. & Jovin, T. M. Oligomerization of epidermal growth factor receptors on A431 cells studied by time-resolved fluorescence imaging microscopy. A

stereochemical model for tyrosine kinase receptor activation. *J Cell Biol* **129**, 1543-58. (1995).

Gadella, T. W., Jr., Vereb, G., Jr., Hadri, A. E., Rohrig, H., Schmidt, J., John, M., Schell, J. & Bisseling, T. Microspectroscopic imaging of nodulation factor-binding sites on living Vicia sativa roots using a novel bioactive fluorescent nodulation factor. *Biophys J* **72**, 1986-96. (1997).

Gadella, T. W., Jr. in *Fluorescent and Luminescent Probes for Biological Activity* (ed. Mason, W.) 467-479 (Academic Press, New York, 1999).

Goldberg, M., Harel, A., Brandeis, M., Rechsteiner, T., Richmond, T. J., Weiss, A. M. & Gruenbaum, Y. The tail domain of lamin Dm0 binds histones H2A and H2B. *Proc Natl Acad Sci U S A* **96**, 2852-7. (1999).

González-Melendi, P., Testillano, P. S., Mena, C. G., Muller, S., Raska, I. & Risueño, M. C. Histones and DNA Ultrastructural Distribution in Plant Cell Nucleus: A Combination of Immunogold and Cytochemical Methods. *Experimental Cell Research* **242**, 45-59 (1998).

Goodrich, J. & Tweedie, S. Remembrance of things past: chromatin remodeling in plant development. *Annu Rev Cell Dev Biol* **18**, 707-46. (2002).

Gordon, G. W., Berry, G., Liang, X. H., Levine, B. & Herman, B. Quantitative fluorescence resonance energy transfer measurements using fluorescence microscopy. *Biophys J* **74**, 2702-13. (1998).

Graziano, V., Gerchman, S. E., Schneider, D. K. & Ramakrishnan, V. Histone H1 is located in the interior of the chromatin 30-nm filament. *Nature* **368**, 351-4. (1994).

Greyling, H. J., Schwager, S., Sewell, B. T. & von Holt, C. The identity of conformational states of reconstituted and native histone octamers. *Eur J Biochem* **137**, 221-6. (1983).

Grynkiewicz, G., Poenie, M. & Tsien, R. Y. A new generation of Ca2+ indicators with greatly improved fluorescence properties. *J Biol Chem* **260**, 3440-50. (1985).

Guex, N. & Peitsch, M. C. SWISS-MODEL and the Swiss-PdbViewer: an environment for comparative protein modeling. *Electrophoresis* **18**, 2714-23. (1997).

Guo, H., Mockler, T., Duong, H. & Lin, C. SUB1, an Arabidopsis Ca2+-binding protein involved in cryptochrome and phytochrome coaction. *Science* **291**, 487-90. (2001).

Hardtke, C. S. & Deng, X. W. The cell biology of the COP/DET/FUS proteins. Regulating proteolysis in photomorphogenesis and beyond? *Plant Physiol* **124**, 1548-57. (2000).

Hare, P. D., Seo, H. S., Yang, J. Y. & Chua, N. H. Modulation of sensitivity and selectivity in plant signaling by proteasomal destabilization. *Curr Opin Plant Biol* **6**, 453-62. (2003).

Haseloff, J., Siemering, K. R., Prasher, D. C. & Hodge, S. Removal of a cryptic intron and subcellular localization of green fluorescent protein are required to mark transgenic Arabidopsis plants brightly. *Proc Natl Acad Sci U S A* **94**, 2122-7. (1997).

Haugland, R. P. in *Handbook of Fluorescent Probes and Research Products* (ed. Gregory, J.) 747-863 (Molecular Probes, Eugene, Oregon, 2002).

Heim, R. Green fluorescent protein forms for energy transfer. *Methods Enzymol* **302**, 408-23. (1999).

Heitz, E. Das Heterochromatin der Moose. *I. Jahrb. Wiss. Bot.* **69**, 762-819 (1928).

Huala, E., Oeller, P. W., Liscum, E., Han, I. S., Larsen, E. & Briggs, W. R. Arabidopsis NPH1: a protein kinase with a putative redox-sensing domain. *Science* **278**, 2120-3. (1997).

Huq, E., Al-Sady, B. & Quail, P. H. Nuclear translocation of the photoreceptor phytochrome B is necessary for its biological function in seedling photomorphogenesis. *Plant J* **35**, 660-4. (2003).

Iglesias, V. A., Moscone, E. A., Papp, I., Neuhuber, F., Michalowski, S., Phelan, T., Spiker, S., Matzke, M. & Matzke, A. J. Molecular and cytogenetic analyses of stably and unstably expressed transgene loci in tobacco. *Plant Cell* **9**, 1251-64. (1997).

Immink, R. G., Gadella, T. W., Jr., Ferrario, S., Busscher, M. & Angenent, G. C. Analysis of MADS box protein-protein interactions in living plant cells. *Proc Natl Acad Sci U S A* **99**, 2416-21. (2002).

Inoué, S. & Spring, K. R. *Video Microscopy* (Plenum Press, New York, 1997).

Ishige, F., Takaichi, M., Foster, R., Chua, N.-H. & Oeda, K. A G-box motif (GCCACGTGCC) tetramer confers high-level constitutive expression in dicot and monocot plants. *Plant J.* **18**, 443-448 (1999).

Jarillo, J. A. NPL1 (accession no. AF053941): a second member of the NPH serine/threonine kinase family of *Arabidopsis*. *Plant Physiol* **117**, 719 (1998).

Jarillo, J. A., Gabrys, H., Capel, J., Alonso, J. M., Ecker, J. R. & Cashmore, A. R. Phototropin-related NPL1 controls chloroplast relocation induced by blue light. *Nature* **410**, 952-4. (2001).

Jasencakova, Z., Meister, A., Walter, J., Turner, B. M. & Schubert, I. Histone H4 acetylation of euchromatin and heterochromatin is cell cycle dependent and correlated with replication rather than with transcription. *Plant Cell* **12**, 2087-100. (2000).

Jefferson, R. A., Kavanagh, T. A. & Bevan, M. W. GUS fusions: β-glucuronidase as a sensitive and versatile gene fusion marker in higher plants. *EMBO J.* **6**, 3901-7 (1987).

Jenik, P. D. & Irish, V. F. The Arabidopsis floral homeotic gene APETALA3 differentially regulates intercellular signaling required for petal and stamen development. *Development* **128**, 13-23. (2001).

Jenuwein, T. & Allis, C. D. Translating the histone code. *Science* **293**, 1074-80. (2001).

Kagawa, T., Sakai, T., Suetsugu, N., Oikawa, K., Ishiguro, S., Kato, T., Tabata, S., Okada, K. & Wada, M. Arabidopsis NPL1: a phototropin homolog controlling the chloroplast high-light avoidance response. *Science* **291**, 2138-41. (2001).

Kam, Z., Hanser, B., Gustafsson, M. G., Agard, D. A. & Sedat, J. W. Computational adaptive optics for live three-dimensional biological imaging. *Proc Natl Acad Sci U S A* **98**, 3790-5. (2001).

Kanda, T., Sullivan, K. F. & Wahl, G. M. Histone-GFP fusion protein enables sensitive analysis of chromosome dynamics in living mammalian cells. *Curr Biol* **8**, 377-85. (1998).

Kato, K., Matsumoto, T., Koiwai, A., Mizusaki, S., Nishida, K., Noguchi, M. & Tamaki, E. In *Fermentation Technology Today* (G. Terui, ed.), pp. 689-695. Soc. Ferment. Technol., Osaka, Japan, 1972.

Kendrick, R. E. & Kronemberg, G. H. M. *Photomorphogenesis in Higher Plants* (Kluver Academic Publishers, Dordrecht,The Netherlands, 1994).

Kim, L., Kircher, S., Toth, R., Adam, E., Schafer, E. & Nagy, F. Light-induced nuclear import of phytochrome-A:GFP fusion proteins is differentially regulated in transgenic tobacco and Arabidopsis. *Plant J* **22**, 125-33. (2000).

Kinoshita, T., Doi, M., Suetsugu, N., Kagawa, T., Wada, M. & Shimazaki, K. Phot1 and phot2 mediate blue light regulation of stomatal opening. *Nature* **414**, 656-60. (2001).

Kircher, S., Kozma-Bognar, L., Kim, L., Adam, E., Harter, K., Schafer, E. & Nagy, F. Light quality-dependent nuclear import of the plant photoreceptors phytochrome A and B. *Plant Cell* **11**, 1445-56. (1999).

Kircher, S., Gil, P., Kozma-Bognar, L., Fejes, E., Speth, V., Husselstein-Muller, T., Bauer, D., Adam, E., Schafer, E. & Nagy, F. Nucleocytoplasmic partitioning of the plant photoreceptors phytochrome A, B, C, D, and E is regulated differentially by light and exhibits a diurnal rhythm. *Plant Cell* **14**, 1541-55. (2002).

Kleine, T., Lockhart, P. & Batschauer, A. An Arabidopsis protein closely related to Synechocystis cryptochrome is targeted to organelles. *Plant J* **35**, 93-103. (2003).

Koning, A. J., Tanimoto, E. Y., Kiehne, K., Rost, T. & Comai, L. Cell-specific expression of plant histone H2A genes. *Plant Cell* **3**, 657-65. (1991).

Kornberg, R. D. & Klug, A. The nucleosome. *Sci Am* **244**, 52-64. (1981).

Kornberg, R. D. & Lorch, Y. Twenty-five years of the nucleosome, fundamental particle of the eukaryote chromosome. *Cell* **98**, 285-94. (1999).

Lakowicz, J. R. in *Principles of fluorescence spectroscopy* 305-341 (Plenum, New York, 1983).

Lakowicz, J. R. *Principles of Fluorescence Spectroscopy* (Kluwer Academic/Plenum Publishers, New York, 1999a).

Lakowicz, J. R. in *Principles of Fluorescence Spectroscopy* 425-443 (Kluwer Academic/Plenum Publishers, New York, 1999b).

Lakowicz, J. R. in *Principles of Fluorescence Spectroscopy* 367-394 (Kluwer Academic/Plenum Publishers, New York, 1999c).

Lakowicz, J. R. in *Principles of Fluorescence Spectroscopy* 95-140 (Kluwer Academic/Plenum Publishers, New York, 1999d).

Lawrence, P. A. & Struhl, G. Morphogens, compartments, and pattern: lessons from drosophila? *Cell* **85**, 951-61. (1996).

Lin, C., Robertson, D. E., Ahmad, M., Raibekas, A. A., Jorns, M. S., Dutton, P. L. & Cashmore, A. R. Association of flavin adenine dinucleotide with the Arabidopsis blue light receptor CRY1. *Science* **269**, 968-70. (1995).

Lin, C., Yang, H., Guo, H., Mockler, T., Chen, J. & Cashmore, A. R. Enhancement of blue-light sensitivity of Arabidopsis seedlings by a blue light receptor cryptochrome 2. *Proc Natl Acad Sci U S A* **95**, 2686-90. (1998).

Lin, C. Blue light receptors and signal transduction. *Plant Cell* **14**, S207-25. (2002).

Liscum, E. & Briggs, W. R. Mutations in the NPH1 locus of Arabidopsis disrupt the perception of phototropic stimuli. *Plant Cell* **7**, 473-85. (1995).

Lorain, S., Quivy, J. P., Monier-Gavelle, F., Scamps, C., Lecluse, Y., Almouzni, G. & Lipinski, M. Core histones and HIRIP3, a novel histone-binding protein, directly interact with WD repeat protein HIRA. *Mol Cell Biol* **18**, 5546-56. (1998).

Luger, K., Mader, A. W., Richmond, R. K., Sargent, D. F. & Richmond, T. J. Crystal structure of the nucleosome core particle at 2.8 A resolution. *Nature* **389**, 251-60. (1997).

Lusser, A., Kolle, D. & Loidl, P. Histone acetylation: lessons from the plant kingdom. *Trends Plant Sci* **6**, 59-65. (2001).

Lyapina, S., Cope, G., Shevchenko, A., Serino, G., Tsuge, T., Zhou, C., Wolf, D. A., Wei, N. & Deshaies, R. J. Promotion of NEDD-CUL1 conjugate cleavage by COP9 signalosome. *Science* **292**, 1382-5. (2001).

Ma, L., Gao, Y., Qu, L., Chen, Z., Li, J., Zhao, H. & Deng, X. W. Genomic evidence for COP1 as a repressor of light-regulated gene expression and development in Arabidopsis. *Plant Cell* **14**, 2383-98. (2002).

Markey, M. K., Boland, M. V. & Murphy, R. F. Toward objective selection of representative microscope images. *Biophys J* **76**, 2230-7. (1999).

Marsden, M. P. & Laemmli, U. K. Metaphase chromosome structure: evidence for a radial loop model. *Cell* **17**, 849-58. (1979).

Martinez, E., Palhan, V. B., Tjernberg, A., Lymar, E. S., Gamper, A. M., Kundu, T. K., Chait, B. T. & Roeder, R. G. Human STAGA complex is a chromatin-acetylating transcription coactivator that interacts with pre-mRNA splicing and DNA damage-binding factors in vivo. *Mol Cell Biol* **21**, 6782-95. (2001).

Martinez-Garcia, J. F., Monte, E. & Quail, P. H. A simple, rapid and quantitative method for preparing Arabidopsis protein extracts for immunoblot analysis. *Plant J* **20**, 251-7. (1999).

Martinez-Garcia, J. F., Huq, E. & Quail, P. H. Direct targeting of light signals to a promoter element-bound transcription factor. *Science* **288**, 859-63. (2000).

Mas, P., Devlin, P. F., Panda, S. & Kay, S. A. Functional interaction of phytochrome B and cryptochrome 2. *Nature* **408**, 207-11. (2000).

McCormick, S. in *Plant Tissue Culture Manual* 1-9 (the Netherlands, 1991).

McCurdy, D. W. & Pratt, L. H. Immunogold electron microscopy of phytochrome in Avena: identification of intracellular sites responsible for phytochrome sequestering and enhanced pelletability. *J Cell Biol* **103**, 2541-50. (1986).

Menkens, A. E., Schindler, U. & Cashmore, A. R. The G-box: a ubiquitous regulatory DNA element in plants bound by the GBF family of bZIP proteins. *Trends Biochem Sci* **20**, 506-10. (1995).

Meyer, P. Chromatin remodelling. *Curr Opin Plant Biol* **4**, 457-62. (2001).

Minta, A. & Tsien, R. Y. Fluorescent indicators for cytosolic sodium. *J Biol Chem* **264**, 19449-57. (1989).

Miyawaki, A. & Tsien, R. Y. Monitoring protein conformations and interactions by fluorescence resonance energy transfer between mutants of green fluorescent protein. *Methods Enzymol* **327**, 472-500. (2000).

Montgomery, B. L. & Lagarias, J. C. Phytochrome ancestry: sensors of bilins and light. *Trends Plant Sci* **7**, 357-66. (2002).

Morin, J. G. & Hastings, J. W. Energy transfer in a bioluminescent system. *J Cell Physiol* **77**, 313-8. (1971).

Muller, W. G., Walker, D., Hager, G. L. & McNally, J. G. Large-scale chromatin decondensation and recondensation regulated by transcription from a natural promoter. *J Cell Biol* **154**, 33-48. (2001).

Mustilli, A. C., Fenzi, F., Ciliento, R., Alfano, F. & Bowler, C. Phenotype of the tomato high pigment-2 mutant is caused by a mutation in the tomato homolog of DEETIOLATED1. *Plant Cell* **11**, 145-57. (1999).

Nagata, T., Nemoto, Y. & Hasezawa, S. Tobacco BY-2 cells as the "HeLa" cell in the cell biology of higher plants. *Internatl. Rev. Cytol.* **132**, 1-30 (1992).

Nagy, F. & Schafer, E. Nuclear and cytosolic events of light-induced, phytochrome-regulated signaling in higher plants. *Embo J* **19**, 157-63. (2000).

Nagy, F. & Schafer, E. Phytochromes control photomorphogenesis by differentially regulated, interacting signaling pathways in higher plants. *Annu Rev Plant Biol* **53**, 329-55. (2002).

Nakayama, J., Klar, A. J. & Grewal, S. I. A chromodomain protein, Swi6, performs imprinting functions in fission yeast during mitosis and meiosis. *Cell* **101**, 307-17. (2000).

Ni, M., Tepperman, J. M. & Quail, P. H. PIF3, a phytochrome-interacting factor necessary for normal photoinduced signal transduction, is a novel basic helix-loop-helix protein. *Cell* **95**, 657-67. (1998).

Ni, M., Tepperman, J. M. & Quail, P. H. Binding of phytochrome B to its nuclear signalling partner PIF3 is reversibly induced by light. *Nature* **400**, 781-4. (1999).

Okamoto, H., Matsui, M. & Deng, X. W. Overexpression of the heterotrimeric G-protein alpha-subunit enhances phytochrome-mediated inhibition of hypocotyl elongation in Arabidopsis. *Plant Cell* **13**, 1639-52. (2001).

Olins, A. L. & Olins, D. E. Spheroid chromatin units (v bodies). *Science* **183**, 330-2. (1974).

Ormo, M., Cubitt, A. B., Kallio, K., Gross, L. A., Tsien, R. Y. & Remington, S. J. Crystal structure of the Aequorea victoria green fluorescent protein. *Science* **273**, 1392-5. (1996).

Osterlund, M. T. & Deng, X. W. Multiple photoreceptors mediate the light-induced reduction of GUS-COP1 from Arabidopsis hypocotyl nuclei. *Plant J* **16**, 201-8. (1998).

Osterlund, M. T., Hardtke, C. S., Wei, N. & Deng, X. W. Targeted destabilization of HY5 during light-regulated development of Arabidopsis. *Nature* **405**, 462-6. (2000).

Osterlund, M. T., Wei, N. & Deng, X. W. The roles of photoreceptor systems and the COP1-targeted destabilization of HY5 in light control of Arabidopsis seedling development. *Plant Physiol* **124**, 1520-4. (2000).

Oyama, T., Shimura, Y. & Okada, K. The Arabidopsis HY5 gene encodes a bZIP protein that regulates stimulus-induced development of root and hypocotyl. *Genes Dev* **11**, 2983-95. (1997).

Patterson, G., Day, R. N. & Piston, D. Fluorescent protein spectra. *J Cell Sci* **114**, 837-8. (2001).

Paulson, J. R. & Laemmli, U. K. The structure of histone-depleted metaphase chromosomes. *Cell* **12**, 817-28. (1977).

Peng, Z., Serino, G. & Deng, X. W. Molecular characterization of subunit 6 of the COP9 signalosome and its role in multifaceted developmental processes in Arabidopsis. *Plant Cell* **13**, 2393-407. (2001).

Pepper, A., Delaney, T., Washburn, T., Poole, D. & Chory, J. DET1, a negative regulator of light-mediated development and gene expression in arabidopsis, encodes a novel nuclear-localized protein. *Cell* **78**, 109-16. (1994).

Pienta, K. J. & Coffey, D. S. A structural analysis of the role of the nuclear matrix and DNA loops in the organization of the nucleus and chromosome. *J Cell Sci Suppl* **1**, 123-35. (1984).

Prasher, D. C. Using GFP to see the light. *Trends Genet* **11**, 320-3. (1995).

Quail, P. H. Phytochrome-interacting factors. *Semin Cell Dev Biol* **11**, 457-66. (2000).

Quail, P. H. Photosensory perception and signalling in plant cells: new paradigms? *Curr Opin Cell Biol* **14**, 180-8. (2002).

Razin, S. V. & Gromova, II. The channels model of nuclear matrix structure. *Bioessays* **17**, 443-50. (1995).

Reymond, P., Short, T. W., Briggs, W. R. & Poff, K. L. Light-induced phosphorylation of a membrane protein plays an early role in signal transduction for phototropism in Arabidopsis thaliana. *Proc Natl Acad Sci U S A* **89**, 4718-21. (1992).

Sakai, T., Kagawa, T., Kasahara, M., Swartz, T. E., Christie, J. M., Briggs, W. R., Wada, M. & Okada, K. Arabidopsis nph1 and npl1: blue light receptors that mediate both phototropism and chloroplast relocation. *Proc Natl Acad Sci U S A* **98**, 6969-74. (2001).

Sakamoto, K. & Nagatani, A. Nuclear localization activity of phytochrome B. *Plant J* **10**, 859-68. (1996).

Sancar, A. Structure and function of DNA photolyase. *Biochemistry* **33**, 2-9. (1994).

Schafer, E. & Bowler, C. Phytochrome-mediated photoperception and signal transduction in higher plants. *EMBO Rep* **3**, 1042-1048 (2002).

Schnitzler, G. R. in *Current Protocols in Molecular Biology* (eds. Ausubel, F. M. et al.) 21.25.21-21.25.25 (Green Publishing/Wiley Interscience, New York, 2000).

Schroeder, D. F., Gahrtz, M., Maxwell, B. B., Cook, R. K., Kan, J. M., Alonso, J. M., Ecker, J. R. & Chory, J. De-etiolated 1 and damaged DNA binding protein 1 interact to regulate Arabidopsis photomorphogenesis. *Curr Biol* **12**, 1462-72. (2002).

Schwechheimer, C., Serino, G., Callis, J., Crosby, W. L., Lyapina, S., Deshaies, R. J., Gray, W. M., Estelle, M. & Deng, X. W. Interactions of the COP9 signalosome with the E3 ubiquitin ligase SCFTIRI in mediating auxin response. *Science* **292**, 1379-82. (2001).

Shacklock, P. S., Read, N. D. & Trewavas, A. J. Cytosolic free calcium mediates red light-induced photomorphogenesis. *Nature* **358**, 753-755 (1992).

Sharrock, R. A. & Quail, P. H. Novel phytochrome sequences in Arabidopsis thaliana: structure, evolution, and differential expression of a plant regulatory photoreceptor family. *Genes Dev* **3**, 1745-57. (1989).

Shimomura, O. & Johnson, F. H. Chemical nature of bioluminescence systems in coelenterates. *Proc Natl Acad Sci U S A* **72**, 1546-9. (1975).

Singh, P. B. & Georgatos, S. D. HP1: facts, open questions, and speculation. *J Struct Biol* **140**, 10-6. (2002).

Smith, H. Physiological and Ecological Function within the Phytochrome Family. *Annu. Rev. Plant Physiol. Plant Mol. Biol.* **46**, 289-315 (1995).

Speth, V., Otto, V. & Schaefer, E. Intracellular localization of phytochrome in oat coleoptiles by electron microscopy. *Planta* **168**, 299-304 (1986).

Speth, V., Otto, V. & Schaefer, E. Intracellular localization of phytochrome and ubiquitin in red-light-irradiated oat coleoptiles by electron microscopy. *Planta* **171**, 332-338 (1987).

Stacey, M. G. & von Arnim, A. G. A novel motif mediates the targeting of the Arabidopsis COP1 protein to subnuclear foci. *J Biol Chem* **274**, 27231-6. (1999).

Strahl, B. D. & Allis, C. D. The language of covalent histone modifications. *Nature* **403**, 41-5. (2000).

Struhl, K. Fundamentally different logic of gene regulation in eukaryotes and prokaryotes. *Cell* **98**, 1-4. (1999).

Svaren, J. & Horz, W. Histones, nucleosomes and transcription. *Curr Opin Genet Dev* **3**, 219-25. (1993).

Sweere, U., Eichenberg, K., Lohrmann, J., Mira-Rodado, V., Baurle, I., Kudla, J., Nagy, F., Schafer, E. & Harter, K. Interaction of the response regulator ARR4 with phytochrome B in modulating red light signaling. *Science* **294**, 1108-11. (2001).

Taylor, B. L. & Zhulin, I. B. PAS domains: internal sensors of oxygen, redox potential, and light. *Microbiol Mol Biol Rev* **63**, 479-506. (1999).

Tepperman, J. M., Zhu, T., Chang, H. S., Wang, X. & Quail, P. H. Multiple transcription-factor genes are early targets of phytochrome A signaling. *Proc Natl Acad Sci U S A* **98**, 9437-42. (2001).

Thoma, F., Koller, T. & Klug, A. Involvement of histone H1 in the organization of the nucleosome and of the salt-dependent superstructures of chromatin. *J Cell Biol* **83**, 403-27. (1979).

Tobey, R. A., Oishi, N. & Crissman, H. A. Cell cycle synchronization: reversible induction of G2 synchrony in cultured rodent and human diploid fibroblasts. *Proc Natl Acad Sci U S A* **87**, 5104-8. (1990).

Tsien, R. Y. Fluorescent indicators of ion concentrations. *Methods Cell Biol* **30**, 127-56. (1989).

Tsien, R. Y. The green fluorescent protein. *Annu Rev Biochem* **67**, 509-44. (1998).

Tsien, R. Y. & Prasher, D. C. *GFP: Green Fluorescent Protein Strategies and Applications* (eds. Chalfie, M. & Kain, S.) (John Wiley & Sons, New York, 1998).

van Holde, K. E., Lohr, D. E. & Robert, C. What happens to nucleosomes during transcription? *J Biol Chem* **267**, 2837-40. (1992).

Verbsky, M. L. & Richards, E. J. Chromatin remodeling in plants. *Curr Opin Plant Biol* **4**, 494-500. (2001).

von Arnim, A. G. & Deng, X. W. Light inactivation of Arabidopsis photomorphogenic repressor COP1 involves a cell-specific regulation of its nucleocytoplasmic partitioning. *Cell* **79**, 1035-45. (1994).

von Arnim, A. G., Deng, X. W. & Stacey, M. G. Cloning vectors for the expression of green fluorescent protein fusion proteins in transgenic plants. *Gene* **221**, 35-43. (1998).

Wallace, W., Schaefer, L. H. & Swedlow, J. R. A workingperson's guide to deconvolution in light microscopy. *Biotechniques* **31**, 1076-8, 1080, 1082 passim. (2001).

Wang, H., Ma, L. G., Li, J. M., Zhao, H. Y. & Deng, X. W. Direct interaction of Arabidopsis cryptochromes with COP1 in light control development. *Science* **294**, 154-8. (2001).

Ward, W. W. *Photochem Photobiol* **35**, 803 (1982).

Wei, N., Tsuge, T., Serino, G., Dohmae, N., Takio, K., Matsui, M. & Deng, X. W. The COP9 complex is conserved between plants and mammals and is related to the 26S proteasome regulatory complex. *Curr Biol* **8**, 919-22. (1998).

Wei, N. & Deng, X. W. Making sense of the COP9 signalosome. A regulatory protein complex conserved from Arabidopsis to human. *Trends Genet* **15**, 98-103. (1999).

Wilkinson, J. Q., Lanahan, M. B., Yen, H. C., Giovannoni, J. J. & Klee, H. J. An ethylene-inducible component of signal transduction encoded by never-ripe. *Science* **270**, 1807-9. (1995).

Wolffe, A. *Chromatin: Structure and Function* (Academic Press, London, 1998).

Workman, J. L., Taylor, I. C. & Kingston, R. E. Activation domains of stably bound GAL4 derivatives alleviate repression of promoters by nucleosomes. *Cell* **64**, 533-44. (1991).

Xia, Z. & Liu, Y. Reliable and global measurement of fluorescence resonance energy transfer using fluorescence microscopes. *Biophys J* **81**, 2395-402. (2001).

Yamaguchi, R., Nakamura, M., Mochizuki, N., Kay, S. A. & Nagatani, A. Light-dependent translocation of a phytochrome B-GFP fusion protein to the nucleus in transgenic Arabidopsis. *J Cell Biol* **145**, 437-45. (1999).

Yang, F., Moss, L. G. & Phillips, G. N., Jr. The molecular structure of green fluorescent protein. *Nat Biotechnol* **14**, 1246-51. (1996).

Yeh, K. C. & Lagarias, J. C. Eukaryotic phytochromes: light-regulated serine/threonine protein kinases with histidine kinase ancestry. *Proc Natl Acad Sci U S A* **95**, 13976-81. (1998).

Zhang, J., Campbell, R. E., Ting, A. Y. & Tsien, R. Y. Creating new fluorescent probes for cell biology. *Nat Rev Mol Cell Biol* **3**, 906-18. (2002).

Zink, D. & Cremer, T. Cell nucleus: chromosome dynamics in nuclei of living cells. *Curr Biol* **8**, R321-4. (1998).